The Thesis Committee for John Littlepage

Certifies that this is the approved version of the following thesis:

Use of Well Testing and Multiple Point Statistics in Analyzing Deep Water Channel Turbidite Reservoirs

APPROVED BY

SUPERVISING COMMITTEE:

Supervisor:_____

Sanjay Srinivasan

_____

Lesli Wood

Use of Well Testing and Multiple Point Statistics in Analyzing Deep Water Channel Turbidite Reservoirs

By

John Stanley Littlepage, B.S.P.E.

Thesis

Presented to the Faculty of the Graduate School of

The University of Texas at Austin

In Partial Fulfillment

of the Requirements

for the Degree of

Master of Science in Engineering

The University of Texas at Austin

August 2011

Dedication

To my loving family for always providing me the support and encouragement to pursue higher learning and to have the strength to persevere when the going got tough. To my friends and water polo team mates for whom without I would not have been able to undergone the necessary breaks from work and allowed me to enjoy life.

Acknowledgements

I would like to express my deepest gratitude to my supervisor, Dr. Sanjay Srinivasan who without this thesis would not have been possible. You have kept me focused and have shown me the way whenever I began to lose hope. I learnt a lot doing my research under you and as a result have become a better engineer and more importantly a better person.

I would also like to thank Dr. Lesli Wood for taking the time to read my thesis as well as providing valuable feedback and knowledge on the geological environments studied in this thesis.

To the faculty members at the University of Texas specifically Jin Lee for all of her administrative help, Roger Terzian and Joanna Castillo for technical help and computer support and all other staff members for sharing there profound knowledge with me.

I would also like to thank the folks at Kappa Engineering for providing me the use of their commercial Well Testing software Ecrin free of charge and for ease of availability on my personal computer.

Finally I would like to thank my lab mates, friends and research team specifically Sayantan Bowhmik, Selin Erzybek, Cesar Mantilla, Brandon Henke and Namdi Azom. Your wealth of knowledge and continuous support made problem solving fun and always gave new insights to make my thesis better.

Abstract

Use of Well Testing and Multiple Point Statistics in Analyzing Deep Water Channel Turbidite Reservoirs

John Littlepage, M.S.E

The University of Texas at Austin, 2011

Supervisor: Sanjay Srinivasan

Well testing has long been used to determine the dynamic characteristics of a reservoir. However due to the increase in interest in exploring deep offshore reservoirs and the expense associated with performing well tests of sufficient duration, alternative methods for retrieving reservoir specific information from tests of limited duration are necessary. This thesis presents analysis of derivative plots from well tests in different locations along a heterogeneous channelized environment and the information that can be derived the shape of these plots. The viability of calibrating a multiple point proxy that captures the reservoir flow connectivity information contained in well test data is explored. Such a proxy can provide useful insight into the nature of reservoir heterogeneity in the vicinity of the well.

The behavior of the log-log derivative plot gives invaluable information about the nature of the reservoir surrounding the penetrating wells. Based on the change in slope of

the derivative plot one can tell if a flow conduit or a low permeability zone is close to the well. Proximity to these features is also indicated in the curvature of the derivative plot with the test plot showing increasing symmetry as flow boundaries are approached. This was found to be true in both systematic simulations as well as in real build up test data.

The calibration of the multiple point permeability proxy also provides information about the connectivity of the reservoir. Single point statistics provide the best estimate for wells either inside a channel or very close to the channel boundary. This is because of the relative homogeneity of permeability values within the spatial template used for averaging. The further the well gets from the channel fewer high permeability blocks will be picked up by the template and thus multiple point models provide the best estimate for effective permeability, K_{eff}. Three point models were found to be the most accurate when the template exhibited complex permeability transition from the mudstone to the channel facies.

Table of Contents

List of Tables……..…xiii

List of Figures……...xiv

Chapter 1: Introduction……1

1.1 Overview……1

1.2 Traditional Well Test…….2

1.3 Technology Assessment in Deep Water Exploration……3

1.3.1 Solutions to problems discovered……4

1.4 Research Objective……6

1.5 Thesis Outline……6

Chapter 2: Literature Review……...8

2.1 Overview……8

2.2 Turbidite Reservoirs……...8

2.2.1 Characteristics of Channel Sinuosity in Deep-Water Turbidites……9

2.2.2 Facies……11

2.2.3 Repeated Cutting and Filling……12

2.2.4 Stacking Patterns……...13

2.3 Outcrop Models for Deep Sea Turbidites……14

2.3.1 Geological Setting of Delaware Basin……..15

2.3.2 Channel Densities of the Columbus Basin ……...17

2.3.3 Quantification of Channel Densities…….18

2.4 Pressure Transient Testing……...19

2.4.1 Use of Well Test for Evaluation of Flow Connectivity……22

2.4.2 Well test Sequence……24

2.4.3 Influence of Geological Features on Well Test Behavior…….25

2.4.4 Well Test Models……..25

2.4.4.1 Semi Infinite Channel with Non Parallel Sides…….30

2.4.4.2 T-Shaped Channels……32

2.4.4.3 Meandering Channels……34

2.4.4.4 Pinch Out Boundary……...36

2.4.4.5 How to Interpret Well Test in these Complex Channelized Reservoirs…….37

2.5 Summary……..40

Chapter 3: Well Test Signature in Different Geological Environments……41

3.1 Overview……..41

3.2 Base Case Well Test Simulation……..41

3.3 Well Test Heterogeneous Systems……...44

3.3.1 Simple Heterogeneous Model……...44

3.3.1.1 Results of Well test for reservoir with Two Different Permeability Values……...45

3.4 Building a Model for a Channel Reservoir……..50

3.4.1 Permeability Averaging for Assessing Channel Boundary Effects..53

3.4.2 Varying Well Location to Asses Effect of Channel……..58

3.5 Conclusion……...61

Chapter 4: Relating Well Test Signature to Spatial Variation in Rock Parameters…..…62

4.1 A Multi-Point Power Average Formulation for Well Test Analysis……...62

4.2 Single Point Power Average……63

4.2.1 Results for Single Point Power Law Model……..……64

4.3 Two Point Permeability Power Average……..68

4.3.1 Results for Two Point Statistical Power Law Model……70

4.4 Three Point Permeability Average……...74

4.4.1 Results for Three Point Statistical Model…….75

4.5 Computing for Different Permeability Channel Maps……82

4.6 Conclusion……...84

Chapter 5: Application to Deep Sea Field in Gulf of Mexico……...86

5.1 Overview……..…86

5.2 Ewing Bank Background…….86

5.3 Well Test Data…….……88

5.4 Well Test Interpretation using the Multiple Point Proxy…….92

5.4.1 Analysis of Well Test……93

5.4.2 Application of the Multiple Point Proxy……...96

5.4.3 Results of Multiple Point Proxy……...……...100

5.5 Conclusion…….101

Chapter 6: Conclusions and Recommendations for Future Work……...103

6.1 Conclusions……103

6.2 Recommendations for Future Work……...105

Appendix A: Python Program for calculating Single Point Statistical Model…….107

A.1 Overview……...107

A.2 Implementation of Single Point Power Law Average……..107

A.3 Implementation of Two Point Statistical Model……...111

A.4 Implementation of Three Point Model……..115

Bibliography……117

List of Tables

Table 2-1 Simplified geometries for sandstone bodies……..26

Table 4-1 Correlation coefficients for two point statistical averages……72

Table 4-2 Correlation coefficients for three point power aw averages……..78

Table 4-3 Results for single point model for lag h=1…….…...79

Table 4-4 Results for two point model for lag h=1…….…...80

Table 4-5 Results for three point model for lag h=1……...…...80

Table 4-6 Results for single, two point and three point models done on varying channel/shale realizations……..83

Table 5-1 Results of multiple point models performance on Well A-04 in Ewing block 873...…….101

List of Figures

Fig 2-1 Sea floor image map showing the sinuosity of channel flows (adapted from Mayall) ……9

Fig 2-2 Simple model of 4 facies in a channel fill (adapted from Mayall And Stewart (2000)) ……...12

Fig 2-3 Summary model showing the potential reservoir distribution and heterogeneity patterns in an erosional channel (adapted from Clark and Pickering (1996))……...…14

Fig 2-4 Location map showing the East Ford and Fort Geraldine units and the outcrop study area with the Delaware Basin (adapted from Dutton et al (1999)) ……15

Fig 2-5 Location of the Columbus basin off the south east coast of Trinidad and the study area where channel densities were accumulated (adapted from Maher) ……..17

Fig 2-6 Parameters measurable on channels from seismic data (adapted from wood and Mize 2010). ……...19

Fig 2-7 log-log plot for drawdown test in a well within an asymmetric channel (adapted from Zambrano 2000))……...27

Fig 2-8 log log plot for drawdown test in a well within a symmetric channel (adapted from Zambrano (2000))……...……..28

Fig 2-9 log-log plot for drawdown test in a well within a sinuous channel (adapted from Zambrano (2000)) ...……...……...29

Fig 2-10 bounded channel with non parallel lateral boundaries (adapted from Zambrano (2000)) ……...31

Fig 2-11 Affect of the wedge on the derivative response (adapted from Zambrano(2000)) …….……...31

Fig 2-12 T-shaped channel in a deltaic depositional environment (adapted from Mijinyawa (2008)) ……...32

Fig 2-13 T-shaped channel combination of a perpendicular channel (adapted from Mijinyawa (2008)) ……32

Fig 2-14 Impact of length on the derivative late-late behavior of a T-shaped channel (adapted from Mijinyawa (2008)) ……33

Fig 2-15 T-channel derivative matched with two perpendicular channels (adapted from Mijinyawa (2008)) ……...……33

Fig 2-16- Meandering Channels in a deltaic depositional environment (adapted from Mijinyawa (2008)) ……...……34

Fig 2-17 Pressure derivative responses for various well locations within a meander (adapted from Mijinyawa (2008)) ……35

Fig 2-18 pressure derivative responses for different angle meander (adapted from Mijinyawa (2008))
……..…….....35

Fig 2-19 Schematic for a well close to a pinchout and the corresponding pressure derivative response (adapted from Mijinyawa (2008))……..36

Fig 2-20 Pressure derivative response for a well near a reservoir pinch-out for various pinch-out angles (adapted from Mijinyawa (2008)) …….37

Fig 2-21 Derivative plots with 3 different interpretations for Gerry Field, West Africa (adapted from Massonant (1993)) …….39

Fig 3-1A PVT input values for CMG reservoir model……..42

Fig 3-1B Rock Fluid data correlations and relative permeability curves for reservoir model…….….43

Fig 3-2 Derivative plot for a well test in a homogenous reservoir……43

Fig 3-3 Permeability Distribution for a simple reservoir model with two permeability regions……45

Fig 3-4 Behavior of log-log derivative plots with channel proximity……...47

Fig 3-5 behavior of log-log derivative plots with varying permeability gradients across channel boundaries…….49

Fig 3-6 Channel and shale permeability maps used in creation of training images……..51

Fig 3-7 Examples of different channel trends for different realizations……53

Fig 3-8 Comparison of permeability from well test and CMG values……...55

Fig 3-9 Example of templates used in determining channel boundary effects……..56

Fig 3-10 Comparisons of $K_{effective}$ and K_{ctual} for a well completed close to a channel/shale boundary……57

Fig 3-11 Effects of channel proximity in determining $K_{effective}$…….59

Fig 3-12 Comparison of derivative plots for short and long-term shut-ins. ……..60

Fig 4-1Single point power law average in determining permeability in the middle of a shale or channel……..65

Fig 4-2 single point power law model in determining permeability for wells completed in a shale in proximity to a channel/shale boundary……..66

Fig 4-3 single point power law model in determining permeability for wells completed in a channel in proximity to a channel/shale boundary……..67

Fig 4-4 Convention for determining two point statistical pairs…….68

Fig 4-5Two point statistical power law averages for wells located in proximity to a boundary completed in a shale zone……..72

Fig 4-6 Two point statistical power law averages for wells located in proximity to a boundary completed in a channel sand……..73

Fig 4-7 Lag configurations in determining three point templates……..75

Fig 4-8 Three point geometrical averages for wells completed in proximity to channel boundaries completed in the shale zone…….77

Fig 4-9 Three point model for a well completed in proximity to channel boundaries completed in the channel sand……...81

Fig 4-10 Comparison of single, two point and three point models for a well completed in the channel in proximity to a boundary…….82

Fig 5-1 Surface location of 18 wells located in the Ewing Block 873 (adapted from Burk, brown and Petro) ……...87

Fig 5-2 Graphic representing the six sand lobes of Ewing Block 873……...87

Fig 5-3 Reservoir Pressure decline for wells in Ewing Block 783 representing different sand lobes……...88

Fig 5-4 Graphic representing the wells with well test data from Ewing Block 873……..89

Fig 5-5 Analysis of Derivative plot for well A- 6……..90

Fig 5-6 Analysis of Derivative plot for well A-10…….92

Fig 5-7 Analysis of derivative plot done on well A-04…….93

Fig 5-8 Analysis of derivative plot done on well A-05…….93

Fig 5-9 Analysis of log-log plot from well A-04……..95

Fig 5-10 Typical log-log profile for well completed within asymmetric channel……96

Fig 5-11 3-D view of reservoir model built to scale Ewing Block 873……97

Fig 5-12 permeability layout of ten layers of Ewing block 873……99

Chapter 1: Introduction

1.1 Overview

For ultra deep water reservoirs, it is not economically feasible to drill numerous appraisal wells to obtain reservoir information. For this reason, companies want to maximize the amount of data or information they obtain from any test or well they drill in such settings. A problem with obtaining large amounts of data from these wells is that, for conducting a well test of adequate duration, the well production is stopped for a significant amount of time to obtain data used to estimate the permeability, reservoir pressure, reservoir size and damage close to the wellbore. The longer duration the well test more thorough the investigation into the reservoir character, however it also means the longer time is spent without producing hydrocarbons. Since rig rates for offshore wells are very expensive, companies often don't want to perform long tests to assess the flow connectivity of the reservoir. As a result it would be best to combine the information obtained from any length well test performed with some geostatistical models to try and characterize the reservoir. Such analysis would enable one to assess and predict the position of wells with respect to depositional facies boundaries, such as deep water channel to overbank, or channel to lobe. This thesis presents a new approach to calibrate a multiple point permeability proxy to a well test and interpret the parameters of that proxy in the context of characteristics of the permeability field. In addition, this enables prediction of the proximity of the well to the facies boundary.

1.2 Traditional Well Test Analysis

Well operators want information regarding the initial well productivity (permeability, skin and pressure evolution), dynamic reservoir characteristics (reservoir limit, lateral extension, fracture extension) and the nature of fluids in place (hydrocarbons, water). The well test is the only way to gather information regarding the dynamic characteristics of the reservoir (Chassagne, 1999). It provides the effective permeability over a much larger scale than core samples and identifies flow boundaries/conduits in proximity to the well. The analysis of the well test data guides the next actions to be carried out on the well. For example low productivity could either be due to good reservoir permeability but degraded interface between well and sand face (+skin). A second example, as this thesis discuses would be drilling into low permeability shale at the fringes of the higher permeability channel. From such a well test you can estimate how far away from the channel boundary the well was completed and the influence of a low permeability zone on the producing characteristics of the well.

Different log-log plot signatures can be identified depending on the location of a well with respect to geological heterogeneities in a reservoir. Past research identifies the behavior of log-log plots in the presence of boundaries, channel wedges, shapes of channel systems and proximity to flow conduits as can be seen in section 2.4. While these are discussed in the literature review section, the main focus in Chapter 3 is on the

development of a technique to identify the proximity of a well to flow conduits and flow in sinuous channels and the effect on well test derivative plots.

It is important to recognize the different responses in the derivative plots to varying heterogeneities in the geology. The more spherical the derivative plot the closer the proximity of a flow conduit to the test well. Alternatively, a positive slope indicates the presence of a low permeability zone or a no-flow boundary close to the wellbore. A flatter derivative plot response with no changes in slope indicates the presence of a large reservoir with no boundaries in the investigated area. However all of these signatures are dependent on the length of the build-up period so it is important to note that during a short test these kinds of boundaries may be missed. As a means of minimizing down time during a well test, technology assessments have been carried out on existing fields to try to improve the reservoir characterization.

1.3 Technology Assessment in Deep Water Exploration

Using the offshore Brazil, the Gulf of Mexico, and offshore Africa as prime examples it has been found that the major problems in producing deep water reservoirs are

1) Daily rig rates and downtime rates: At rig rates approaching 1,000,000$/day any downtime places a huge expense on any company. (Chassagne, 1999)

2) High reservoir temperature if reservoirs are buried very deep below the sea floor- this limits the options of mud-pulse telemetry and measurements. (Wood, 2000)

3) Risk of paraffin deposition- low water temperature causes paraffin deposition in subsea flow lines (Lucchesi, 1998)

4) Unconsolidated sandstone- deep-water reservoirs are generally poorly cemented and thus have poor poroperm relations and increasing risk of sand production in wells. (Lucchesi, 1998)

5) Difficulty of drilling non-conventional wells- unconsolidated sands and overburden shales make it risky to produce from angled/horizontal wells that are very enticing given the cost of drilling ultra deep wells. (Lucchesi, 1998)

6) Narrow pore pressure/fracture gradients- requires multiple casing runs to prevent wellbore instability, kicks, lost circulation and shallow water flows during the drilling process. (Lassoued, 2002)

7) Presence of salt diapirs that make it very difficult to spot reservoir quality layers in seismic sections.

1.3.1 Solutions to problems discovered

To help with rig times, logging while drilling (LWD) has presented great opportunities. Through different types of LWDs such as nuclear, acoustic and electromagnetic tools a good match can be applied to any system. The opportunity to get instant bore-hole images delivered to the rig personnel via the mud pulse telemetry allow quick decisions to be made to help save on rig up and rig down times. A full formation

evaluation program can thus be created by measuring the azimuthal density, neutron, resistivity and sonic tools (Lassoued, 2002).

It has been revealed that using LWD has increased drilling efficiency almost two-fold when implemented correctly. The density-neutron measurements are used to enhance the quality of measurements and to yield a medium-resolution image of the bore hole with density and P_{ef} data. The sonic measurement have to be calibrated with the distance between the transmitter and receiver to be approximately 10.2 ft in order to allow for a greater time separation between compressional, shear and also to improve the ability to measure formation travel time beyond the damaged formation (Chassagne,1999).

In order to obtain a better image of the reservoir it has been proposed to use a new seismic imaging technique known as 3-D high-resolution (HR3D). In offshore Ivory Coast., a noticeable difference between the resolution of the HR3D and HR2D model was observed. The HR3D was also compared with 3D exploration seismic data that was run on this area and results were a 2:1 to 3:1 improvement in vertical resolution (Wood 200).

One big factor in evaluating a deep-water prospect is trying to determine future well production. Due to the scarcity of early exploration data and the geological complexity of turbidite formations in deep-sea reservoirs the prediction of reservoir performance and therefore development planning becomes fairly difficult. Some major subsurface challenges include compaction, compartmentalization and completion failures. Well design is also important and certain factors should be taken into consideration. Considerations such as the expected economic life of the field, how many

reservoirs will be produced from each well are crucial. To cover the economic cost of producing from a deep water prospect drilling and completing a well that could survive in the subsea environment for at least two decades should be one of the first executable challenges (Kindi, 2006).

1.4 Research Objective

The objective of my research is to effectively characterize the geological heterogeneities in deep water channelized deposits, essentially channelized turbidite reservoirs by combining the results of the derivative plots obtained via a well test with a geostatistical model that will allow us to estimate reservoir characteristics around that well location. It is important to point out that a reservoir model is needed in order to estimate the effective permeability of a region as the statistical model relies on surrounding data blocks to make its calculation. This points to the importance of developing representative analog model for a reservoir such the relationship between the reservoir flow characteristics and the well flow response can be calibrated. The primary research objective is to ultimately find a way to minimize the amount of time spent doing a well test. The feasibility of obtaining valuable information about the reservoir characteristics in the vicinity of the well while at the same time running the well test for a limited duration will be assessed.

1.5 Thesis Outline

In Chapter 2, a literature review discussing the geological heterogeneities that can be expected from a channel turbidite reservoir are discussed as well as the effect these

heterogeneities have on the derivative plots in a pressure transient test. The information summarized in Chapter 2 was used to create a reservoir model that was then tested in the later chapters. Chapter 3 gives a description of the procedure carried out for performing well tests on this reservoir model and identifying the effects of heterogeneities on the derivative plots depending on the location of the well in the reservoir.

Chapter 4 introduces the implementation of a multiple point geostatistical model to determine the effective porosity for a well in a given location. It explains the difference and challenges between using a single point, double point or triple point statistical model. Chapter 5 looks at a real data set in Gulf of Mexico and applies the multiple point proxy expression to characterize the location of the wells with respect to channel and fault boundaries.

Chapter 6 discusses the conclusions drawn from this research work and suggestions for any future work on this subject.

Chapter 2: Literature Review

2.1 Overview

This chapter presents relevant literature related to the modeling of channel turbidite reservoirs and the use of well tests to characterize heterogeneity near the wellbore. We begin with a discussion of the common depositional environments of deep-water turbidites and the facies distribution in such reservoirs. Next, outcrop studies that are used for characterization of ultra deep plays are reviewed and the techniques for quantifying channel morphologies are discussed. This information is later used to construct reservoir models for ultra deep plays presented in this thesis. At the end, a review of the effect of heterogeneities on well test results reported in literature is presented.

2.2 Turbidite Reservoirs

Deep-water turbidites will be a prime target for oil and gas exploration and production activities for at least the next 25 years according to Stow and Mayall (1999). The targets will be along any deep water margin with source-rock recharge potential. Turbidites deposited in channels are important but often-complex reservoirs in the exploration, appraisal and development of deep water facies. Over the past 10 years, interest in channelized turbidite reservoirs and more so in deep-water reservoirs has motivated several studies. According to Navarre *et al.*(2002) much of the knowledge

about channel systems in turbidite reservoirs was made possible by the increasing availability of high quality 3D seismic data, particularly from West Africa. Mayall *et al* (2006) indicated that each channel is unique and that there is no one model or series of models that can be superimposed to classify a reservoir. Mayall *et al* believes that the problem of interpreting turbidite channels can be broken into four aspects:

1) The nature of the sinuosity
2) The facies distribution
3) The recognition of repeated cutting and filling episodes
4) The stacking patterns of channels

2.2.1 Characteristics of channel sinuosity in deep-water turbidites

A typical channel turbidite channel can be observed on sea-floor image maps as shown in Fig 2-1. Sinuosity varies from occasional bends in the channel to highly sinuous channels with numerous cut-off bends. There are at least four causes of sinuosity in turbidite channels according to Mayall *et al.* (2006): initial erosive base, lateral stacking, lateral accretion and sea floor topography.

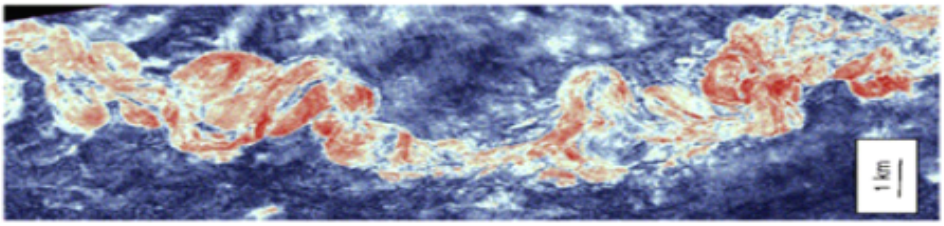

Fig 2-1 Sea floor image map showing the sinuosity of channels due to erosional base and sea floor topography (Mayall, 2006)

Initial erosive base is where an erosional effect caused by turbidite flows carve out a path for future sediment flow as the flow moves. The initial erosion of the sub-flow strata causes turbidites to preferentially flow through the erosional features and that results in further erosion of the slope until a channel is formed. The sinuosity of the channel generated in this fashion generally tends to have an accumulation of sand upstream of the channel as a result of flow stripping.

Lateral stacking occurs when a bend is formed due to lateral shifts in the sediment flow. This can occur due to channel filling, shifting slightly laterally and re-incising. However it is difficult to determine what caused the lateral stacking - whether it is due to depositional processes or if it is a function of changes in sea floor topography.

Lateral accretion occurs when sinuosity is created due to the lateral migration of an open channel. This case is most like the sinuosity and lateral accretion of channels for meandering fluvial systems, with erosion on the outside bank and deposition in the inside bank creating a point bar as pointed out by Kolla *et al.* (2001). However, in deep sea turbidites sinuosity of this type is rare and also creates relatively thin (<10m) channels. The final channel is predominantly mud filled as evidenced by low amplitude seismic and convex down compaction indicated by Abreu *et al* (2003).

A big factor in channel sinuosity is sea floor topography. Sea-floor topography affects sinuosity due to the obstacles that the turbidite encounters while flowing down slope. These obstacles control the down slope route and can cause major diversions of

the channel orientation. On a smaller scale, faults can also cause significant bends in the channels according to Mayall and Stewart (2000). It was found by Cronin (1995) that flow stripping at sharp channel bends may result in sands being deposited upstream of the bends

It should be realized that a combination of the four cases described above is often present causing complexity of turbidite channels.

2.2.2 Facies

The sedimentary features observed in turbidite channels can range from boulders and conglomerates to mud fills and can be a result of gravity-driven depositions, high and low density turbidites, mud flows, debris flows, sediment slides and slumps. However Mayall and Stewart (2000) found it practical to group all these variations into four main facies as seen in Fig 2-2.

- Basal lags of coarse sand/conglomerates, mudclast conglomerates or shale drapes
- Slump and debris flows which can be caused from collapse of channel walls or long distance transport due to evidence of extra-formational clasts which are coarser than the facies seen in the channel
- High net:gross stacked channels which form the best quality reservoirs since they are dominated by massive sands with thin mudclasts marking the base of each channel.
- Low net:gross channel-levee caps the channel fill and may spill beyond the original erosional confinement. Channel fills are predominantly muddy and levees

dominated by patchy sands at the base and thinly interbedded sands and muds in the bulk of the levee.

Mayall and Stewart (2000) recognized these facies in seismic data sets, and they also turn out to be important factors when predicting reservoir distribution and heterogeneity factors and they often occur in vertical sequences.

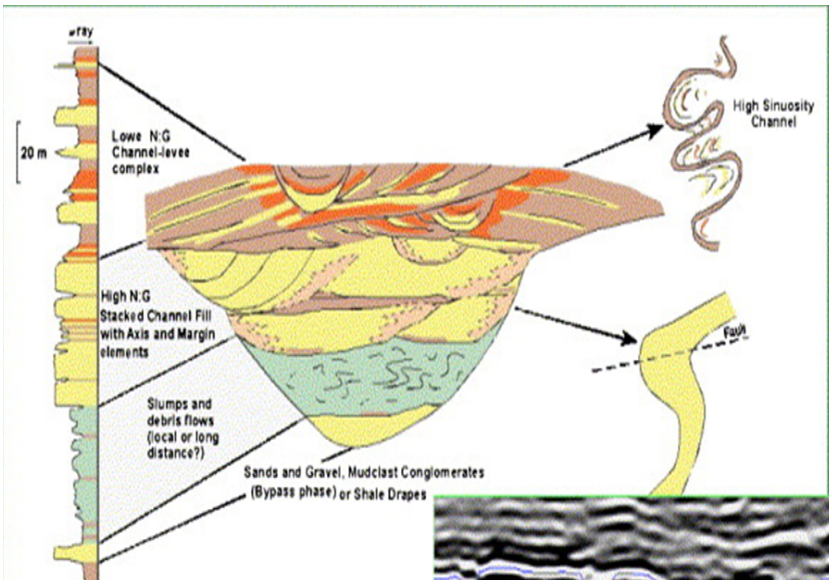

Fig 2-2 Simple model of four facies in a channel fill (Mayall and Stewart, 2000)

2.2.3 Repeated Cutting and Filling

This process results in very complex stratigraphy since earlier episodes of channel fill are preserved as nothing but erosional remnants. Three important implications for reservoir distribution are;

- When erosion is prevalent earlier channel-fill deposits are only preserved as erosional remnants scattered throughout the channel. This case is very difficult to identify on even very good quality seismic.
- The facies at the base of each 4/5th order infill sequence is critical to connectivity. If the facies is composed of mudclasts barriers and baffles within the reservoir may be created
- If a channel fill is made up of muddy slumps then the channel can act to compartmentalize the reservoirs within the erosional remnants of earlier channel fills.

2.2.4 Stacking Patterns

A wide variety of stacking patterns are witnessed in reservoirs. Patterns may be vertical, lateral either systematic in one direction or alternating on either side of a pre-existing channel or a combination of all of these. Clark and Pickering (1996) found that changes in stacking patterns are very common along the length of a channel and are actually expected. It is essential to identify the stacking pattern prior to developing a field since there is a risk that the facies at the base of a channel may act as a permeability barrier.

A summary model showing the potential reservoir distribution and heterogeneity patterns in a large 3rd order erosional channel can be seen in Fig. 2-3. Each channel is unique but can be interpreted considering the sinuosity, the four main facies (basal

lags, slumps, high net:gross and levees), repeated cutting and filling and stacking patterns.

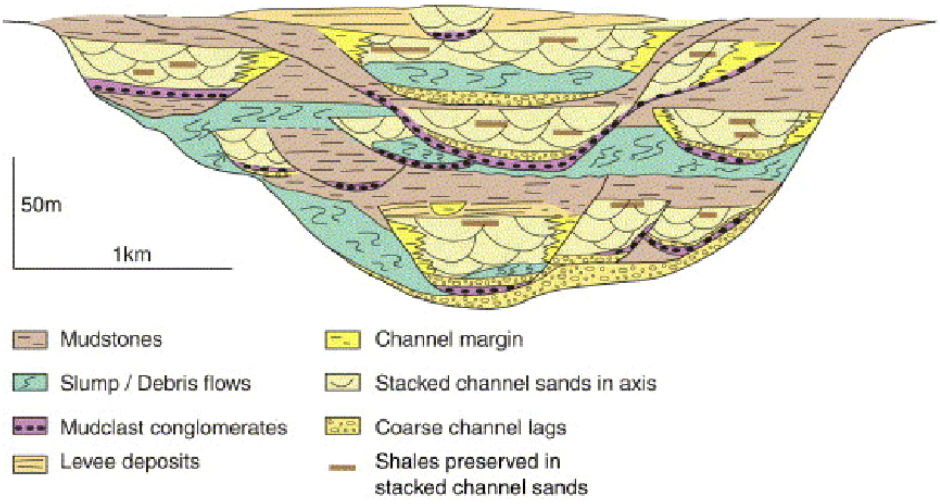

Fig 2-3 Summary model showing the potential reservoir distribution and heterogeneity patterns in an erosional channel. (Clark and Pickering, 1996)

2.3 Outcrop models for Deep Sea Turbidites

Since the spatial distribution of channel facies under subsurface conditions is difficult to predict, we can use outcrops of similar deep water channelized turbidites deposits to lend insight into the detailed architecture and nature of these deposits. Studies in such outcrops have been done around the world. A popular area of detailed outcrop studies is the Delaware basin (Fig 2-4) located in West Texas and southeastern New Mexico. The Delaware mountain group strata consist of a 3500 ft thick succession of slope and basin deposits that are important contributors to Permian Basin petroleum production.

A significant drawback to such outcrop studies is their limited spatial extent. They lack the three-dimensionality and spatial density to see entire geometries. Alternatively, 3D seismic studies provide spatial extent but often lack the temporal detail of outcrops of core. A nice compromise is study of the relatively near seafloor surface using 3D seismic. One such study is that of Maher (2007) in a study of the shelf-edge-structural influence on sources of deep-water sands in the Columbus basin of offshore Trinidad. This study was focused on the relationship between delta clinoform architecture (i.e., prograding, aggrading or oversteepened) and slope channel density and nature, as well as fault magnitudes in the upper slope and slope morphology. These two studies will be used to condition initial models in this thesis and are both discussed in more detail below.

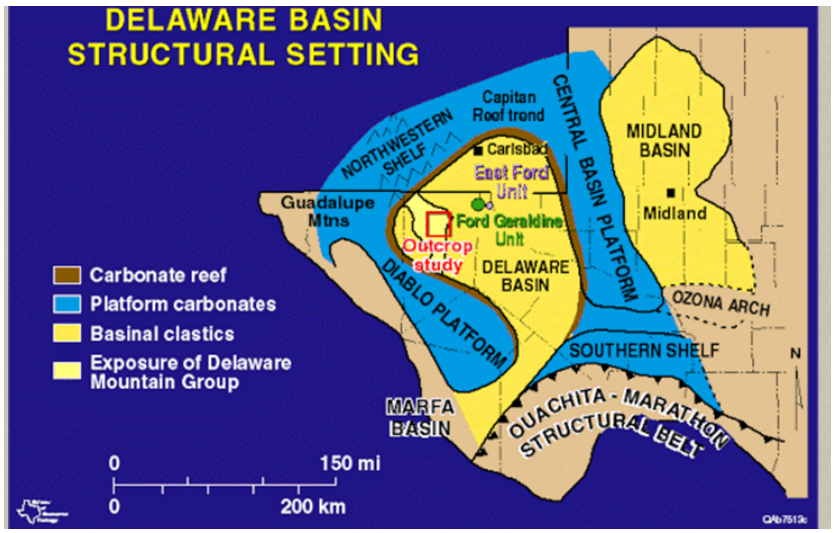

Fig 2-4 Location map showing the East Ford and Fort Geraldine units and the outcrop study area with the Delaware basin (Dutton *et al* (1999))

2.3.1 Geological Setting of Delaware Basin

The Delaware basin is partly open to the seaway on its south boundary while surrounded by an extensive carbonate shelf and reef complex to the north. Correlations indicate that water depths were between 1,000 and 2,000 ft at the time of deposition of the Bell Canyon formation. The Delaware basin is divided into cyclic successions of sandstone and siltstone at several scales. Thick limestones or organic rich siltstones divide the Delaware mountain group into three clastic wedges: Brushy canyon, Cherry Canyon and Bell Canyon formation which are each 1,000 to 1,500 ft thick.

According to Dutton *et al.* (1999) the facies relationships indicate that the sandstones were deposited by turbidites in a basin-floor system of channels and levee sharing attached lobes that initially prograded basinward, aggraded and then turned around and steeped back toward the shelf. The lobe deposits are made up of convoluted sandstones with dewatering structures indicating that they were deposited rapidly from high-density turbidity currents. What we are interested in, the channels of this area are approximately 1200 ft wide and 15 - 35 ft thick and overlie and cut into the lobe deposits. The channels consist of crossbedded sandstones deposited from high-density turbidity currents. The channel margins are characterized by rippled and convoluted sandstones interbedded with siltstones forming levees thought to be caused by overbanking of low-density turbidity currents. Dutton *et al.* also characterized the petrophysical properties of the area and found that for permeability of 1 md, porosity was greater than 15%, water saturation was less than 60% and the clay proportion was less than 15%.

The values for channel length, width, thickness, porosity and water saturations were used from this outcrop and combined with the channel frequency calculations of Maher (2007) in formation of the training images for channel flow used in this thesis.

2.3.2 Channel Densities of the Columbus Basin

The Columbus basin off the southeastern coast of Trinidad (Fig 2-5) is believed to have total hydrocarbon reserves of 486 MMbbl of oil and 23.4 TCF of gas, the majority of which is trapped in shelf edge reservoir deposits (Bowman, 2003). The basin consists of cyclic stacked sandstone packages ranging from tens to hundred of meters thick with net to gross ratios between 0.75 and 0.95 and porosities between 25-30%, and permeabilities of 1000 md. Controls on the density (frequency) of slope channels of the Columbus Basin were investigated in Maher (2007).

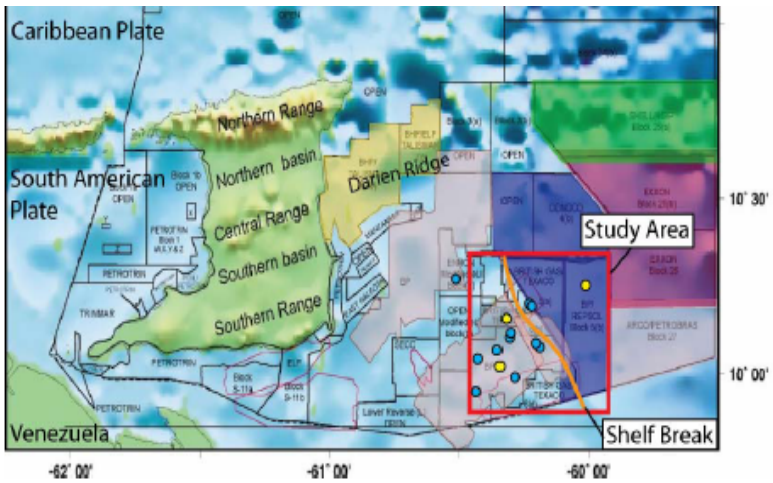

Fig 2-5 Location of the Columbus basin off the south east coast of Trinidad and the study area where channel densities were accumulated (after Maher, 2007).

Three types of shelf edge delta trajectories were identified in Maher (2007); aggradational, progradational and over-steepened. Over-steepened shelf edge trajectories give the highest density of bypassed slope channels and lowest level of aggradation. Most of the channels are straight except on lower angle slopes down dip of the progradational province where channels show sinuosity. Channel densities from aggradational and over-steepened provinces decrease basin-ward from the shelf break and fault. Progradational slope channel densities remain constant or increase basin-ward.

2.3.3 Quantification of Channel densities

Important information gathered from Maher's Thesis (2007) includes measures of channel densities and sinuosity in the Columbus basin. To quantify channel densities, first the shelf edge and slope was divided into province types based on the nature of the shelf margin (progradational, aggradational and over-steepened). Five transects were then made parallel to the shelf break and each time the transect would intersect a channel on the seismic map it was noted and the channel density then calculated using Equation 2.1

$$\rho_c = Ct/Lt \qquad (2\text{-}1)$$

Where

ρ_c = channel density

Ct = number of channels along a transect
Lt = length of transect

Sinuosity was then measured from the root mean squared (RMS) seismic amplitude extractions and the values were compared to the trajectory provinces and the regional fault throw from where the channels initiated. At least one single complete meander loop was needed to calculate sinuosity. Equation 2-2 was used to calculate sinuosity based on the terminology in Fig 2-6.

$$Si = La / Lm \quad (2\text{-}2)$$

Where
Si = sinuosity
La = Radius of Curvature
Lm = meander length

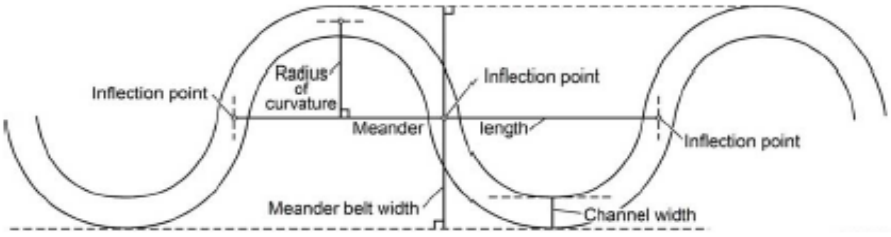

Fig 2-6 Diagram illustrating the parameters measurable on channels from seismic data (after Wood and Mize, 2010).

2.4 Pressure Transient Testing

Permeability is a measure of the porous medium's ability to transmit fluids. Permeability can be determined in the field either by core analysis, which gives readings

on a small scale or using pressure transient tests, which measure permeability of the reservoir rock on a large scale. A transient test consists of recording the changes in bottomhole pressure at well while varying the flow rate. The evolution of the pressure profile in response to the rate changes is dependent on the fluid and rock properties and this dependence is exploited to infer reservoir property variations in a reservoir knowing the fluid properties and some details about the well.

For this thesis we look at build up tests which correspond to a well that flows at a particular rate and is then shut in for a period of time. The dimensionless pressure variation during a build up test is given in equation 2-3

$$P_{DBU} = \frac{1}{2}\ln\left[\frac{t_p + \Delta t}{\Delta t}\right] \tag{2-3}$$

The preceding equation in terms of dimensionless pressure and time allow the solution to be written independent of the actual dimensions of the well and the reservoir and specific reservoir and fluid properties. In the actual units of the data, the pressure variation during a build up test for an infinite acting reservoir is give as:

$$P_{ws}\left(\Delta t\right) = P_i - \frac{162.6 q \mu B}{kh}\log\left(\frac{t_p + \Delta t}{\Delta t}\right) \tag{2-4}$$

Where

t_p = producing time, hours

Δt =time spent shut-in, hours

q = flow rate, STB/day

μ =viscosity, cp

k =permeability, md

B = formation volume factor RB/STB

h = thickness, ft

Pi = initial reservoir pressure, psi

Equation 2-4 is known as the Horner pressure build up equation. If the well flow rate can be reduced to zero instantaneously (shut in), then a graph of bottom hole pressure v.s. Horner time, $\left(\frac{t_p + \Delta t}{\Delta t}\right)$, will be linear with a slope equal to - $\frac{162.6 q \mu B}{kh}$. From this plot, we can estimate the initial reservoir pressure by extrapolating the Horner line to an infinite shut in time (actually not that easy due to all the fluid production prior to well shut in) and the permeability from the slope of the Horner line knowing all the other fluid properties.

Other plots used in this research are the log-log and semi-log plots. These plots are used to account for identifying the important flow regimes during a well test such as the wellbore storage dominated flow period, the transition period, the onset of the infinite acting flow period etc. It is important to construct these plots first to identify the interval of data that should be fitted to the semi-log line. The pressure wave initiated due to the well shut in first traverses through the near well bore region whose property might have been altered due to the drilling fluids or due to well stimulation. This alteration called skin, can be calculated using the following formula:

$$S = 1.1513\left[\frac{P_{wf}\left(t_p\right) - P_{ws}\left(1hr\right)}{-\left(\frac{162.6q\mu B}{kh}\right)} - \log\left(\frac{k}{\phi\mu c_t r_w^2}\right) + 3.23\right] \tag{2.5}$$

Where P_{ws}(1 hr) is read on the horner plot.

Another important aspect of the log-log plot is the shape of it as the shape is highly indicative of the depositional environment it is in. This aspect is incorporated in this thesis to identify channel boundaries and locations and will be discussed later in more detail in section 2.4.3.

A recent development in well test analysis is the use of deconvolution to analyze the pressure data. According to Gringarten (2008) deconvolution is the process that converts pressure data at variable rates into a single drawdown at constant rate. This is important in practice since flow rates are never constant during the operation of a well. Deconvolution allows us to use more data in an interpretation than originally where only constant rates were able to be analyzed. As a result of this it is now possible to see boundaries in deconvolved data compared to conventional analysis in which boundaries could be missed due to the averaging of rates. The bulk of the analysis used in this thesis was completed using the commercial software Saphir by Kappa Engineering group (2011) which incorporates the analytical equations shown above.

2.4.1 Use of well test for evaluation of flow connectivity

A major thrust in oil and gas exploration is in deeper offshore environments where the reservoirs are expensive to explore and develop. We need to be able to evaluate

a reservoir and determine the producible reserves using very limited data. A reservoir may look good at first production but the pressure may decline quickly and the returns will not offset the costs of drilling in an ultra-deep environment. One of the ways of testing and establishing the size of reservoirs and its flow characteristics is by performing a well test. Evaluation of reservoir connectivity over large distances from the well requires relatively long and expensive well tests. The decision to do this test thus becomes a balance of how much information do I need from this reservoir to understand it. Long tests will give you plenty information however might not be economic. These costs however may be worth it since we can ascertain if the well is placed in a big, well connected reservoir or whether it intersects a small/compartmentalized formation. Combining the data obtained from short tests due to necessary shut-ins combined with the geo statistical knowledge gained in this thesis may make well testing more economic and just as knowledgeable.

A well test may last from several days to several weeks but the longer the length of the test the larger the investigated reservoir volume and thus the more information we will obtain about the reservoir. Although we can determine some rock properties from alternative means such as well logging which however only help with the short term productivity of the well, well testing remains the only method for direct evaluation of reservoir connectivity over large distances within the reservoir as pointed out by Levitan (2006).

Levitan continues to say that if a well is in a limited size reservoir compartment the well bottom hole pressure will develop a decreasing linear trend a lot quicker than expected. A quick decreasing trend can also indicate that the connected reservoir volume is smaller than the volume the test was designed to prove, if on the other hand the reservoir pressure declines less than was expected then the reservoir volume is larger than what it was designed for.

2.4.2 Well Test Sequence

Levitan points out that once we have an idea of how big a reservoir should be based on seismic imaging and using other reservoirs in the area as analogs we should have an idea how much fluid we will need to take out of the reservoir to cause a measureable pressure decline. We then evaluate the reservoir pressure by performing a pressure build up test. In order to determine the reservoir pressure change caused by the production targeted for the test we need to perform two build up tests ; one after the initial flow and one immediately after the main production.

Well Test Sequence:-

1) initial flow – remove completion fluid from wellbore (volume of fluid produced should be small so reservoir pressure won't be affected)
2) initial build up test
3) main flow- estimated from size of reservoir we think we have.

4) final build up test- provides main pressure transient data used for well test analysis and how well reservoir pressure is supported. This should be longest of the two build ups

From the well test we will be able to relate the reservoir pressure change to connected reservoir volume provided the test is sufficient duration as well as determine the effective permeability of the well from the derivative plots.

2.4.3 Influence of Geological Features on Well Test Behavior

Since a well test is generally used to determine average reservoir properties it should be expected that because each well may encounters different depositional architectures, each well test will behave differently and likewise data coming from the well will look differently. For example in the calculation of the dynamic reservoir characteristics such as reservoir limits, the difference between a well-connected reservoir where the reservoir boundaries are far away depicting a large reservoir body will be very different to a compartmentalized reservoir which will depict the influence of the close boundaries as pointed out by Zambrano (2000)

By combining the results from numerous well tests done in numerous fields, a very good estimate of the depositional environment encountered can be made by looking at the appropriate well test diagnostic plot(s) as discussed in the following section.

2.4.4 Well Test models

Zambrano combined different models and compared the effect on a well test. The different models discussed in this section can be seen in Table 2-1 below

PLAN VIEW	XY-profile	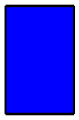	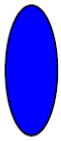	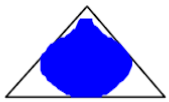	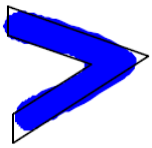
		Straight	Elongated	Fan/Lobate	Sinuous
THICKNESS -PROFILES	YZ-profile (Longitudinal)		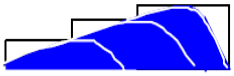	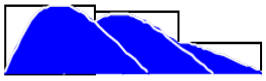	
		Constant	Increasing Composite	Decreasing Composite	
	XZ-profile (Transverse)		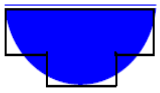	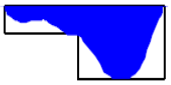	
		Constant	Symmetrical Composite	Asymmetrical Composite	

Table 2-1 Simplified geometries for sandstone bodies

For a well within a straight channel with an asymmetric thickness profile the log-log plot will exhibit two stabilizations: one after the initial well bore storage and one after the effects of the channel are felt which can be seen after 10^6 dimensionless time in fig 2-7 below.

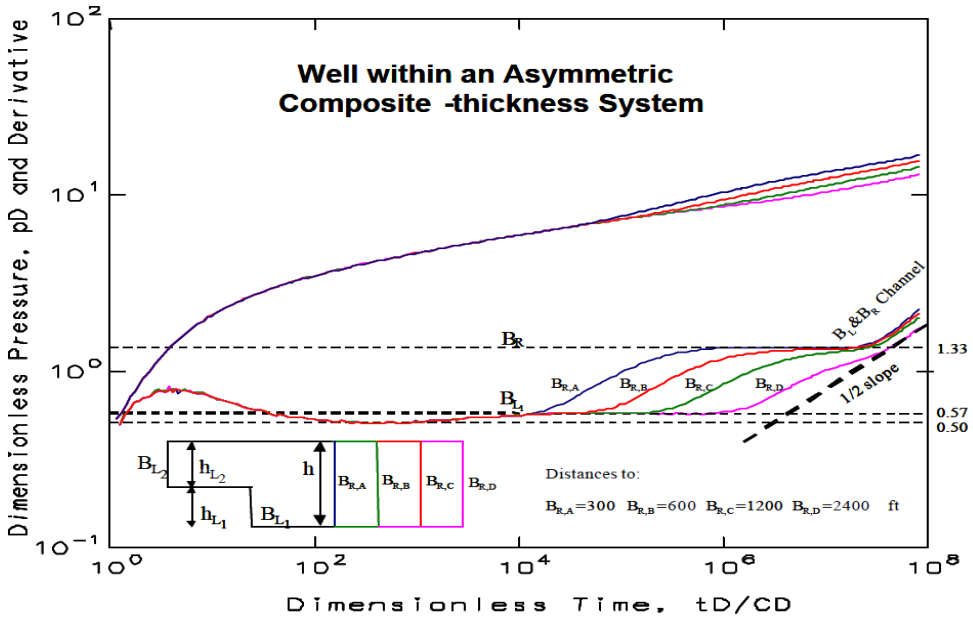

Fig 2-7 log-log plot of drawdown test in a well within a channel with asymmetric composite thickness profile. The change in slope indicates the location of a flow boundary or lower permeability close by (Zambrano, 2000)

The pressure stabilization at a higher level is due to the presence of the well in the channel. This occurs when the inner boundary B_{L1} is observed.

For a well located within a straight channel with a symmetric composite thickness profile the late time log-log plot indicates two stabilizations above the radial flow stabilization. The trend can be seen below in Fig 2-8.

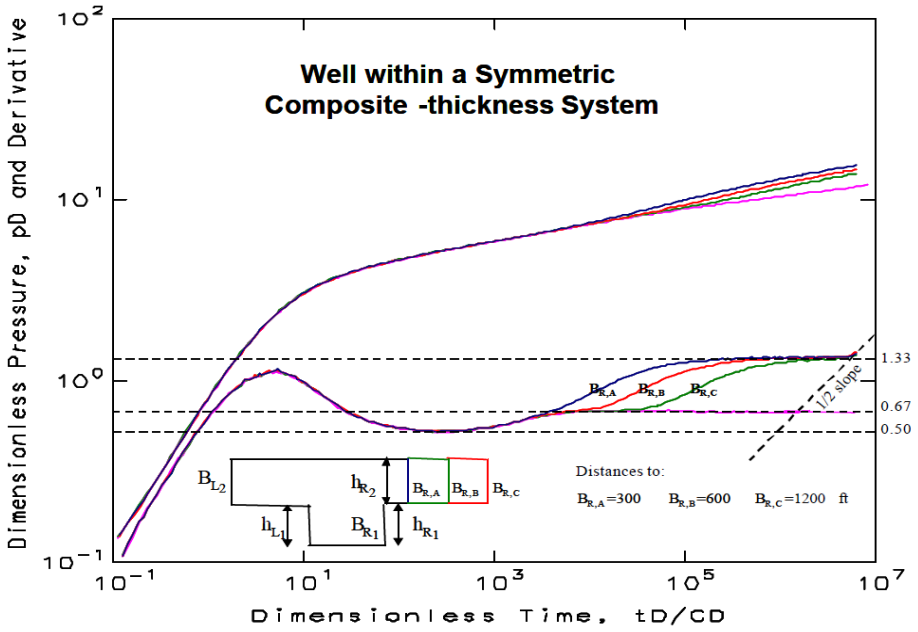

Fig2-8 Log-log plot of drawdown test on well within a channel with symmetric composite thickness profile (Zambrano, 2000)

The stabilization of the pressure is at a higher level than the radial flow is due to a decrease in reservoir thickness from h to h_{L2} which is observed when both inner boundaries, B_{R1} and B_{L1} are seen.

For a well within a meander channel with constant thickness the well test resembles that of a linear channel. As the channel width increases, the effect of the closest wedge is seen on the pressure derivative plot. At late time a one half slope line develops due to the presence of two intersecting straight line channel segments. This pattern is shown below in Fig 2-9.

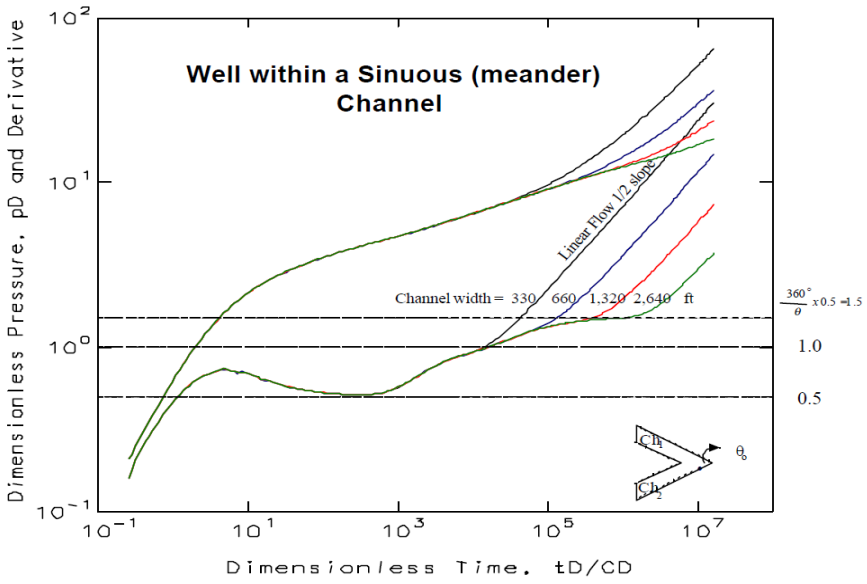

Fig2-9 log-log plot of drawdown test on well within a sinuous channel with constant thickness (Zambrano, 2000)

These results indicate that well test analysis can provide information on reservoir large-scale features specifically:

1) Average thickness between a thicker zone penetrated by a well and a thinner zone away from it for example a linear channel with asymmetrical composite thickness profiles as in Fig 2-7
2) Thicker zone to thinner zone thickness ratio in a symmetric system such as a linear channel with a symmetric composite thickness profile as in Fig 2-8.
3) Channel curvature wavelength to amplitude ratio as in fig 2-9.

In a later paper looking at the influence of reservoir and different geologic features on well test response, Mijinyawa (2008) took a wider approach and investigated four complex models

1) a semi- infinite channel with non parallel boundaries
2) a T-shaped channel (such as a distributary or meandering channel system)
3) a meandering channel with different well locations and meander angles
4) a pinch-out boundary

Mijinyawa found that these four complex models can all be modeled by combining simpler known behaviors.

The semi infinite channel can be modeled by two sequential wedges. The T-shape is equivalent to two linear channels either perpendicular to each other or positioned one after the other. The location of a well in the meandering system affects the early-time and middle-late time behavior of the pressure and pressure derivative responses but has no effect on the late time behavior. Layer pinch outs are similar to a single sealing fault but with a longer transition after the main radial flow stabilization in the derivative plot.

2.4.4.1 Semi-infinite channel with non parallel sides

This channel type is modeled using two wedges as shown in Fig 2-10. Different channels are modeled by controlling the angle of wedge W_2. At zero degrees an open rectangle is modeled and at 90 degrees two perpendicular boundaries are modeled.

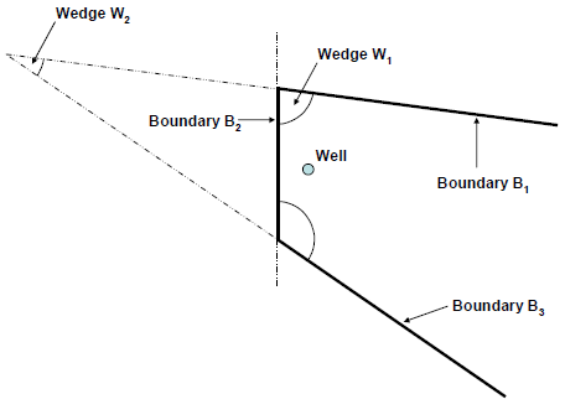

Fig2-10-bounded channel with non parallel lateral boundaries (Zambrano, 2000)

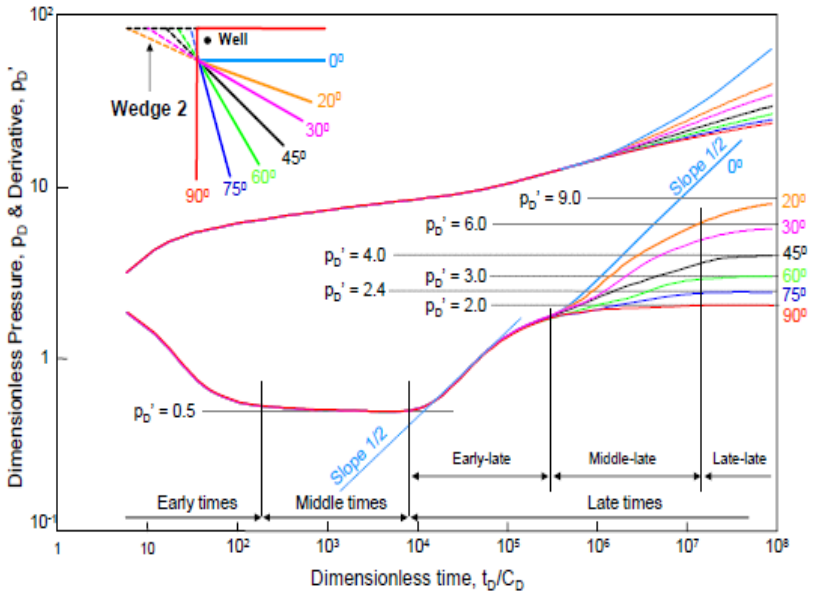

fig2-11-effect of the wedge W_2 angle on the derivative response (Zambrano, 2000)

Fig 2-11 above displays different W_2 angles for the simplified case of W_1 being 90 degrees. For other variations Mijinyawa's (2008) paper should be looked at. Fig 2-11

depicts a channel with non parallel boundaries bounded on one side, for which no analytical solution exists. The analytical solution for such a channel can now be analyzed by superimposing the solution for two successive wedges, for which solutions do exists.

2.4.4.2 T-Shaped Channels

T-shaped channels used to model distributary and meandering channel systems such as those shown in Fig 2-12. The two channel system is broken up into a main branch, CH_1 and a tributary branch CH_2 as shown in Fig 2-13.

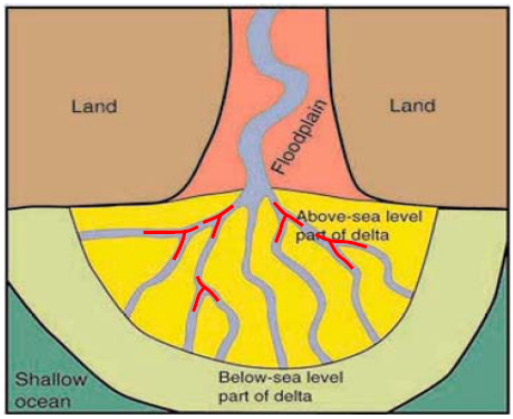

Fig 2-12 T-shaped channels in a deltaic depositional environment (Mijinyawa, 2008)

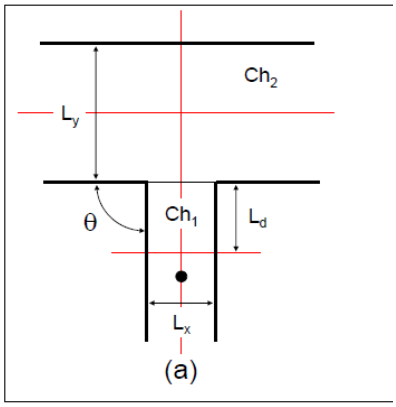

fig2-13 T-shaped channel combination of a perpendicular channel (Mijinyawa, 2008)

When the well is located in the middle of the main branch, CH_1 the derivative plot (fig 2-14) exhibits two half unit slope log-log straight lines after radial flow. The first half-slope corresponds to CH_1 (early late times in Fig 2-15) while the second channel only contributes to the plot when the Ly/Lx > 1 (see above figure for an explanation of these symbols). Fig 2-15 suggests that a T-channel exhibits an identifiable derivative

behavior that can be analyzed with two successive wedges when the well is located in the main branch, the first wedge deals with width of the branch and the lateral distance from the boundaries while the second one yields the sum of the widths of the main and tributary branches.

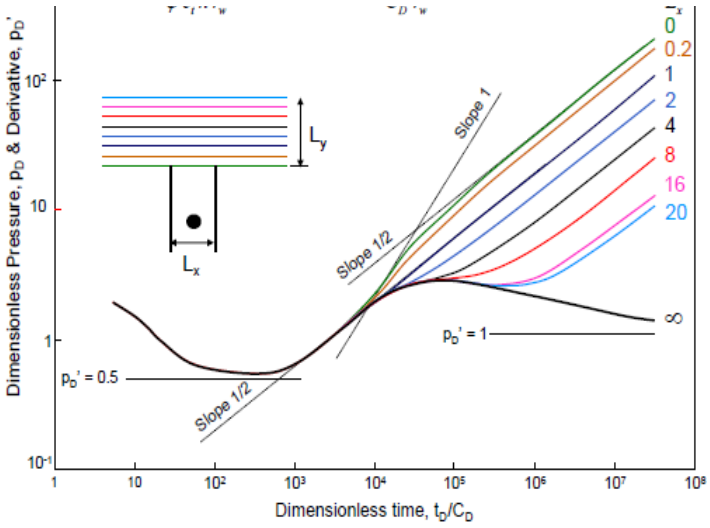

Fig2-13-impact of L_2 on the derivative late-late behavior of a T-shaped channel (Mijinyawa, 2008)

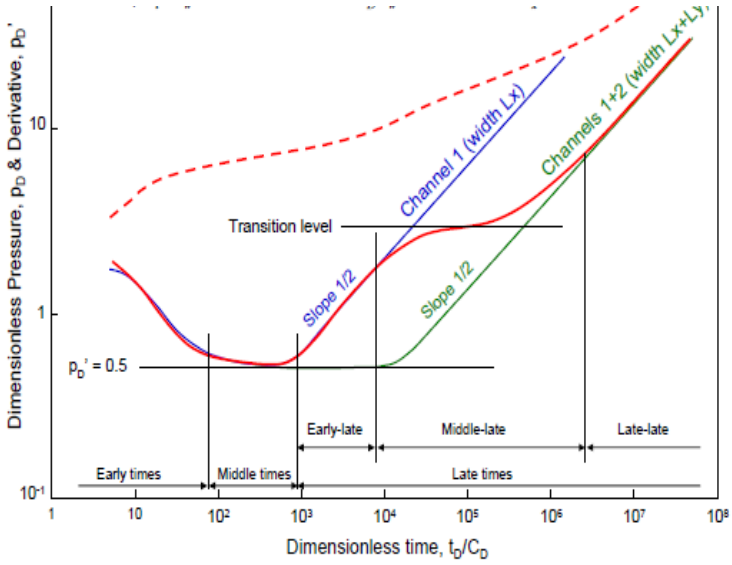

fig2-14 T-channel derivative matched with two perpendicular channels (Mijinyawa, 2008)

It is to be noted that when the well is located in the tributary branch the behavior is different. It is similar to that of a well that is off center between two parallel sealing faults.

2.4.4.3 Meandering Channels

The derivative plots (Fig 2-17 and Fig 2-18) for a meandering system (Fig 2-16) show that all behaviors start with a radial flow dimensionless stabilization of the derivative P_D' despite the angle of the meander and end with a half-unit slope log-log straight line at late-late times. The late-late time behavior represents the combined effect of the channel on both sides of the meander, bounded by the boundaries of the channel.

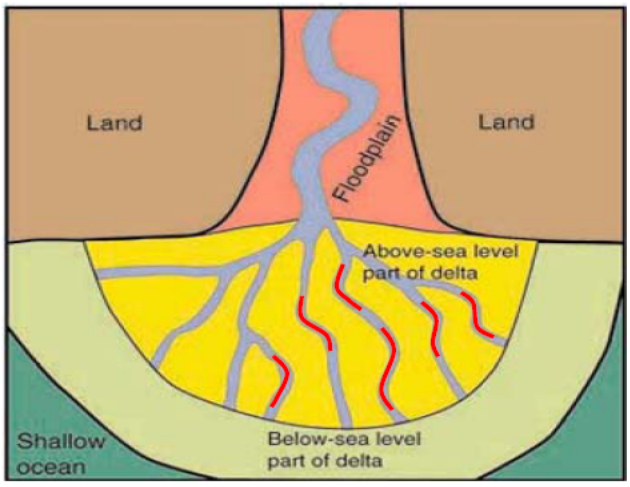

Fig2-16- Meandering channels in a deltaic depositional environment (Mijinyawa, 2008)

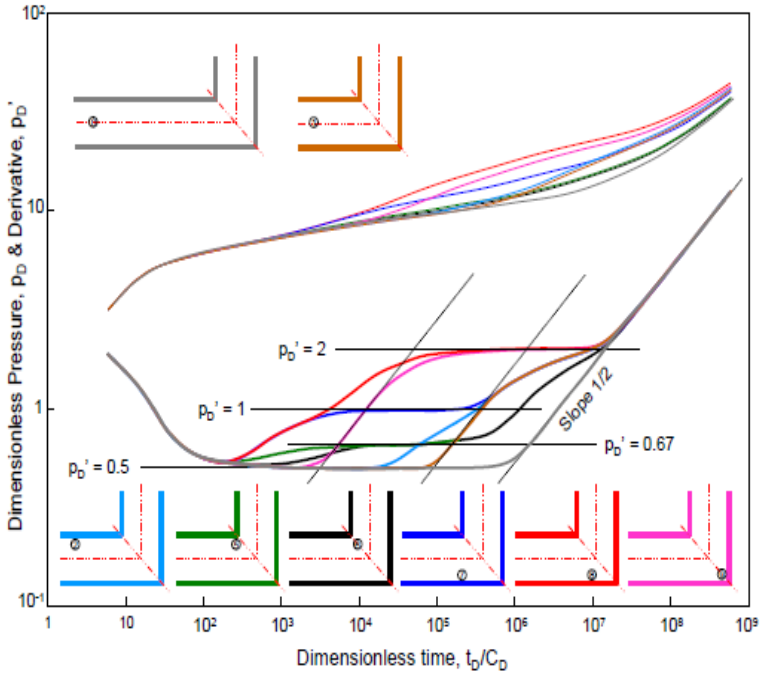

Fig2-17 P_D and P_D' responses for various well locations within a 90° meander (Mijinyawa, 2008)

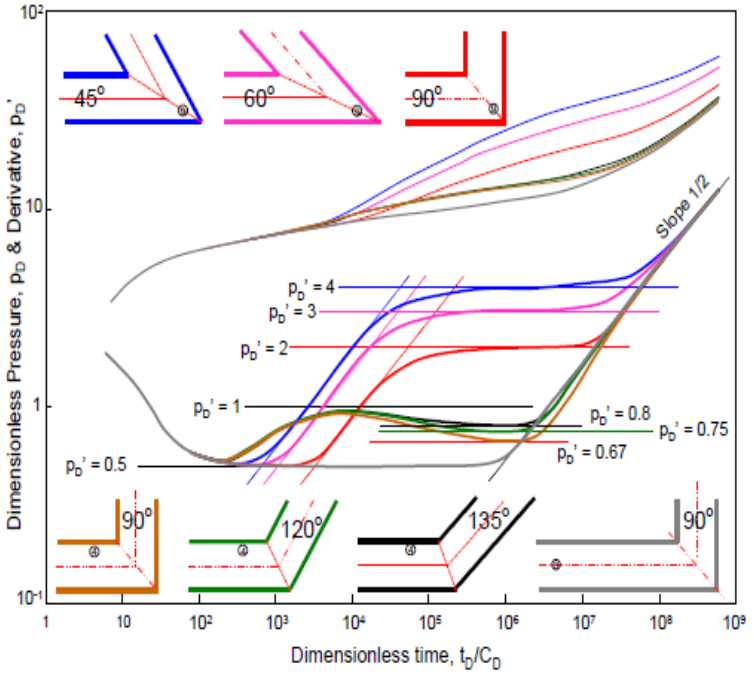

Fig2-18 P_D and P_D' responses for different angle meanders (Mijinyawa, 2008)

Fig 2-17 and 2-18 thus suggest that a meandering channel can be analyzed by a well test by combining one or two wedge models and a channel model. Analysis yields the meander angle, the arithmetic average of the widths of the channel on each side of the meander, and the distance to the well closest lateral boundary.

2.4.4.4 Pinch Out Boundary

For a well close to a pinch-out, the derivative plot (Fig 2-19) exhibits a spherical type behavior at late times, characterized by a negative half-unit slope log-log straight line. This is due to increase of reservoir thickness away from the pinch out.

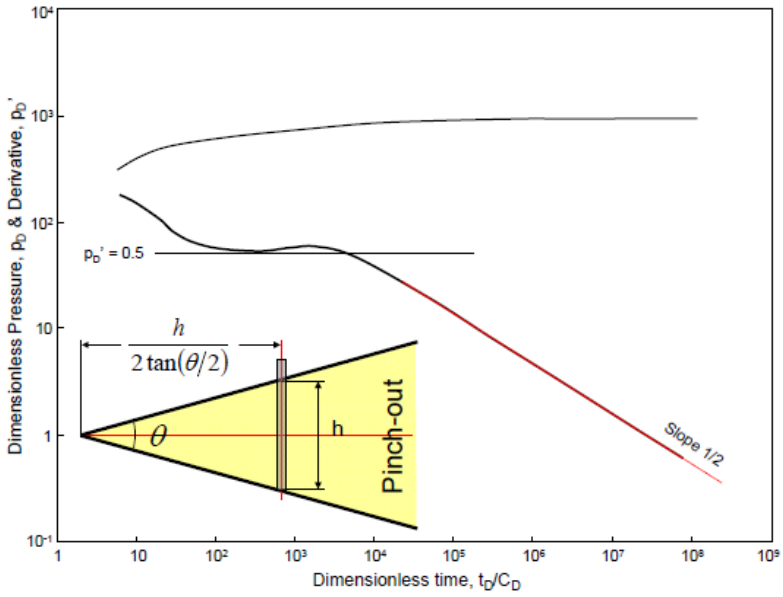

Fig2-19 Schematic for a well close to a pinchout and the corresponding pressure derivative response (Mijinyawa, 2008)

When the well is away from the pinch-out, the reservoir thickness will be constant in one direction while in the direction of the pinch out a gradual decrease in thickness will be experienced. The pinch-out derivative response (Fig 2-20) is characterized by a final stabilization level at twice the radial flow stabilization level, as with a sealing fault.

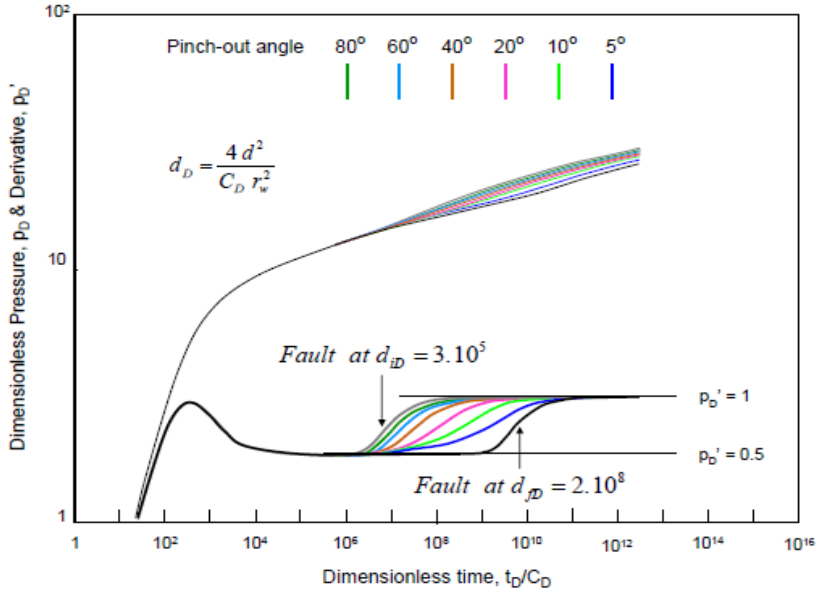

Fig2-20 Pressure and derivative response for a well near a reservoir pinch-out for various pinch-out angles (Mijinyawa, 2008)

2.4.4.5 How to interpret Well Test in these Complex Channelized Reservoirs

For simple geological areas, interpretation of well tests is done analytically however for more difficult geological models as the ones described above a different approach is needed. Massonnat (1993) gives an outline on the approach to be followed for complex geologic environments

The study is normally done in four steps

1) A field example is used to define the problem: a pressure transient test is interpreted in terms of complex geology by combining analytical solutions
2) Known reservoir geometry from say an outcrop study is input into a well test flow simulation model.
3) A more complex reservoir model is generated using stochastic techniques
4) A new analytical solution is developed to reflect the behavior of the stochastic model and that allows for the correct interpretation of the original field example

In Massonant (1993) these steps were used to model the Gerry Field located offshore West Africa. The Gerry Field reservoirs were deposited in a deep-sea fan environment, characterized by channels and overbank deposits (levees and crevasse splays) . The original interpretation of the pressure derivative uses a two parallel boundary channel model (Fig2-21a). The match was then improved by using a radial composite model but the radius of investigation was too large compared to the known lateral extension of the stratigraphic trap (Fig2-21b). This assumption of the radial composite model is also inconsistent with the probable elongate nature of sand bodies. Therefore the two above strategies deemed unusable data since in Fig 2-21a the match wasn't a good one and in Fig 2-21b the reasoning did not match the geology of the area. It was then decided to combine the theory of the radial composite and the homogenous with parallel boundaries model. It was also assumed that the channels exist at the edge of a channelized zone. Using this interpretation Massonnat was able to determine the permeability of both the individual channels and the channelized zone. The first stabilization was interpreted as

the pressure response with the elementary channel, and the second as a response to the larger channel belt width. This interpretation provided a good match (fig2-21 c) which indicated an elementary channel width of 80m and a channelized zone of 500m. These figures agree with the geological and seismic data.

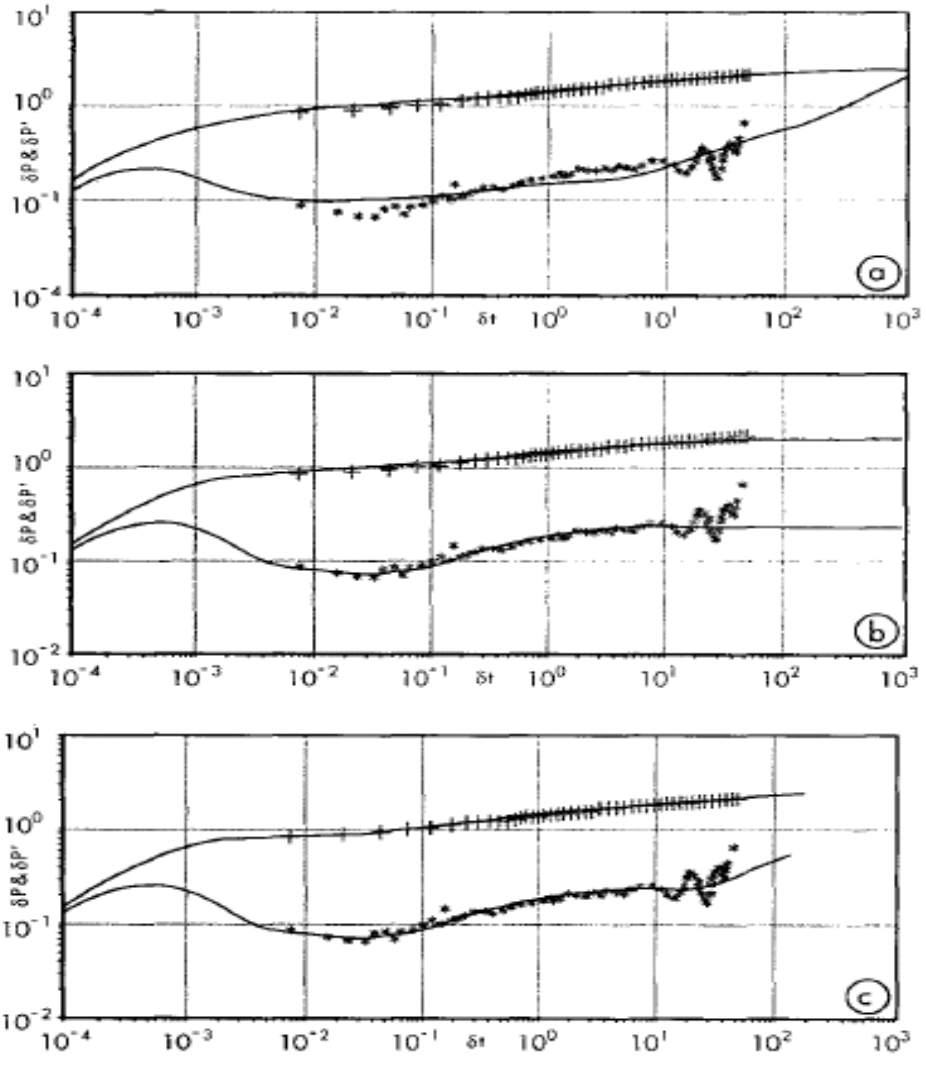

Fig 2-21 Derivative plots with 3 different interpretations for the Gerry Field, West Africa. (Massonnat (1993)) a.)using an non homogenous reservoir model with parallel no flow-boundaries, b.) With radial-composite model, c.)With a radial-composite no flow boundary solution

Using the results from the three different cases above (fig 2-21a - 2-21c), two stochastic models were developed one using the width from the homogenous-with-parallel-boundaries and one using the width from the derived combination model and these models were used for different purposes during the reservoir development phase.

2.5 Summary

Based on the findings in this literature review we have some idea of what to expect when analyzing build up test derivative plots. We can expect certain trends and shapes and can come to better understand the geology involved in the deep sea turbidite models used in this thesis.

Models can also be scaled to be more realistic based on the outcrop studies discussed in this literature review specifically the petrophysical and channel geometries found by Dutton and the channel density findings of Maher's thesis. Due to these findings accurate representation of thickness, orientation, amplitude, length and channel density are taken into account in building the reservoir models.

Chapter 3: Well Test Signature in Different Geologic Environments

3.1 Overview

This chapter presents a systematic analysis of well tests performed in different simulated geological environments. Specifically, the chapter probes the sensitivity of the well test response to the transition of permeability at the boundary of a channel system. The ultimate goal is to determine how far these well needs to be to pick up channel boundary effects as well as to determine the sensitivity of the power law parameter determined in chapter 4.

3.2 Base Case Well Test Simulation

To test the accuracy of the well test and to ensure that the interpretation of the derivative plots give accurate results, a synthetic base case was constructed. This base case considers a homogeneous reservoir represented in a 200x200x1 grid system (with grid block dimensions 10,000'x10,000'x100'). The permeability was specified to be constant 4.82 md across the reservoir with a porosity of 0.3. Rock fluid properties and PVT data used for the simulation can be seen in Figure 3-1. A well was placed in the middle of the grid and flowed at 4000 bbl/day for 12 hours followed by a shut in period of 24 hours taking data readings every minute.

The resultant variation in bottom hole pressure at the well as a function of test time were then imported into Saphir well testing software and the log-log, semi-log, Horner and derivative plots were constructed. The inputs into Saphir include the oil

viscosity and formation volume factor, $B_{o,}$ at the pressure conditions in the reservoir. Since this pressure is decreasing during the flow period and increasing during the shut in period, an estimate of the PVT parameters at reference conditions is needed. Using the PVT data showed in fig 3.1, the viscosity corresponding to the bubble point of 3277 psia was used first and then adjusted until the best match was obtained for permeability. This value for viscosity was found to be 0.187 cps and the formation volume factor was found to be 1.6 rbbls/STB.

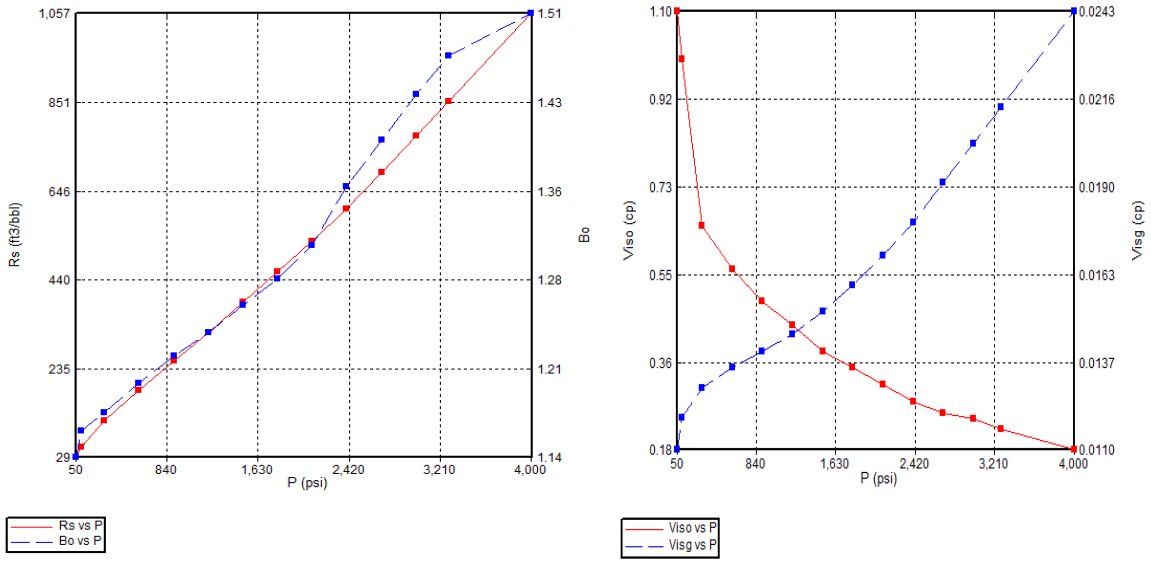

Fig 3.1a Input Parameters in CMG for the PVT region of the reservoir

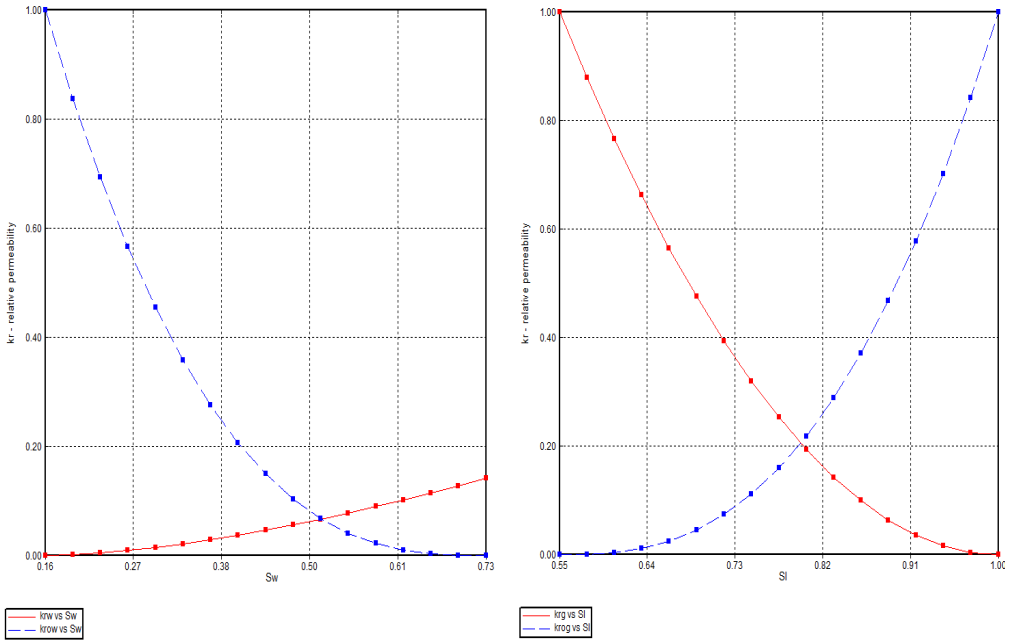

Fig 3.1b Rock fluid data correlations for the reservoir and the resulting relative permeability curves

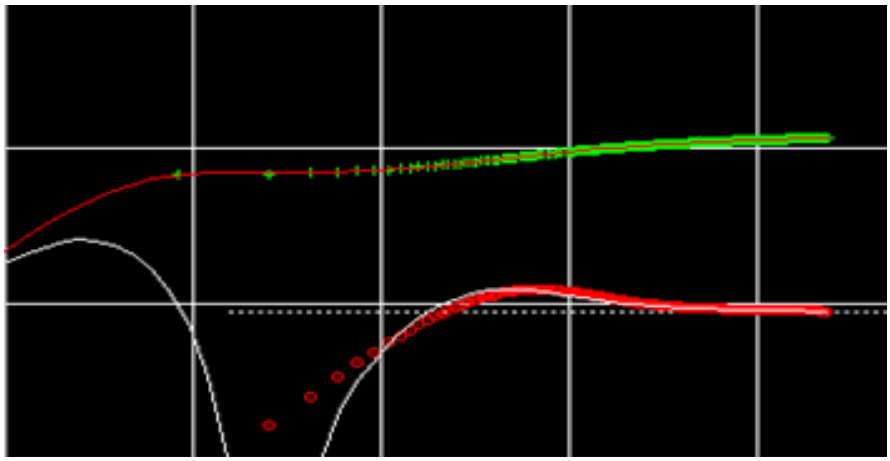

Fig 3.2 Typical shape of a log-log plot (red dots) for a Well Test in a homogeneous reservoir with permeability=4.82 and porosity=.3

Using these parameters the effective permeability estimated by the well test came out to be 4.88 md which is very close to the constant permeability specified for the flow

simulation model. The derivative plots for this case can be seen in fig 3.2. The derivative plot does not have the characteristic “bump” indicative of the transition from the wellbore to the near-well reservoir flow condition. There is no skin transition zone around the well assumed in the simulation. From the log-log plot in this scenario the flattening out of the plot(red dots) indicates a zone with no variations in geology has been investigated. If a zone of lower permeability was near a positive slope change would be observed and if a zone of higher permeability is picked up a negative slope change.

3.3 Well Test in Heterogeneous Systems

This main objective of this study is to assess the influence of channel heterogeneity on the well test response. The base case simulation was repeated this time for a heterogeneous reservoir model. The first well test simulation model was performed to test the drainage radius for a well test in an inhomogeneous reservoir.

3.3.1 Simple Heterogeneous model

Using the same PVT properties and rock fluid data as the base case a model with spatially varying permeability distribution was created. The permeability distribution can be seen in Fig 3.3. The red values of permeability are 1000md and the blue values are 4.82md.

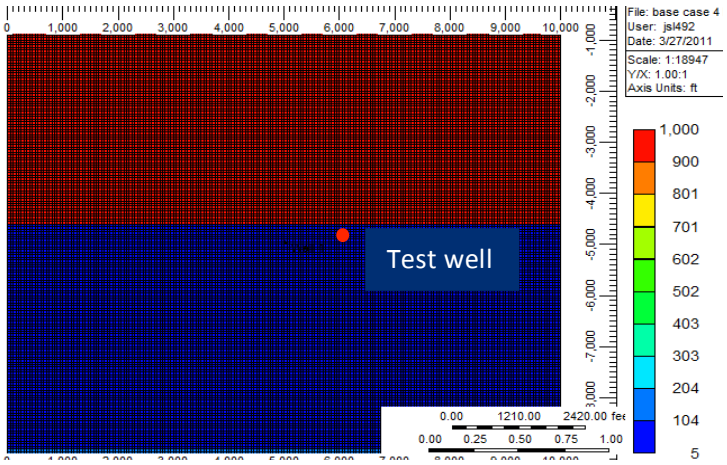

Fig 3.3 Permeability distribution for a Reservoir model with two permeability regions and the location of the well on the boundary of the two permeabilities in the shale region

A build up test was carried for a well 1 block (50ft) away from the boundary between the high and low permeabilities. The $K_{effective}$ from the well test was calculated and the well test signatures were compared to the results of well test in different geological environments talked about in the Literature review. The well was then moved in a southerly direction and analyzed until the effect of the boundary was no longer seen on both the log-log plot and in the calculation of $K_{effective}$.

3.3.1.1 Results of Well test for Reservoir with two different permeability values

As pointed out in the Literature review, the well test next to a boundary exhibits a log-log plot that has an almost spherical shape with no leveling of the log-log plot. As the well moves south one grid block at a time we can see in fig 3.4 that the log-log plot becomes less spherical and begins leveling off after the initial well bore storage period. Well test response when the well is one block and two blocks away from the permeability

contrast boundary reveals that the log-log plot never levels out. When the well is moved to three and four grid blocks away from the boundary, the log-log plot levels out after the initial well bore storage and at the end shows a characteristic increase in slope indicative of the boundary. When the well is seven grid blocks away the derivative plot shows no increase in slope indicating that for the length of the test carried out the boundary effect is not felt. The value for $K_{effective}$ vs. K_{actual} is also a good indicator for where the channel begins to have an effect on well response. For 1 and 2 blocks away the $K_{effective}$ value of 88md is significantly higher than K_{actual} at the well location of 18 md. When the well is completed four grid blocks away from the boundary between the high and low permeability region, the $K_{effective}$ approximately equals K_{actual}.

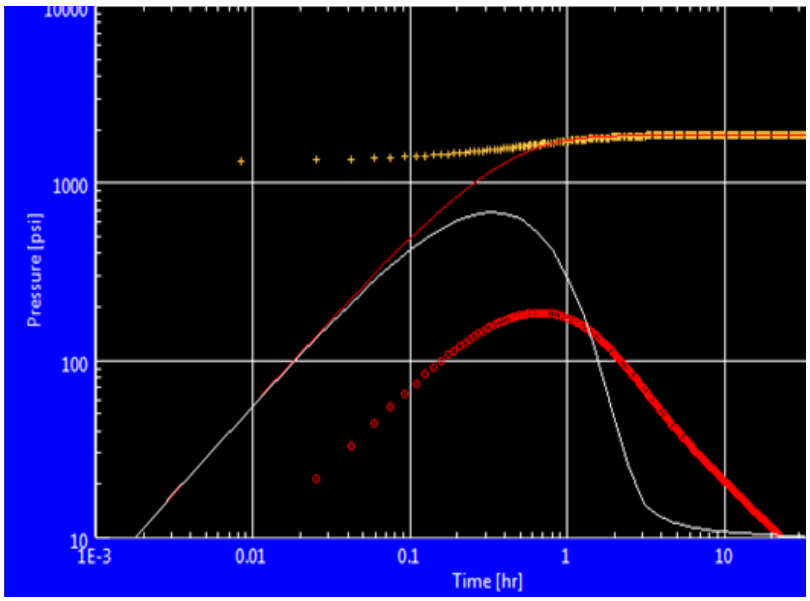

(A)

Fig 3.4

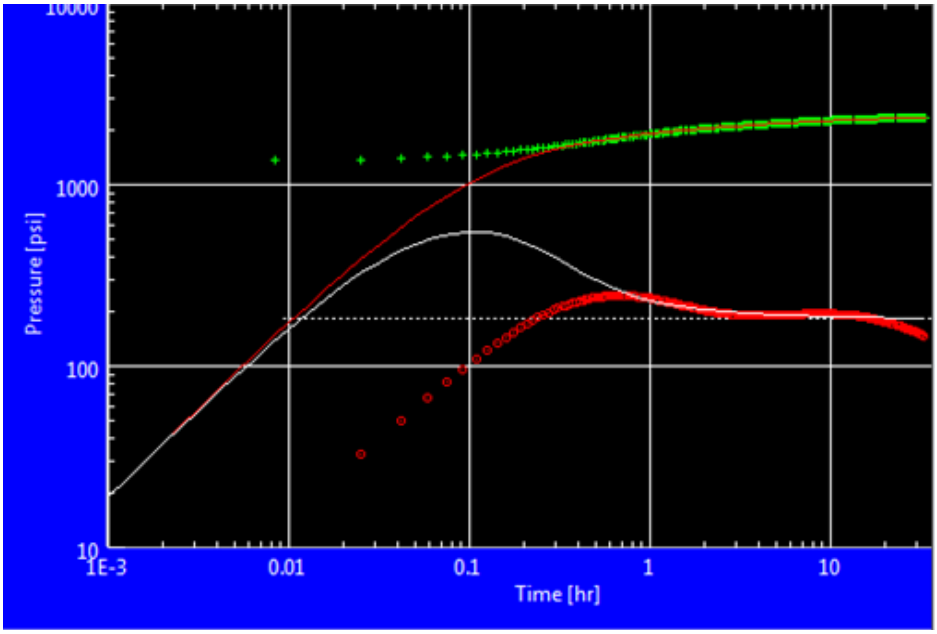

(B)

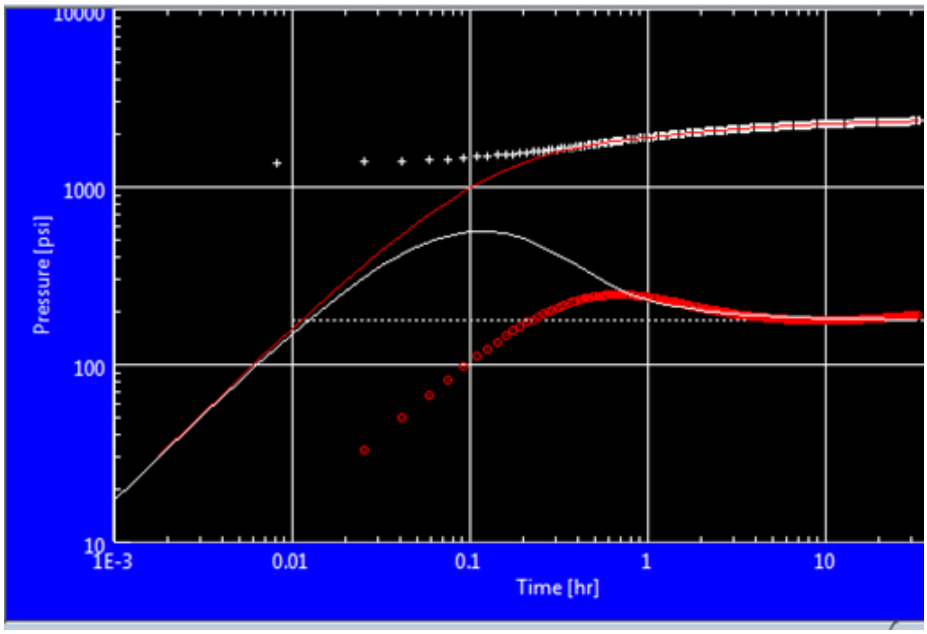

(C)

Fig 3.4 Log-log plot (red dots) response to channel effects in heterogeneous environments (A)-Log-log plot very rounded at 1 block away (B) Log-log plot levels out after storage then slope changes due to boundary 3&4 grid blocks away (C) After well bore storage log-log plot levels out and no evidence of channel felt at 7 blocks away for this length test where the red dots represent the log-log plot

To investigate the dependence on permeability variation between the channel and shale regions the above experiment was repeated for models where the permeability of the shale region is increased. Three new models were done where the permeabilities of the bottom zone were increased from 4.82 – 110 – 800 md while the upper zone is held fixed at 1000 md. The results can be seen in Fig 3.5. It should be noted for the first two models (4.82 md and 110 md the oil rate was held at 400 bbl/day while at the others it was held at 10,000 bbl/day in order to keep the bottom hole pressure above the bubble point pressure as well as to view a significant pressure decline in the higher permeability models.

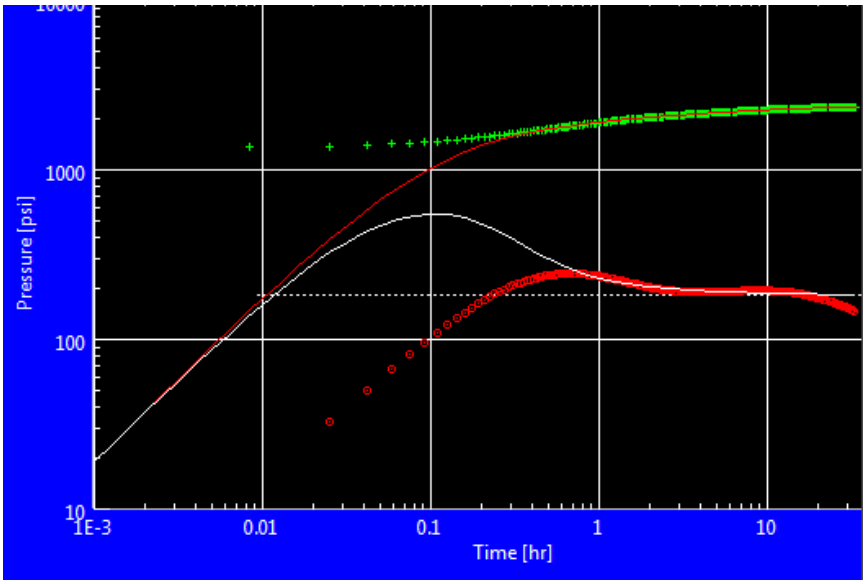

(A)

Fig 3.5

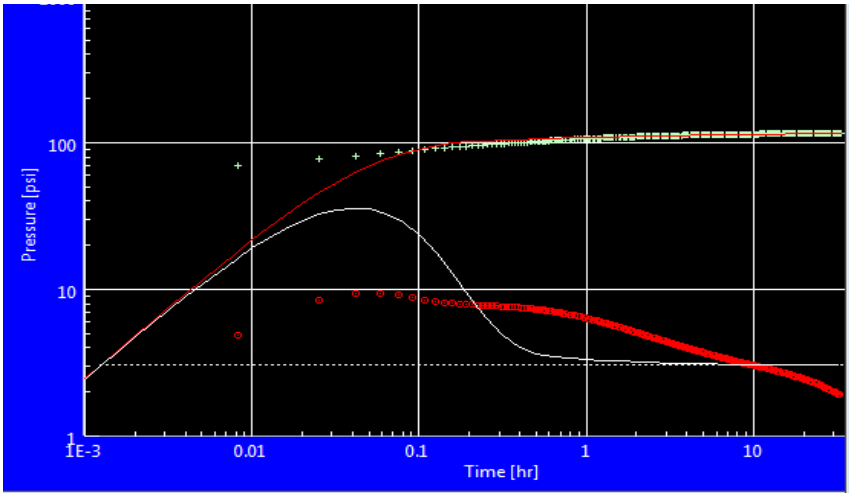

(B)

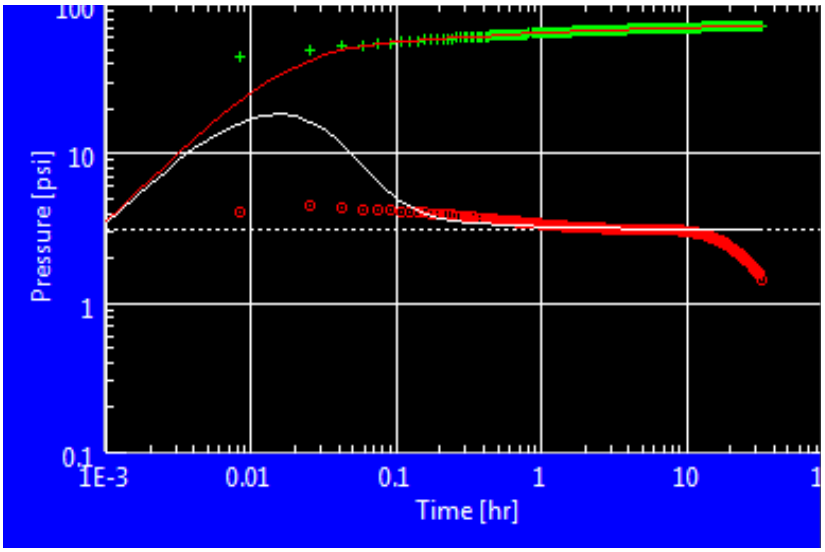

(C)

Fig 3.5 Log log plots for a well located four blocks away from a 1000md channel for different permeability gradients across the boundary (A) shale= 4.82 md, channel response felt at 10 hr but for this low flow rate it would take longer for the boundary to be felt. If flow rate was at 10000 bbls response will be felt earlier. (B) shale= 110 md-hint of boundary but steady decline observed. (C) shale=800md, very low gradient between shale/channel boundary derivate very shallow feels increase of permeability late on. The red dots represent the log-log derivative plots in each figure.

Based on the results in Fig 3-5 the best way of indicating the presence of a channel or the productivity of the zone the wellbore is completed in is to view the Pressure decline. If there is no significant pressure decline increase the flow rate and then see if any boundaries can be picked up. If there is significant pressure decline we can then look at the log log plot to see if any channel effects are picked up and at what time these are picked up. Based on the result regardless of the gradient the channel boundary is still picked up at about the same time, only the initial derivative that changes.

3.4 Building a Model for a Channel Reservoir

Using the data pertaining to channel width, length, thickness, orientation, amplitude and wavelength in Maher (2007) and Dutton (1999), hundred training images were constructed using Remy's *et al (2009)* SGEMS (Stanford Geostatistical Modeling Software)) for reservoir systems with channels. The channel facies models obtained using SGEMS were combined with models for channel and turbidite permeabilities constructed using sequential Gaussian simulation. These simulations were conditioned to the data at nine data locations for locations in a reservoir with an expected permeability of 1000md for the channels and 10md for the shales.

A range of 200 - 2000 md was selected for the target histogram of permeability in the channel facies, while for the shale/mudstone a range of 5-50 md was specified. The models for permeability in channel and mudstone are shown in Figure 3-6.

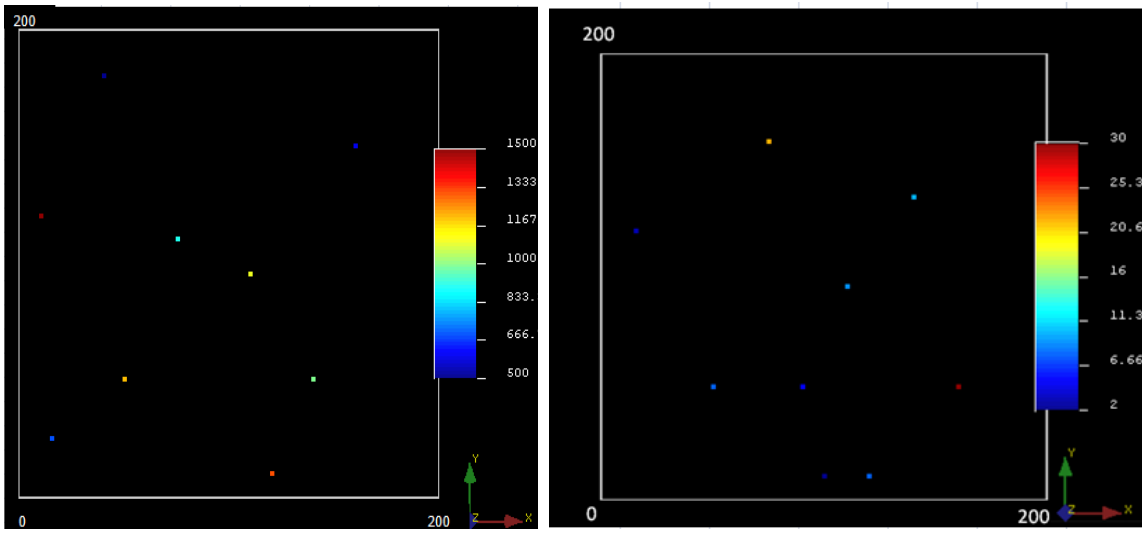

(A) (B)

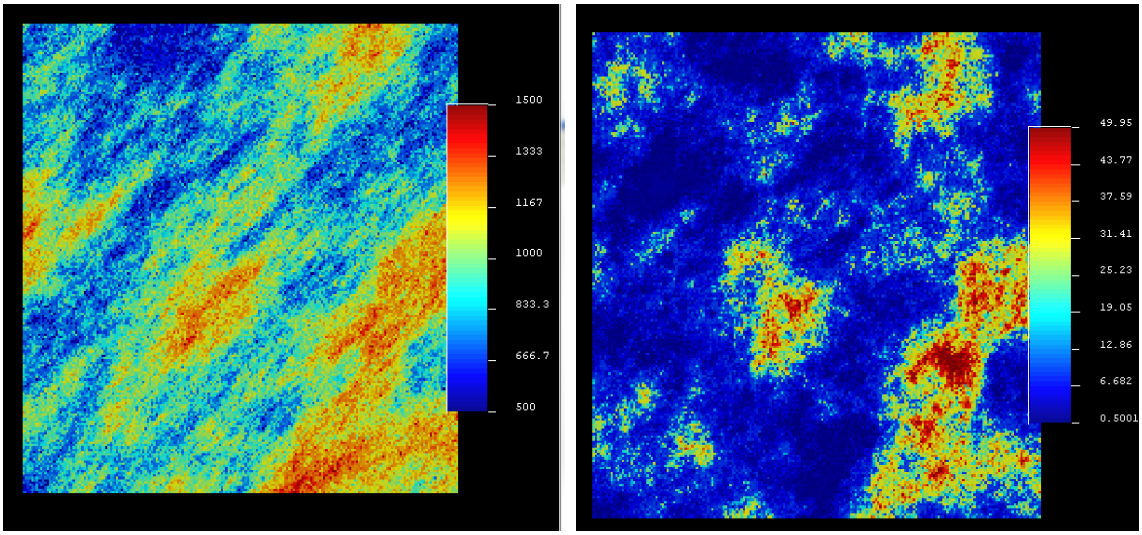

(C) (D)

Fig 3-6 (A) Location map for channel permeabilities used to create training image in Fig3-6c(B) Location map for shale permeabilities used to create training image in Fig 3-6D (C) Training image for channel permeabilities (range 500md-1500md)(D) Training image for shale permeabilities (range .5-50 md)

Combining the two realizations shown in figure 3.6 with the channelized training image, a grid with permeabilities was constructed using the cookie-cutter approach. In this approach, if a channel is present at a grid location, the value for channel permeability is assigned from the permeability model for the channel. On the other hand, if shale is present at a location, the permeability from the shale turbidite model is assigned. The resultant combined permeability model is shown in Figure 3-7 for different training images.

The permeability model was imported into the flow simulator CMG-IMEX (Computer Modeling Group Ltd.'s Implicit-Explicit Black Oil Simulator (2006)) to simulate the well test response. The well location for the flow test was changed systematically to assess the response at various locations within the channel models. Wells completed in the middle of shales where no channels were close, in the middle of channels, close to channel boundaries, close to shale boundaries, and in channel wedges were assumed.

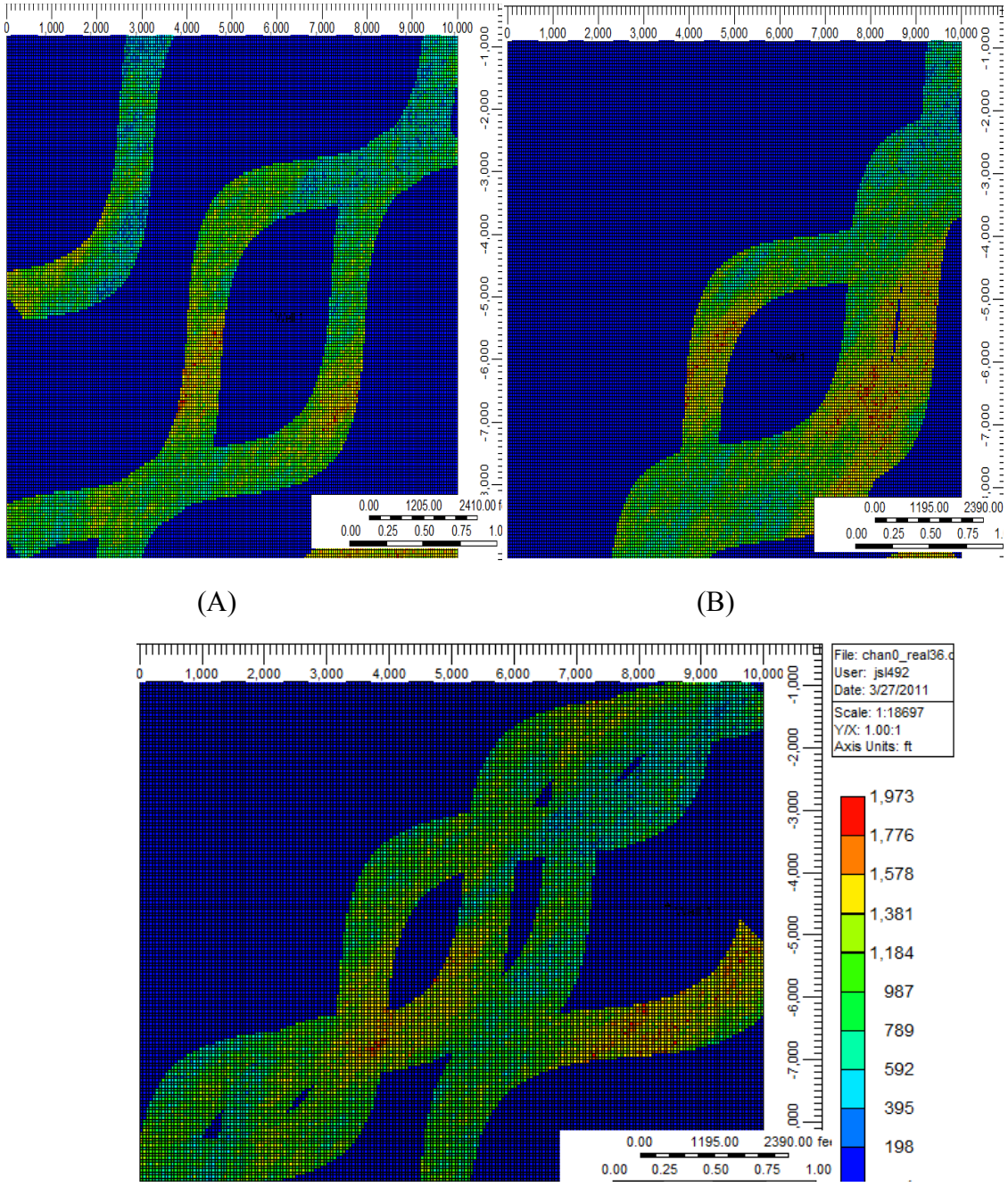

Fig 3-7 Permeability Trend for channel models for different realizations (A) Realization 1 (B) Realization 12 (C) Realization 36

3.4.1 Permeability averaging for assessing channel boundary effects

These first set of cases probe the concept of a single effective permeability representative of the well test behavior observed in a heterogeneous reservoir. The reference case is the well test response for the fully heterogeneous reservoir. This response was compared against the response of a model where a 3x3 grid around the well is selected and assigned a constant value equal to the arithmetic average of the 9 blocks in the template. This process was repeated for a template of 5x5 grid blocks around the well and lastly for a 7x7 template around the well. These averaging schemes are indicated in Equations 3.1-3.3

$$k_{average3x3} = \frac{1}{9}\sum_{1}^{9} k_i \qquad \text{equation 3.1}$$

$$k_{average5x5} = \frac{1}{25}\sum_{1}^{25} k_i \qquad \text{equation 3.2}$$

$$k_{average7x7} = \frac{1}{49}\sum_{1}^{49} k_i \qquad \text{equation 3.3}$$

The plots show the average permeability over the grids of different size for different permeability models versus $K_{effective}$ calculated from the well test for that model. These wells tests are in the shale/mudstone region with no channels in the vicinity.

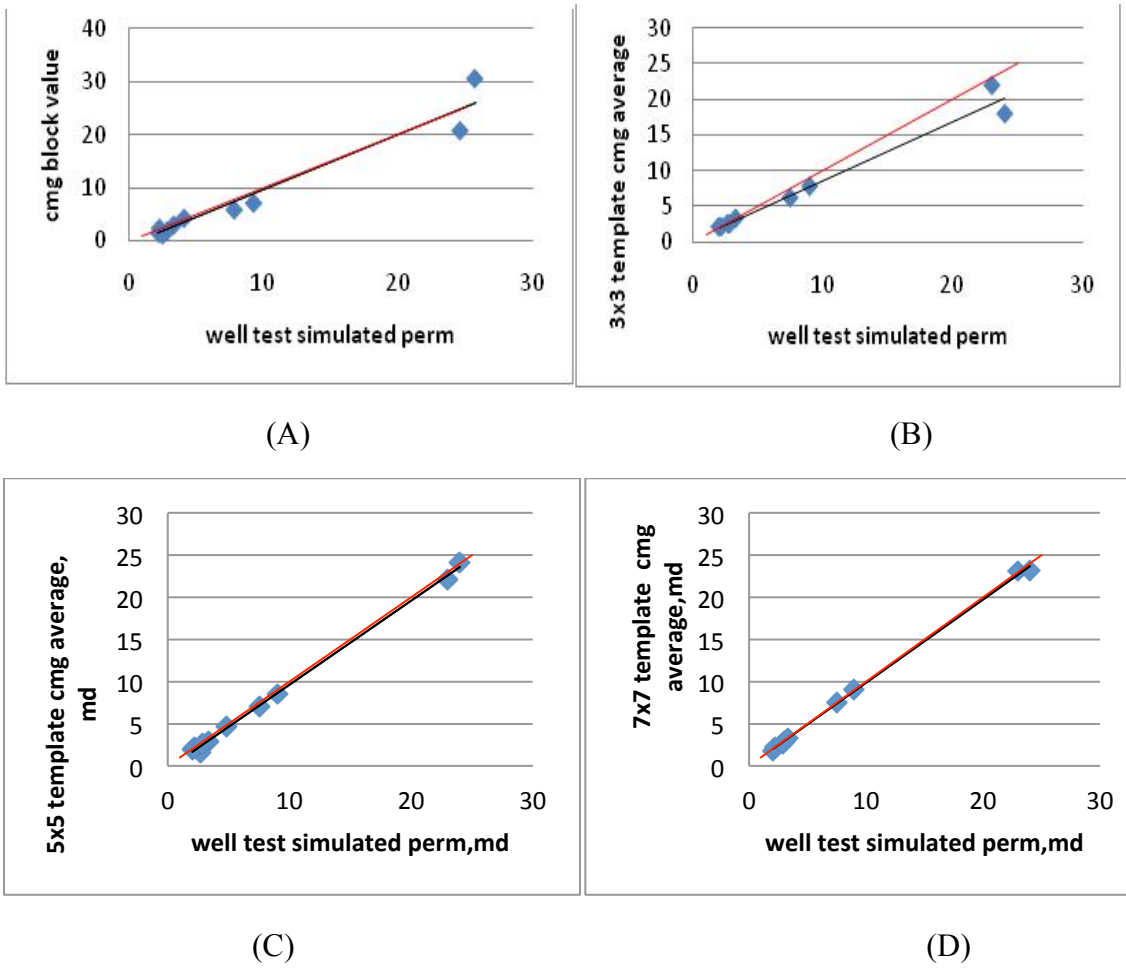

Fig3-8 $K_{CMG\ grid\ value}$ vs. $K_{effective\ from\ well\ test}$ for 10 simulations completed in the shale for realization 1. The red line signifies a perfect match while the black line is a linear fit of the actual results (A) No template applied (B) 3x3 constant permeability template applied (C) Constant 5x5 template applied (D) Constant 7x7 template applied

It can be concluded that generally, the average permeability values converge to the corresponding well test response as the size of the averaging grid increases. It can be seen in Figure 3-8a that even though the shale exhibits minor heterogeneity, the average permeability does not yield a good representation of the actual well test response when the size of the averaging template is small. . In Fig 3-8b that spread is reduced and the

correlation coefficient has improved but there is still some spread around the actual well test response. In Fig 3-8c because the size of the averaging template is quite large, the computed correlation coefficient between the actual well test response in the heterogeneous reservoir and that for the model with values over the 7 x7 grid replaced by the arithmetic average is very high. Similar results were obtained for well test done in the center of the channels where the well was more than 5 grid blocks away from the boundary in any direction.

The next series of cases are for well locations that are close to the channel/mudstone boundary. The same averaging grids were used for these cases: 3x3 , 5x5, and 7x7 arithmetic averages. In these cases, as the averaging grid is increased the permeability averages exhibit wide variations. An example of the evolution of average permeability around the well is shown in Fig 3-9.

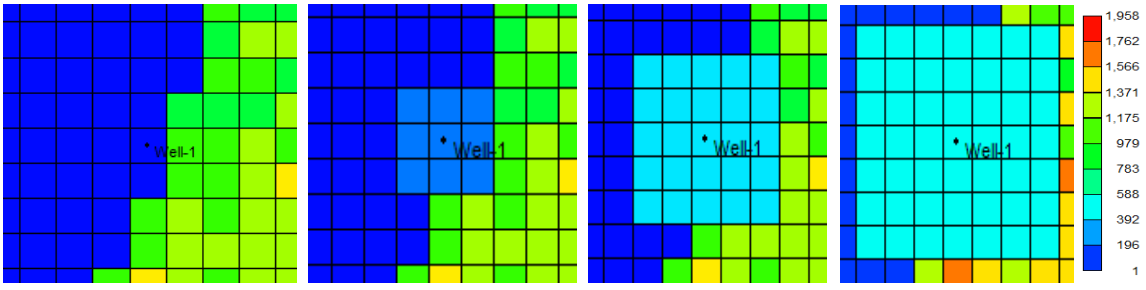

(A) (B) (C) (D)

Fig 3-9 permeability trend for 4 templates for a well completed next to the boundary (A) no template k=4.51md, (B) 3x3 template where k_{3x3}=330.7md (C) 5x5 template where k_{5x5}=426md (D) 7x7 template where k_{7x7}=482.07

In these cases, a scatter between the well test response for a grid with average permeability and that for the actual heterogeneous field is observed. The effect of the high permeability channel not only decreases the rate at which pressure declines but greatly increases the $K_{effective}$ of the tested zone. From Fig 3- 10 we can see that the correlation coefficient improves with the size of the template and the $K_{effective}$ approaches the true well test permeability.

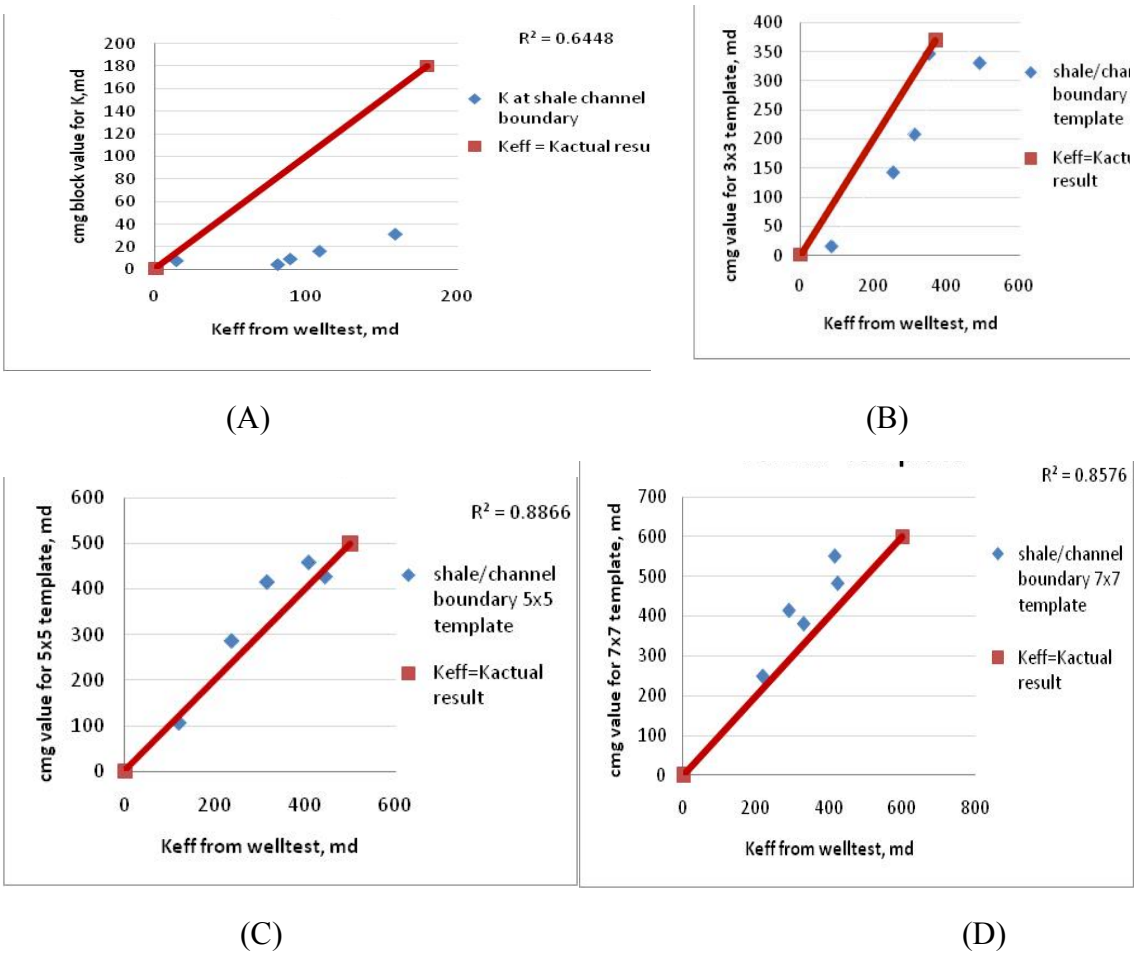

Fig 3-10 $K_{CMG\ template\ average}$ vs. $K_{effective\ from\ well\ test}$ for five wells located one grid block away from the channel. As template size increase the correlation between the permeability obtained from the well test and the permeability from CMG improves (A) No template applied, well located one block away from high permeability channel- K_{eff} much greater than $K_{wellbore}$ (B) 3x3 template applied- influence of homogeneity improves

correlation between K_{eff} and $K_{wellbore}$ however channel influence is still felt (C) 5x5 template applied- the well test value becomes close to the wellbore value indicating the presence of the channel is becoming less effective (D) 7x7 template- good correlation between K_{eff} and $K_{wellbore}$ for a 7x7 homogeneous template around the wellbore.

The derivative plots for these cases also show the same trend as in Fig 3-4 in that as the template size increases the log-log plot becomes flat after the initial well bore storage followed by a change in slope due to the effects of the channel.

3.4.2 Varying Well Location to Assess Effect of Channel

In this section, we investigate moving the location of the well to pick up the effect of channel boundaries.

The test well was located one grid block away from a channel/shale boundary and a build up test was performed. The test was repeated with the well moved one block further away from the channel and repeated. This was done until the well was four grid blocks away which corresponds to the 3 x 3 template grid for which the results were presented in the previous section. The base case heterogeneous model discussed in chapter 3.3.1 was used to perform these well test simulations. A plot of 10 different wells that lie in the shale region were chosen randomly and there respective distances (1 grid block = 50ft) from the channel boundary can be seen in Fig 3-11.

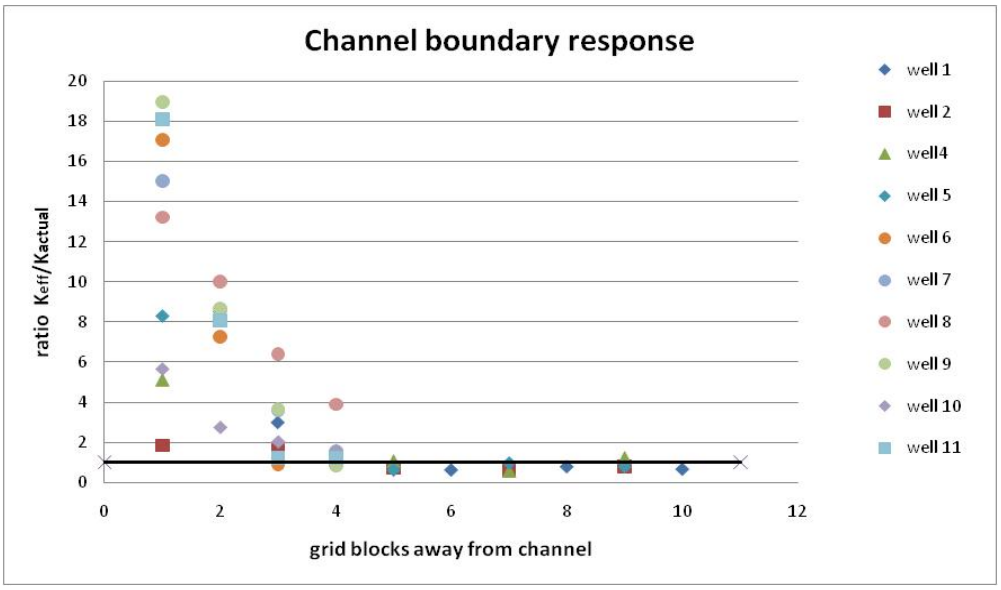

Fig 3-11 Graph depicts the effect of distance on the $K_{effective}$ obtained from the well test. From about 4 grid blocks away the $K_{welltest} = K_{actual}$ indicating an good indicator of the distance where channel effects are no longer significant on the performance of the well.

Fig 3-11 shows that for the duration of test implemented (12 hour flow period followed by 24 hour shut in), the channel boundary's influence on the test stops when the well is about 4-5 grid blocks from the boundary and for distances greater than that $K_{average} = K_{effective\text{-}well\ test}$. The data for this case was taken from a wide array of channel locations for realization 1so it can be concluded that channel effects for this length of test occurs from distances less than 250 ft.

To investigate the effects if the shut in period is increased thus giving the reservoir more time to build up to original reservoir pressure the shut in time was increased by two days to 72 hours. This can be possible by design or by necessity such as in the case during a hurricane shut down. The log-log plots for one of the locations tested above can be seen Fig 3-12

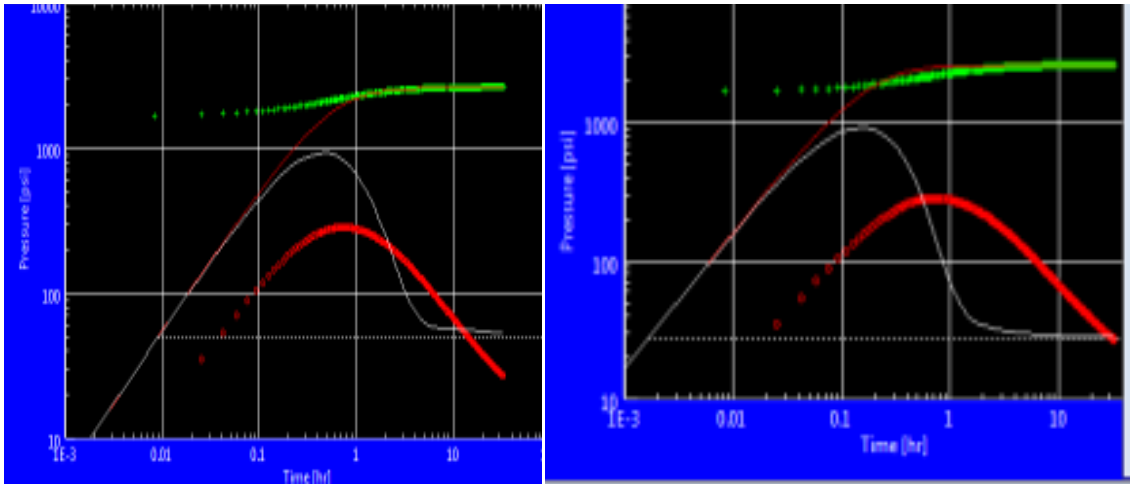

(A)

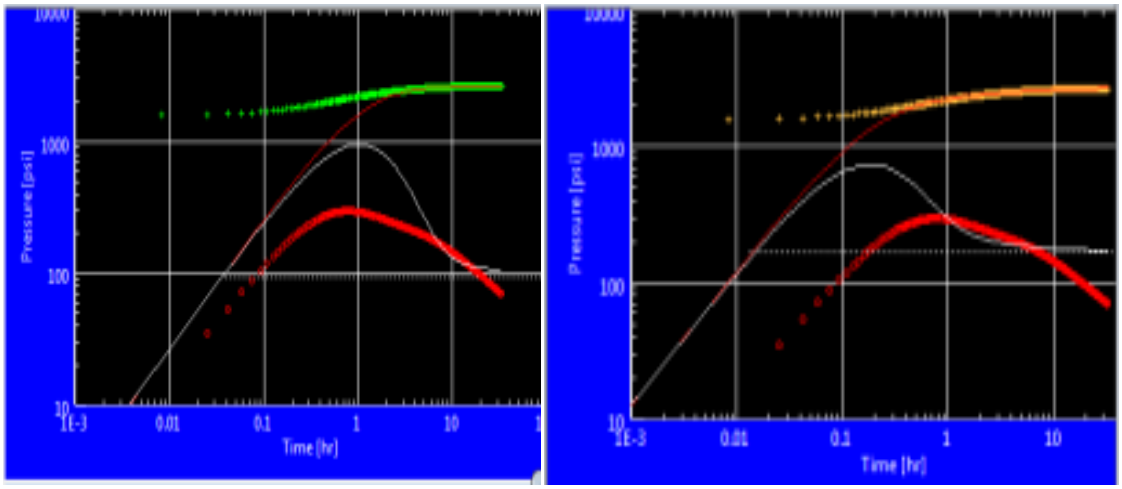

(B)

Fig 3-12 graphs comparing the difference between a 24 hour shut in period (right) and a 72 hour shut in period (left) which is seen to give more data . (A) Log-log plots for a well completed two blocks away from the channel, the derivative plots seem almost identical thus yielding similar K_{eff} . (B)Log-log plots for a well completed three blocks away from channel, again plots look identical

The results shown in Fig 3-13 show that the length of the buildup period does not play an important role once the boundary has been felt already. In this case the build up

period did not need to be longer than 20 hours. If however the build up was only 1 or 6 hours which is common offshore we would not have detected the presence of the channel.

3.5 Conclusion

The results obtained from the cases presented in this chapter are valuable for the rest of this thesis. It allows us to use geostatistical models discussed in the next chapter to determine where channel effects will have an effect on the build up test. Analysis of the signature of the log-log plot also allows us to know a bit more about the channel configuration and gives some idea of the level of variation of permeability between the grid blocks. The results also indicate that the complete suite of well test analysis including pressure derivative analysis, Horner analysis and analysis of pressure profile is necessary to detect the influence of the channel boundary.

The results indicate that for a 36 hour build up test (12 hours flowing, 24 hours shut in) and pressure decline of about 1000 psia the presence of the channel can be felt from about 200ft away regardless of the permeability gradient across the boundary. The deciding factor is more dependent on the flow rate used to investigate the reservoir space. If the pressure decline is to low the depth of investigation would not be deep enough.

Chapter 4: Relating Well Test Signature to Spatial Variation in Rock Parameters

Overview

In chapter 3 the variations in well test drawdown and buildup characteristics due to well placement at different locations with respect to facies boundaries are demonstrated. It was observed that the derivative plot could be used to identify whether a well was completed close to a channel or in an area with low variation in permeability. In this chapter, an attempt will be made to quantify the permeability variations in the reservoir in the vicinity of the test well using multiple point (mp) permeability averaging. The exponents of the mp averages can then be related to the particular spatial characteristics of the permeability field in the vicinity of the well.

4.1 A multi-point power average formulation for well test analysis

Srinivasan (2000) studied the relationship between well test response and the spatial characteristics of the permeability field using a multiple point proxy function. Such a function utilizes higher-order permeability product terms as indicated in the expansion below:

$$f \doteq \lambda_o + \lambda_1 . \sum_{u_i \in T} [k(u_i)]^{\omega_1} + \lambda_2 . \sum_{u_i, u_j \in T} [k(u_i) \cdot k(u_j)]^{\omega_2} + \lambda_3 . \sum_{u_i, u_j, u_k \in T} [k(u_i) \cdot k(u_j) \cdot k(u_k)]^{\omega_3} + \cdots$$

(1)

The permeability products are computed using nodes within a spatial template T. The response function f can be a static quantity such as a effective permeability interpreted from a well test test or it could be a dynamic variable such as a pressure profile recorded during a test. In that case, the coefficients l_i and w_i would be time dependent.

It is clear by looking at the proxy expression (1) that if the expansion is terminated at the linear (first) order term and the coefficient l_o is nominally set to zero, then the resultant expression is the familiar power average expression given by:

$$\dot{f} = \lambda_1 . \sum_{u_i \in T} [k(u_i)]^{\omega_1}$$

If further, the exponent w_1 is set to 1, then we have the familiar arithmetic average expression. On the other hand when w_1=0, the expression resolves to a harmonic average. When only the two-point product term $\sum_{u_i,u_j \in T}[k(u_i) \cdot k(u_j)]^{\omega_2}$ is retained and the exponent w_2 is set to 0.5, then we recover the geometric average. The full expansion including all the terms captures the complex connectivity of the permeability field as described by the spatial template T.

. The evaluation of such averages and the interpretation of the exponents and weights for well tests performed in different reservoir environments is discussed in the next sections.

4.2 Single point power average

As seen from the above discussion, the single point arithmetic average simply amounts to truncating the proxy expression at the first order term and setting w = 1. In

the following cases, the arithmetic average of permeability was calculated over a 7x7 grid around the wellbore. This grid defines the spatial template T in Expression 1. The arithmetic average was calculated as in equation 4-1:

$$K_{average} = \frac{1}{49}\sum_{1}^{49} K_i \qquad (4\text{-}1)$$

It was seen in Chapter 3 that while this single point arithmetic average model proved accurate for wells completed in the middle of a shale or channel, it was very inaccurate when the well is placed close to the transition between the channel and mudstone. To reduce this discrepancy, a power law average was combined with equation 4-1:

$$K_{average} = \left[\frac{1}{49}\sum_{1}^{49} K_i^{\omega}\right]^{\frac{1}{\omega}} \qquad (4\text{-}2)$$

As has been discussed earlier, an ω value of -1 signifies harmonic average, while ω=1 signifies arithmetic average. In the analysis presented below, the parameter w was varied until a match to the well test interpreted permeability is obtained on the average over the suite of models.

4.2.1 Results for Single Point Power Law model

For areas where the permeability variation is small for example for wells in the middle of overbank deposit or a channel, any of the conventional averages; a simple

arithmetic average (ω=1), a harmonic average (ω= -1) or a geometric average can be used to fit the well test response (Fig 4-1).

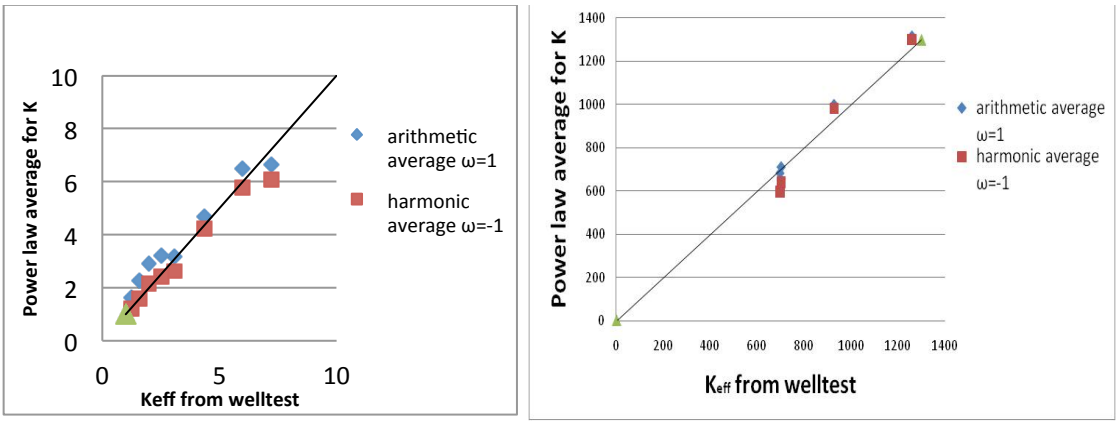

(A) (B)

Fig 4-1 Use of single point power law average in a location where permeability variability is low (A) Well completed in middle of mudstone with no channels in proximity (B)Well completed in the middle of a channel with no mudstone or other transition facies in proximity

For the cases where the well is located close to a channel/levee boundary as in Fig 3-11 this proved not to be the case. For ω ranging from -1 to 1, the dispersion of the scatterplot between the well test calculated effective permeability and $K_{average}$ calculated using the power average is much greater. It was also found that ω varied as a function of the distance from the boundary. For locations close to the boundary (<50ft) , ω=0.1 gave the best match to the well test effective permeability (Fig 4-2A). As the well moves farther away from the boundary, the optimum values for w increases and is close to a value of 0.7 for the case when the well is 4 grid blocks or 200 ft away from the boundary (Fig 4-2D). For ω to be considered optimum the minimum value for the sum of the difference squared between the values of the calculated effective permeabilities and the

effective permeability obtained from the well test were found. This optimum value of ω gave the best correlation between the two readings if a straight line was plotted where $K_{effective}$ is equal to $K_{average}$.

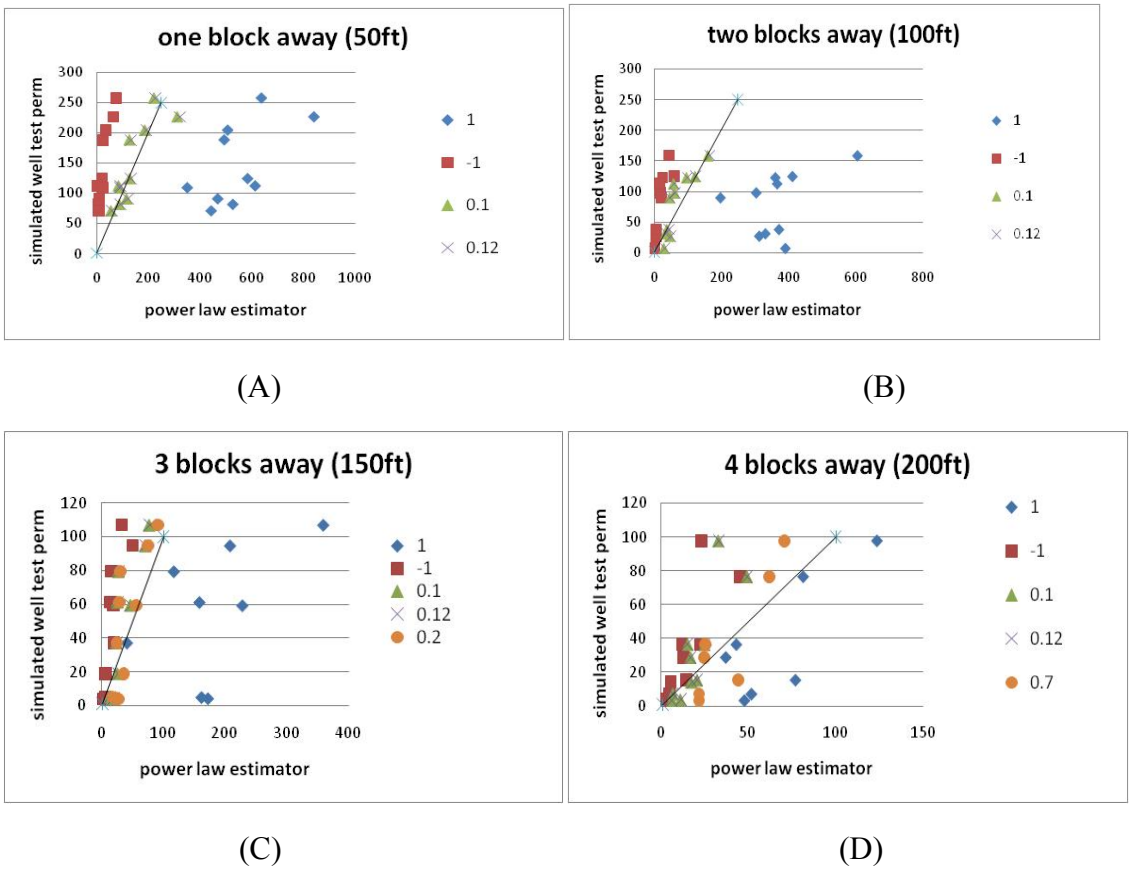

Fig 4-2. Single point power law averages for 10 wells completed in realization 1 close to channel boundaries (A) Wells completed 50 ft away from channel (B) Wells completed 100 ft away from channel (C) Wells completed 150 ft away from channel (D) Wells completed 200 ft away from channel. For locations close to the boundary the optimal value of ω=0.12 and as we move further away ω tends to 1

As the well gets farther from the channel/turbidite boundary as in the middle of a shale/channel, ω approaches a value of 1. As seen in Fig 4-2c, when the well is 150 ft from the channel boundary, ω =0.2 and this systematic variation in w points to the

usefulness of the power law exponent to detect the characteristics of permeability variations in the reservoir and the position of the well with respect to facies boundaries.

The previous cases were for a well in mudstone as it is progressively moved closer to the channel boundary. Now reversing those cases and starting with a well in the middle of a channel and moving it closer to the channel fringes yields a value of ω close to 1 which is slightly higher than when the well is in the middle of mudstone. This ω value indicates that no weight is needed for the power law average if the well is located in a channel sand. The simulated permeability average is close to the average of the template and thus an arithmetic average can be used. This is also true for when the well is moved away from the boundary as seen in figure 4-3B for a well in the middle of a channel.

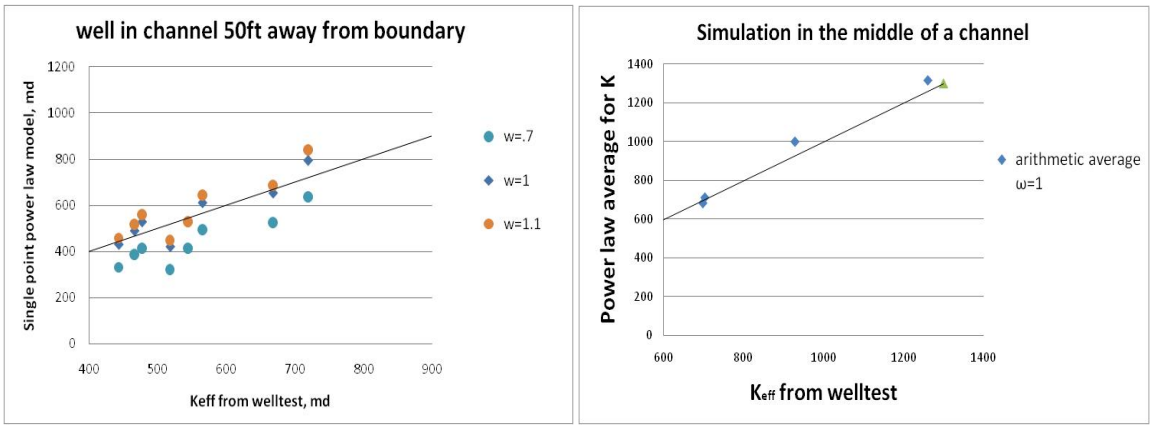

(A) (B)

Fig 4-3 Application of single point power law model completed in the high permeability channel sands at distances away from the channel/shale boundaries and the corresponding ω's used to best fit the data. (A) well completed 50 ft from the channel/shale boundary (B) well completed far from the channel/shale boundary

4.3 Two point permeability power average

To further investigate the connectivity between neighboring grid blocks the spatial template for averaging was expanded to include up to the second order term in the proxy expression shown in Eq. 4-1. The two point averaging terms were calculated for different lag distances. A code developed for this purpose in Python programming language can be seen in Appendix A.2. Three different lag distances were taken: neighboring grid blocks (lag1), one block in between (lag 2), and two grid blocks in between (lag3). The lags were taken at 45^{o} and 135^{o} orientations as seen in Fig 4-4a to 4-4f. A 7 x 7 square template was taken and all pairs separated by the chosen lag within that square domain were utilized to compute the average.

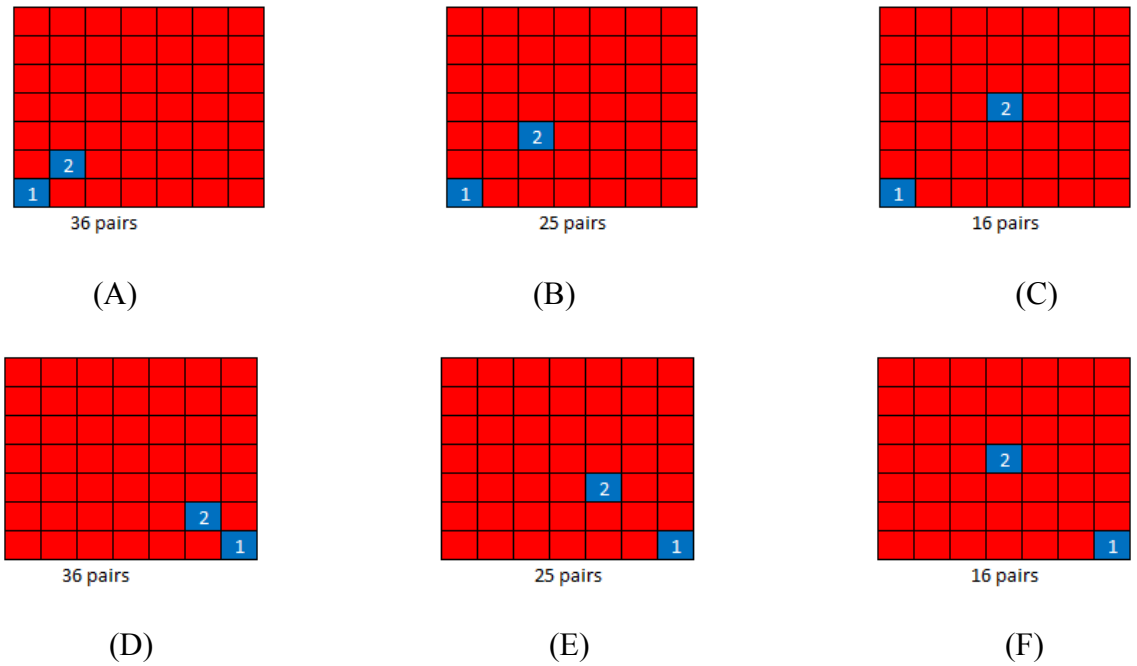

Fig 4-4 Convention for choosing two point statistical pairs for different lags and orientations from the 7x7 template with the accompanying number of pairs available in

the template (A) lag1, 45 degrees (B) lag2, 45 degrees (C) lag 3, 45 degrees (D) lag 1, 135 degrees (E) lag 2, 135 degrees (F) lag 3, 135 degrees

The equation used for this two point model is shown in equation 4-3. The ω_1 from the single point was fixed to be the optimum value for ω from section 4.2. The two point model was thus used as a second order term to minimize the sum of the differences between k_{eff} and $k_{average}$

$$k_{average} = \left[\frac{1}{n}\sum_{i=1}^{n} k^{\omega_1}(\mathbf{u}_i)\right]^{\frac{1}{\omega_1}} + \left[\frac{1}{n_h}\sum_{i=1}^{n_h} k(\mathbf{u}_i)\cdot k(\mathbf{u}_i+\mathbf{h})\right]^{\omega_2} \qquad (4\text{-}3)$$

In Equation (4-3),n_h is the number of pairs that are available on the 7x7 template. For $|\mathbf{h}|$=1 in the 45^o direction, n_h=36, for lag $|\mathbf{h}|$=2, n_h=25 and for $|\mathbf{h}|$=3, n_h=16. This equation enables us to gain a better approximation for the well test effective permeability when the well is completed at greater distances from the boundary and thus less channel permeabilities were picked up by the template. Instead of weighting each block equally, the relationships between neighboring blocks are taken into account. It was found as in the single point case that the ω_1 and ω_2 parameters assume more significance when the well is moved close to the channel/shale boundary. As mentioned previously, the ω_1 value was assumed to be the optimum value calculated previously for the single-point averaging case. The Microsoft Excel function solver was used to calculate the optimum ω_2 by taking the minimum of the difference squared between the $K_{effective}$ from the well

test and the $K_{average}$ from the two point statistical analysis for each lag distance and orientation.

4.3.1 Results for Two Point Statistical Power Law Model

The results for the two point statistical model can be seen in Fig 4-5 below. The values for ω_1 were found from section 4.2. For a well 50 feet away from the channel fringes, ω_1=0.1, for a well 100 feet away from the fringe ω_1=0.12, for a well150feet away ω_1=0.2, and finally ω_1= 0.7 for a well in mudstone, 200 feet away from the channel boundary. The correlation coefficient for each lag can also be seen in table 4-1 below

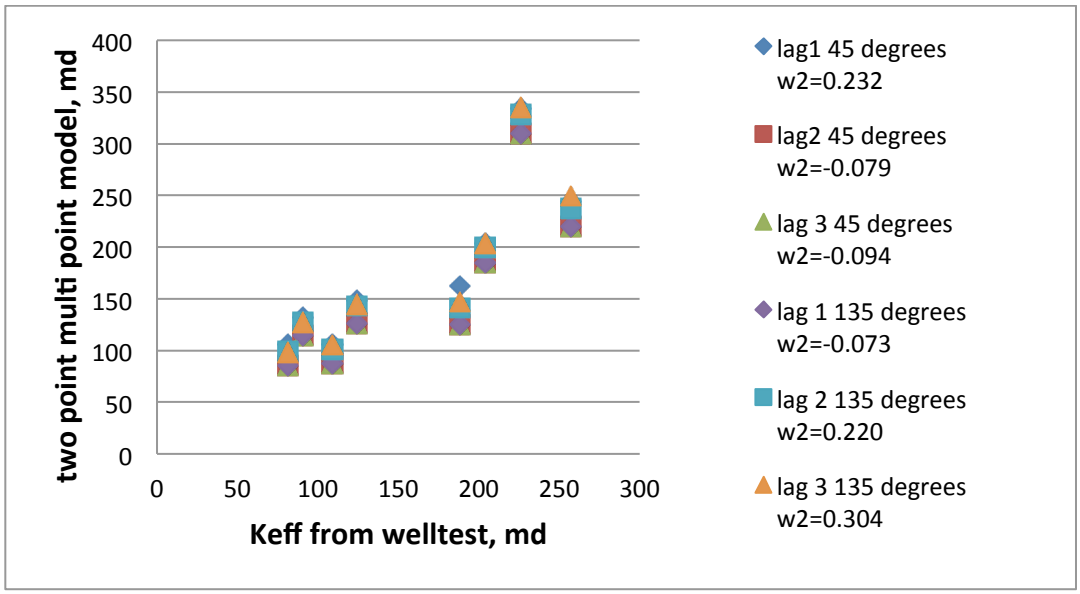

(A)

Fig 4-5

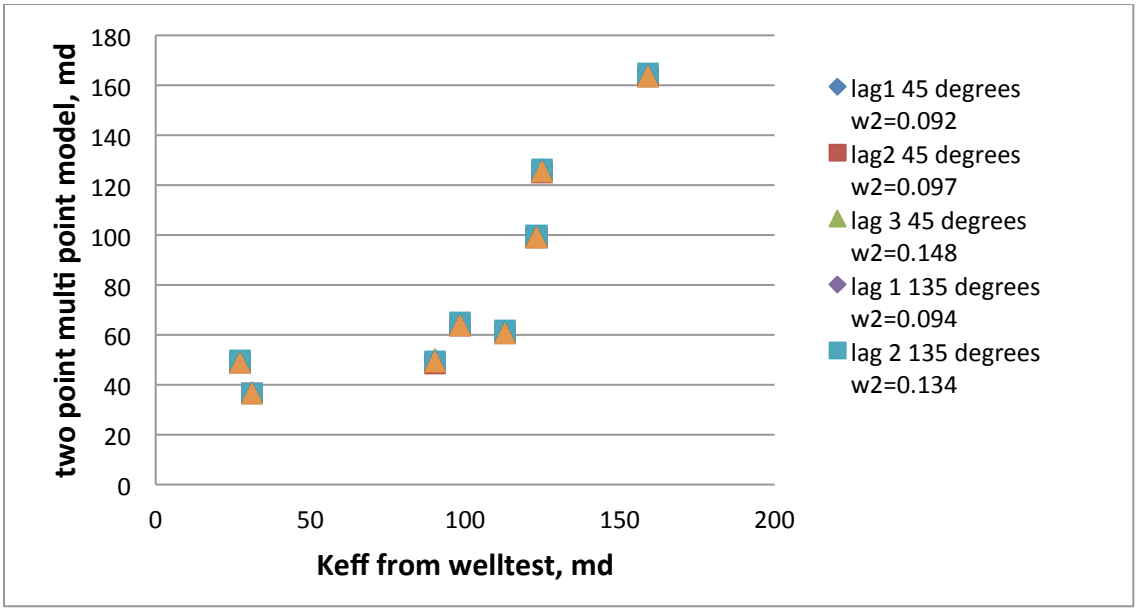
two point multi point model, md
180
160
140
120
100
80
60
40
20
0
0
50
100
150
200
Keff from welltest, md
lag1 45 degrees w2=0.092
lag2 45 degrees w2=0.097
lag 3 45 degrees w2=0.148
lag 1 135 degrees w2=0.094
lag 2 135 degrees w2=0.134

(B)

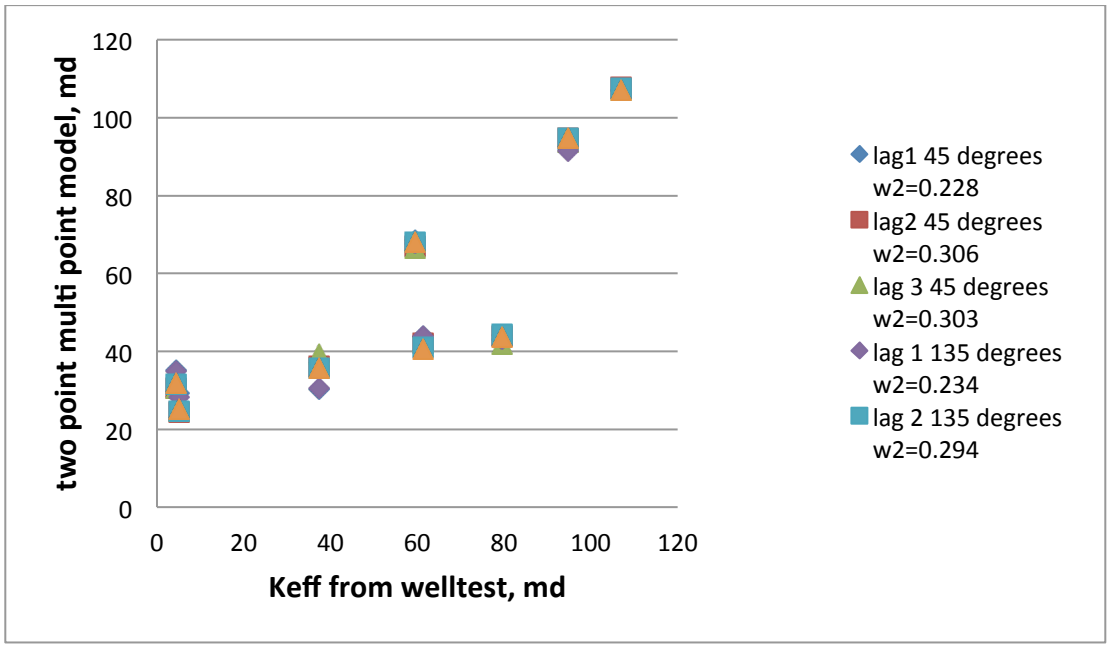
two point multi point model, md
120
100
80
60
40
20
0
0
20
40
60
80
100
120
Keff from welltest, md
lag1 45 degrees w2=0.228
lag2 45 degrees w2=0.306
lag 3 45 degrees w2=0.303
lag 1 135 degrees w2=0.234
lag 2 135 degrees w2=0.294

(C)

Fig 4-5

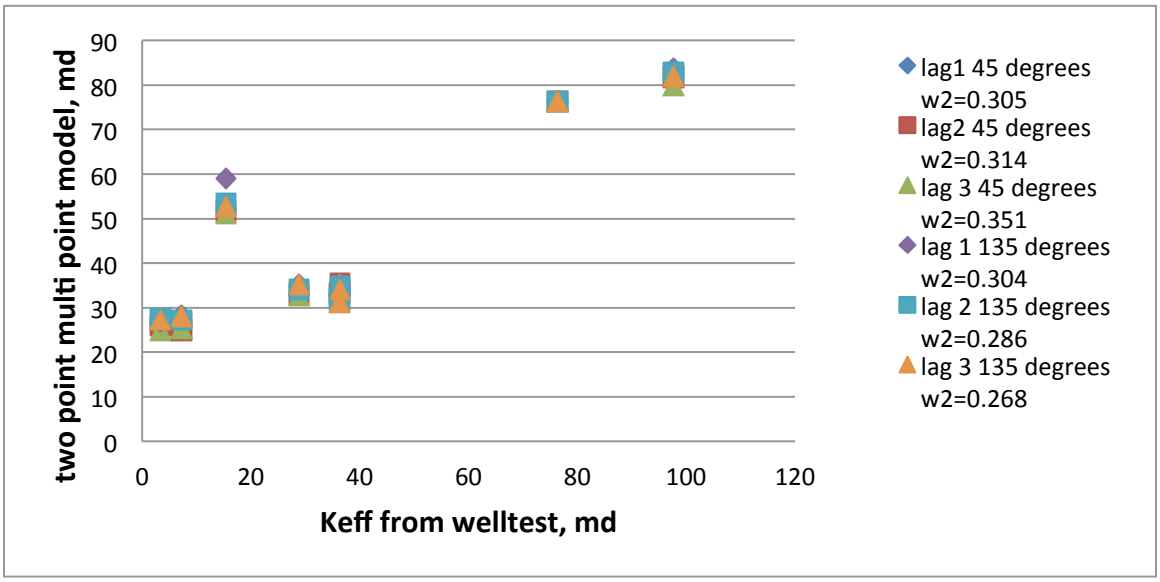

(D)

Fig 4-5 Two point geometrical averages for 10 wells completed for all lags and orientations where Keff = effective permeability calculated from the well test, and w2 is the parameter ω_2 from equation 4-3 at (a) 50 feet from the channel boundary(B) 100 feet from the channel boundary (C) 150 feet from the channel boundary (D) 200 feet from the channel boundary

	R^2 value			
	50ft	100ft	150ft	200ft
lag1	0.7109	0.6859	0.6883	0.7853
lag2	0.6748	0.6854	0.7366	0.7967
lag3	0.6748	0.6912	0.722	0.7863
lag1 135deg	0.6748	0.6862	0.69	0.71
lag2 135 deg	0.6798	0.6903	0.7247	0.7657
lag3 135 deg	0.7104	0.689	0.7169	0.7641

Table 4-1 Correlation coefficients for the graphs shown in Figures 4-5 where R^2 is the correlation coefficient, ft = feet, deg. = degrees

After comparing the results for different lags for each well position, it was found that the two point average corresponding to lag |**h**|=1 in the 45 degree direction gave the highest correlation (R^2=0.72) for a well completed one block away from the shale/channel boundary. The further away the well is located from the boundary, the larger the lag |**h**| that yields the best correlation.

Comparison of the results for a well completed in the channel close to the boundary at distances of 50 ft and 150 ft can be seen in Fig 4-6a,b corresponding to the template orientation of 45° and 135° respectively. For these cases ω_1 was held at 0.8 for the well completed 50 ft away and 1 for a well completed 150 ft away. The ω_2 established by regression was found to be similar regardless of the orientation of the template, with ω_2= 0.48 for the well close to the boundary and ω_2=0.46 for a well completed 150 ft away.

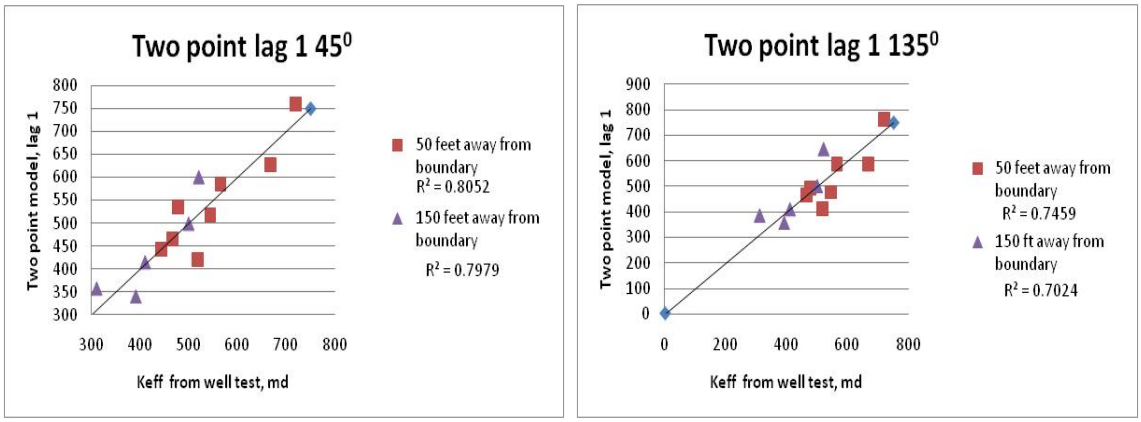

(A) (B)

Fig 4-6 Two point permeability averages for wells completed in a channel at distances 50 and 150 feet away from the mudstone boundary. (A) for a multiple point model taken in

the direction of the channels, 45° and (B) a multiple point model taken in the direction perpendicular to the channel, 135°

4.4 Three Point Permeability Average

The proxy expression was now terminated at the three-point term. This expanded expression now becomes:

$$k_{average} = \left[\frac{1}{n}\sum_{i=1}^{n} k^{\omega_1}(\mathbf{u}_i)\right]^{1/\omega_1} + \left[\frac{1}{n_h}\sum_{i=1}^{n_h} k(u_i)\cdot k(\mathbf{u}_i+\mathbf{h})\right]^{\omega_2} + \left[\frac{1}{n_g}\sum_{i=1}^{n_g} k(\mathbf{u}_i)\cdot k(\mathbf{u}_i+\mathbf{h})\cdot k(\mathbf{u}_i+2\mathbf{h})\right]^{\omega_3} \quad (4\text{-}4)$$

Because now we have to account for the joint occurrence of three permeability values on a template, the size of the template grid was expanded to 9x9 model. However, subsequently it was found that the results obtained using this expanded template grid were essentially the same as for a 7x7 template grid and so the reduced grid was utilized for all subsequent analysis. The Python code to calculate the three point averages can be seen in Appendix A.3.

In expression 4-4, n_h is the number of pairs observed in the template grid and n_g is the number of three-point occurrences in the 7x7 template. The three-point lags used for the calculation of the averages can be seen in Figure 4-6. The three-point averages were only calculated for lag $|\mathbf{h}|=1$ in the 45° and 135° directions.

(A) (B)

Fig 4-7 Lag configurations used for calculating three-point averages on a 7x7 template grid around the well: (A) 3 point 45 degrees (in orientation of channel) (B) 3 point 135 degrees (perpendicular to orientation of channel). . The corresponding number of occurrences of these lags in the 7 x 7 template grid are also noted.

The Microsoft Excel function solver was used to calculate the optimum ω_2 and ω_3 exponents by minimizing the square difference between the $K_{effective}$ from the well test and the $K_{average}$ calculated from equation 4-4. Like in the two point permeability average case, the optimum ω_1 from section 4.2 were used for each case of well location with respect to the channel.

4.4.1 Results for Three Point Statistical Model

After using the solver to optimize the ω_2 and ω_3 values, the following results were obtained as seen in Fig 4-8

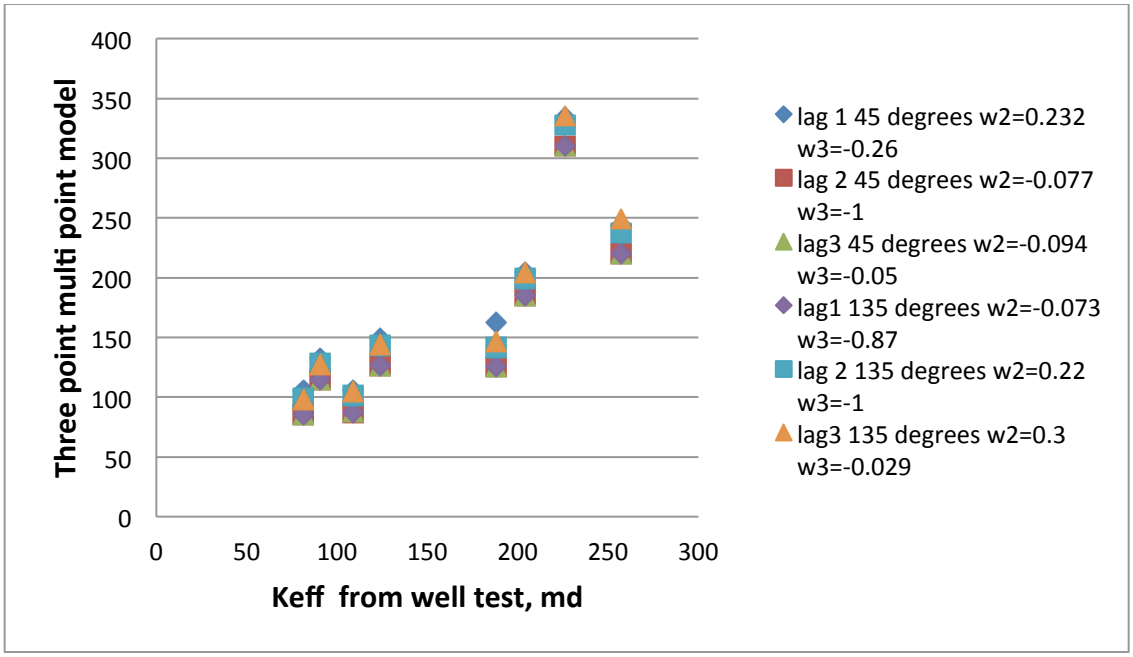
Three point multi point model
400
350
300
250
200
150
100
50
0
0
50
100
150
200
250
300
Keff from well test, md
lag 1 45 degrees w2=0.232 w3=-0.26
lag 2 45 degrees w2=-0.077 w3=-1
lag3 45 degrees w2=-0.094 w3=-0.05
lag1 135 degrees w2=-0.073 w3=-0.87
lag 2 135 degrees w2=0.22 w3=-1
lag3 135 degrees w2=0.3 w3=-0.029

(A)

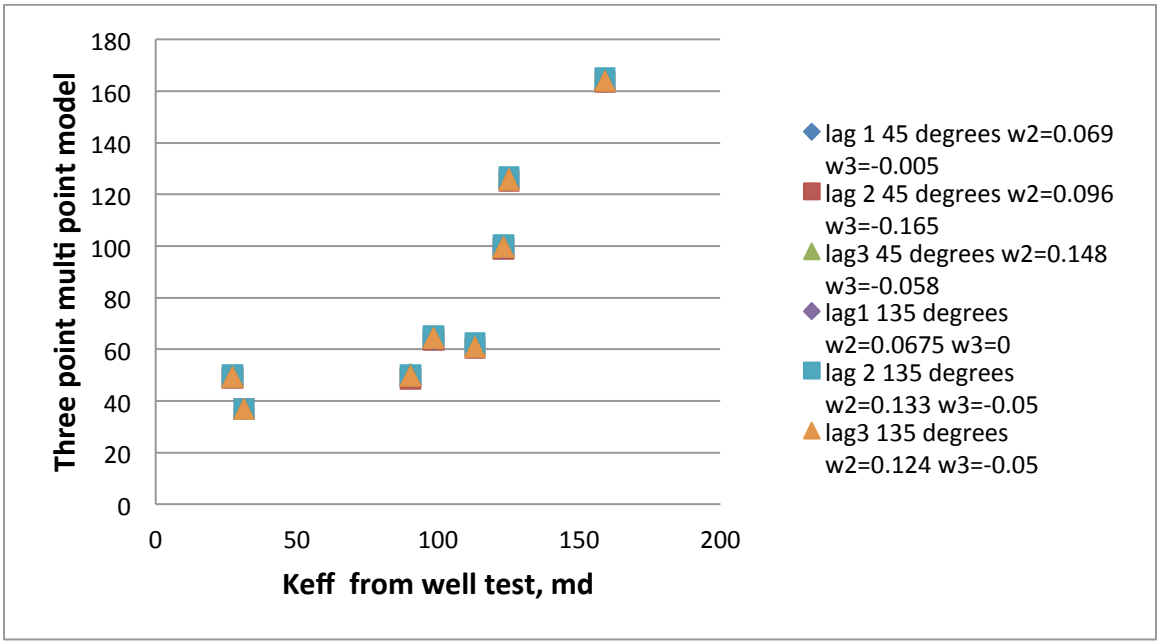
Three point multi point model
180
160
140
120
100
80
60
40
20
0
0
50
100
150
200
Keff from well test, md
lag 1 45 degrees w2=0.069 w3=-0.005
lag 2 45 degrees w2=0.096 w3=-0.165
lag3 45 degrees w2=0.148 w3=-0.058
lag1 135 degrees w2=0.0675 w3=0
lag 2 135 degrees w2=0.133 w3=-0.05
lag3 135 degrees w2=0.124 w3=-0.05

(B)

Fig 4-8

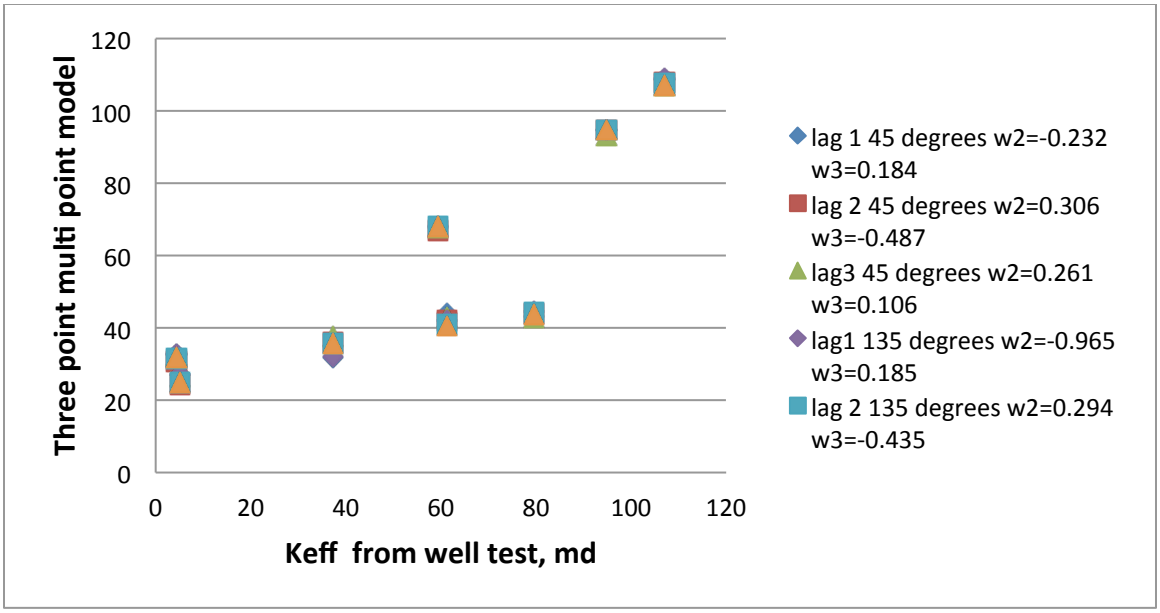

(C)

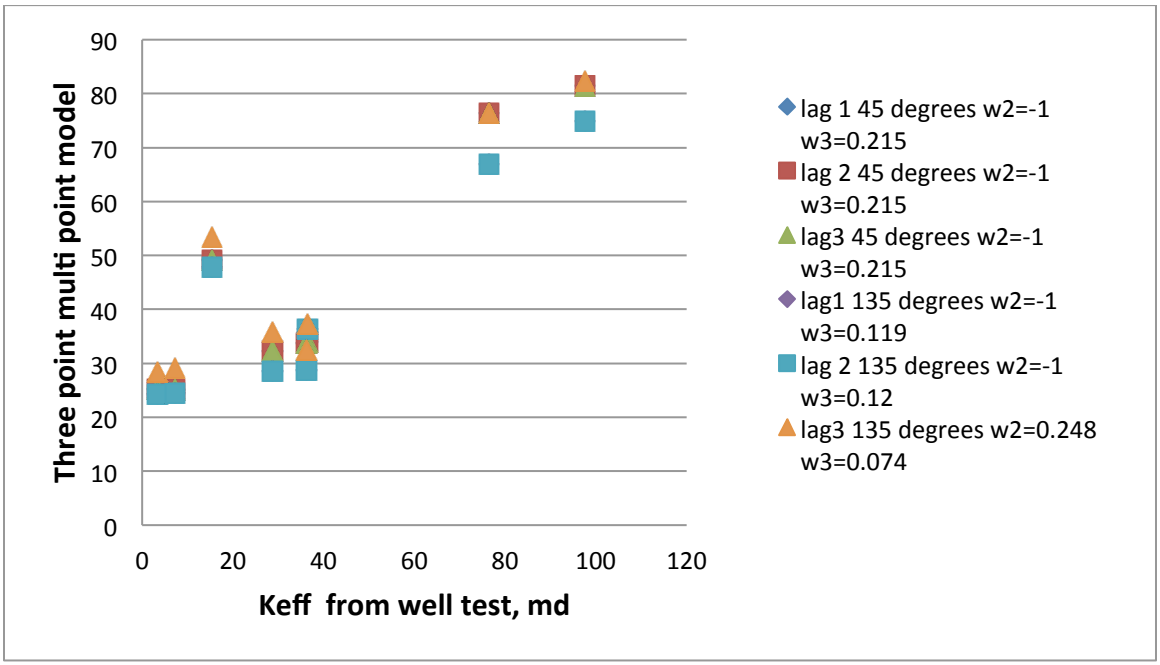

(D)

Fig 4-8 Three point geometrical averages for 10 wells completed for all lags and orientation s at (a) 50 feet from the channel boundary(B) 100 feet from the channel boundary (C) 150 feet from the channel boundary (D) 200 feet from the channel boundary

	R^2 value			
	50ft	100ft	150ft	200ft
lag1	0.7108	0.686	0.7107	0.819
lag2	0.6747	0.6855	0.7366	0.819
lag3	0.6747	0.6914	0.7142	0.819
lag1 135deg	0.6748	0.6861	0.712	0.786
lag2 135 deg	0.6798	0.6903	0.7247	0.786
lag3 135 deg	0.7091	0.689	0.7169	0.7743

Table 4-2 Correlation Coefficients for graphs shown in Figures 4-8 where R^2 is the correlation coefficient between the K_{eff} from the well test and the $K_{average}$ from the geostatistics

From the plots in Fig 4-8 it can be seen that for a well completed 4 blocks away from the channel boundary, the optimal exponent for the two-point term is often close to ω_2=-1 for most of the lags. This implies that the two-point average contributes very little to the total permeability average. When the well is located some distances say 200ft away from the boundary, the R^2 for the 3-point permeability average increases significantly from the two-point model. As the well moves closer to the boundary, the R^2 value remains fairly the same as the two-point model.

Because it is not obvious, whether the two-point and the three-point terms carry redundant information, the permeability average was computed again by retaining only the three-point term:

$$k_{average} = \left[\frac{1}{n}\sum_{i=1}^{n} k^{\omega_1}(\mathbf{u}_i)\right]^{1/\omega_1} + \left[\frac{1}{n_g}\sum_{i=1}^{n_g} k(\mathbf{u}_i)\cdot k(\mathbf{u}_i+\mathbf{h})\cdot k(\mathbf{u}_i+2\mathbf{h})\right]^{\omega_3} \quad (4\text{-}5)$$

The solver function in Microsoft Excel was then used to minimize the difference between k_{eff} from the well test and $k_{average}$ from equation 4-5 and compared to the $k_{average}$ for the two point model from equation 4-3. The results for the single-point permeability average, the two-point permeability average and the three-point average using Eq. 4-5 were compared for the 45 degree and 135 degree template orientation for lag $|\mathbf{h}|=1$. The results can be seen in table 4-3- table 4-5.

	single point average	
	ω_1	R^2
50ft	0.1	0.6748
100ft	0.1	0.6848
150ft	0.2	0.64
200ft	0.7	0.7434

Table 4-3 Results for the single point model with the calculated optimum parameter, ω_1 from equation 4-2 and correlation coefficient R^2

	two point average for lag h=1		
	ω_1	ω_2	R^2
50ft	0.1	0.232	0.7109
100ft	0.1	0.092	0.6859
150ft	0.2	0.228	0.6883
200ft	0.7	0.305	0.7853

Table 4-4 Results for the two point model with the calculated optimum parameters, ω_1 and ω_2 from equation 4-3 and correlation coefficient R^2

	three point average for lag h=1			
	ω_1	ω_2	ω_3	R^2
50ft	0.1	0.232	0.26	0.7109
100ft	0.1	0.069	0.005	0.686
150ft	0.2	0.232	0.184	0.7107
200ft	0.7	-1	0.215	0.819

Table 4-5 Results for the three point model with the calculated optimum parameters, ω_1, ω_2 and ω_3 from equation 4-3 and correlation coefficient R^2

It is observed in table 4-3- table 4-5 that when the well is located sufficiently close to the channel boundary, all the averages perform equally well and the correlation coefficient is fairly uniform regardless of what model is used. When the well moves to more than 100 ft away from the boundary, templates in the direction of the channel (45^o) provide the best estimate. The three point model gives the highest correlation coefficient

in these cases indicating that the spatial connectivity of the permeability field influences the well test response.

Figure 4-9 summarizes the results using Eq. 4-5 for the templates in the 45^o and 135^o orientations respectively. The ω_3 were fairly constant for different orientations; ω_3=0.32 and 0.31. The correlation coefficient was fairly constant for different distances away from the boundary and can be viewed in Fig 4-9

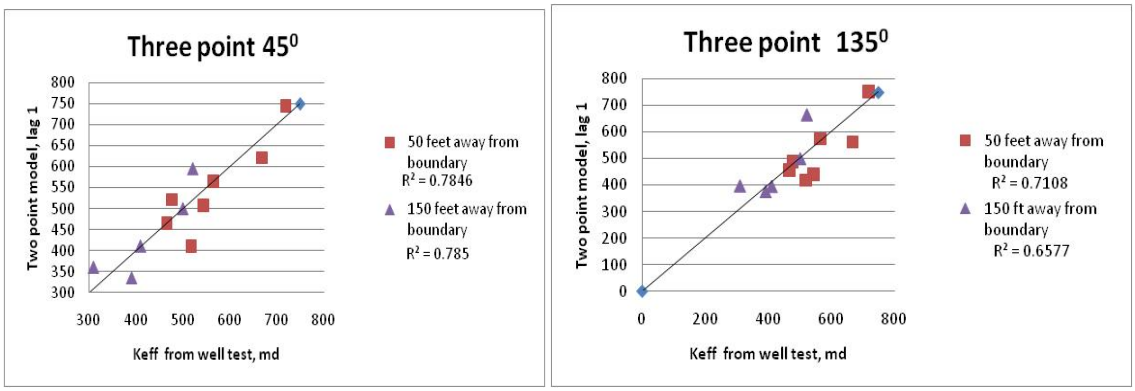

(A) (B)

Fig 4-9 Three point model for a well completed in a channel at distances 50 and 150 feet away from the mudstone boundary. (A) In direction of channel orientation (45^o), (B) perpendicular to channel orientation (135^o)

The preceding cases corresponded to cases where the well was moved from inside the channel to locations close to the boundary and then on to the mudstone. The analysis was repeated when the well is moved from mudstone to close to the channel boundary. Fig 4-10 shows that for wells completed close to the boundary the best fit is from the single point model while the multiple-point models provide better fits as the well moves farther from the boundary.

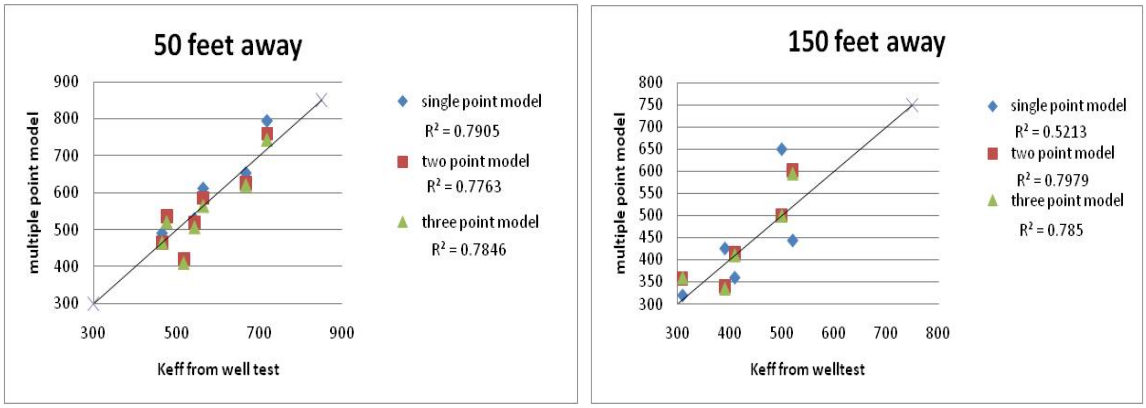

(A) (B)

Fig 4-10 Comparison of the Three statistical models for a well completed in the channel at a distance away from the mudstone boundary for (A) 50 feet away from the mudstone region, (B) for 150 feet away from the mudstone region.

4.5 Computing for Different Permeability Channel Maps

To ensure that the trend discussed above hold for different training images the same process was repeated for two other realizations that are shown in in Figures 3-7b and Figure 3-7c. The two and three point averages were computed for $|\mathbf{h}|=1$ since that lag configuration provided the best results for realization 1. After solving for the optimum ω_2 and ω_3, similar trends were seen as the results of realization 1 with the single point average being optimal for wells completed less than 100 ft away from the channel-mudstone boundary, while the three-point average worked best when the well was completed at a distance greater than 100 ft away from the boundary. The ω values can be seen in Tables 4-6A, B, C and D below.

50 ft from boundary

Statistical Method	realization 1	realization 12	Realization 36
single point			
ω_1	0.1	0.1	0.1
R^2	0.6748	0.6029	0.9138
Two Point			
ω_1	0.1	0.1	0.1
ω_2	0.232	0.26	0.240
R^2	0.7108	0.6431	0.920
Three Point			
ω_1	0.1	0.1	0.1
ω_2	0.232	0.250	0.240
ω_3	0.260	0.270	0.240
R^2	0.7108	0.668	0.920

(A)

100 ft from boundary

Statistical Method	realization 1	realization 12	Realization 36
single point			
ω_1	0.11	0.11	0.12
R^2	0.6634	0.5674	0.7531
Two Point			
ω_1	0.11	0.11	0.12
ω_2	0.23	0.25	0.21
R^2	0.6859	0.5874	0.7723
Three Point			
ω_1	0.11	0.11	0.12
ω_2	0.069	0.12	0.09
ω_3	0.005	0.009	0.003
R^2	0.686	0.59	0.773

(B)

150 ft from boundary

Statistical Method	realization 1	realization 12	Realization 36
single point			
ω_1	0.2	0.2	0.2
R^2	0.6451	0.5803	0.8078
Two Point			
ω_1	0.2	0.2	0.2
ω_2	0.228	0.29	0.243
R^2	0.6883	0.63	0.6521
Three Point			
ω_1	0.2	0.2	0.2
ω_2	-0.232	-0.431	-0.413
ω_3	0.184	0.256	0.232
R^2	0.7107	0.6634	0.6749

(C)

200 ft from boundary

Statistical Method	realization 1	realization 12	Realization 36
single point			
ω_1	0.7	0.7	0.7
R^2	0.7434	0.6103	0.8611
Two Point			
ω_1	0.7	0.7	0.7
ω_2	0.305	0.283	0.341
R^2	0.7853	0.6453	0.89
Three Point			
ω_1	0.7	0.7	0.7
ω_2	-1	-1	-1
ω_3	0.215	0.243	0.198
R^2	0.819	0.684	0.91

(D)

Table 4-6 Results for the multiple point models done on the three realizations for (A) well completed 50 feet from the boundary (B) 100 feet from the boundary (C) 150 feet from the boundary (D) 200 feet from the boundary

From Table 4-4 we can see that the single-point average exponent ω_1 holds constant from realization to realization but the performance of that average gets progressively worse the further away from the channel the well is completed. The performance of the average improves with the inclusion of multiple-point terms. The exponents ω_2 and ω_3 are fairly stable from one realization to the next indicating that even though the realizations may appear to be different from each other superficially, they exhibit similar connectivity characteristics that can be quite reliably calibrated from the well test. The correlation coefficient however was still highest when the three-point permeability average was computed in all the cases.

4.6 Conclusion

Based on the results obtained in this chapter it was found that the performance of the permeability average is very dependent on the distance of the well from the channel/mudstone boundary. For wells completed less than 100 feet from the boundary a single point model is sufficient. From table 4-4 it can be seen that the R^2 value does not change with the higher order terms for small distances away from the channel. In such a case, the nodes in the template grid are divided almost equally between the high-permeability channel values and the low permeability shale values and thus equal weight assigned to each template node provides a good average. However as the well moves further from a boundary and fewer nodes have either high-permeability channel values or alternatively low-permeability mudstone values, more weight will need to be applied to those less-frequent node values. For this reason, the multiple-point $k_{average}$ tend to be more

accurate. This is reflected in Table 4-3 and Table 4-4 as the R^2 are improved significantly with the addition of higher order terms.

It also seemed that the only constant between realizations was the value of ω_1. The ω_2 and ω_3 values especially for the cases when the well is far from the channel boundary tend to vary significantly from one realization to the next. Nevertheless, the results in this chapter point to the feasibility of using the exponents of the multiple point averages to detect proximity of well to facies boundary in a typical turbidite system for a specific case but not from realization to realization.

Chapter 5: Application to Deep Sea Field in Gulf of Mexico

5.1 Overview

The previous results relating to the performance of the multiple point permeability proxy were all for synthetic cases. This chapter applies the proxy to analyze the well test data for the Lobster field (Ewing bank) in the Gulf of Mexico. The field is about 1400 acres in area and is characterized by a highly channelized turbidite lobe environment. The reservoir is thought to consist of three main lobes that span over different lengths in different parts of the field. This chapter will attempt to analyze the well test to determine the proximity of the wells to lobe and channel boundaries .

5.2 Ewing Bank Background

Data available for this study consists of 18 wells spread over the reservoir area as shown in Fig 5-1. The reservoir consists of six different sand lobes within the three compartments that can be seen in Fig 5-2. These compartments have been established on the basis of pressure surveys, 3D seismic analysis and log analysis.

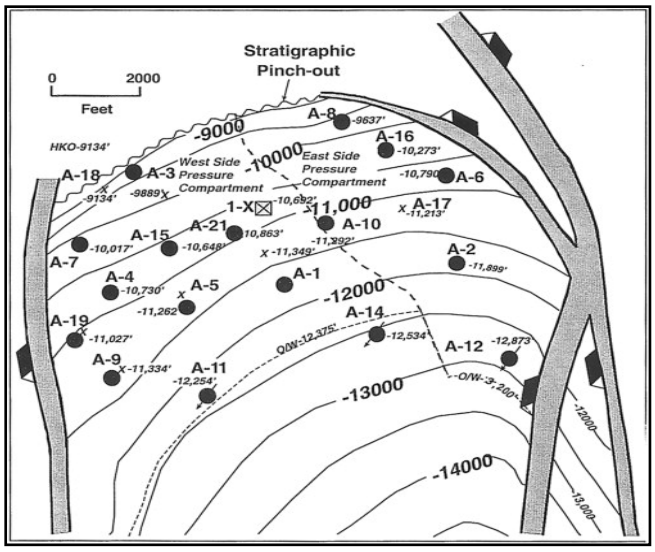

Fig 5-1 Surface location of the 18 wells located in the Ewing block 873 (**after Burk, Brown, & Petro., 1999**)

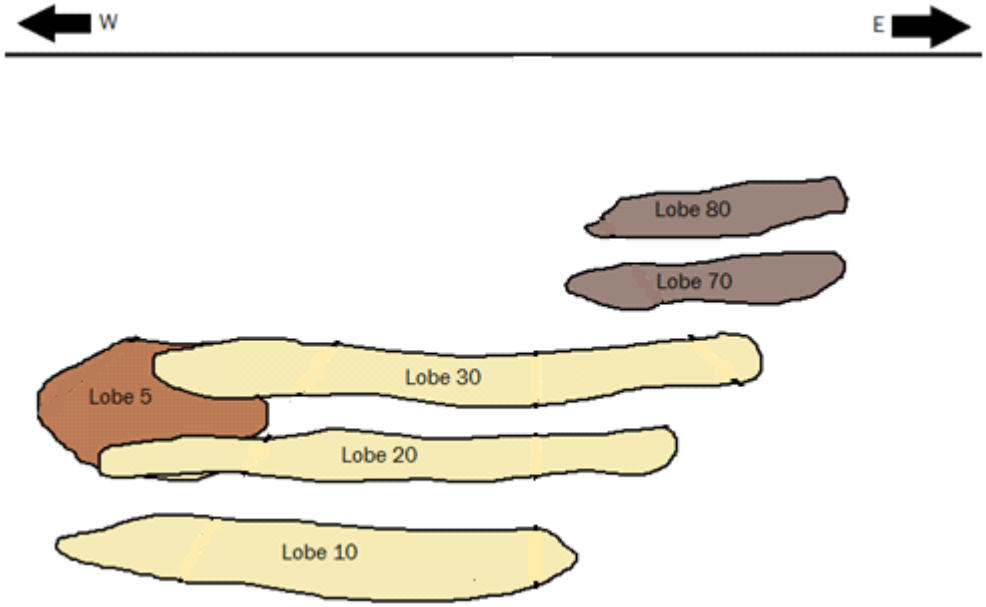

Fig 5-2 The arrangement of six sand lobes in the Ewing block 783 reservoir area.

The three different compartments in the area is evidenced in the pressure decline observed in these different regions as shown in Fig 5-3.

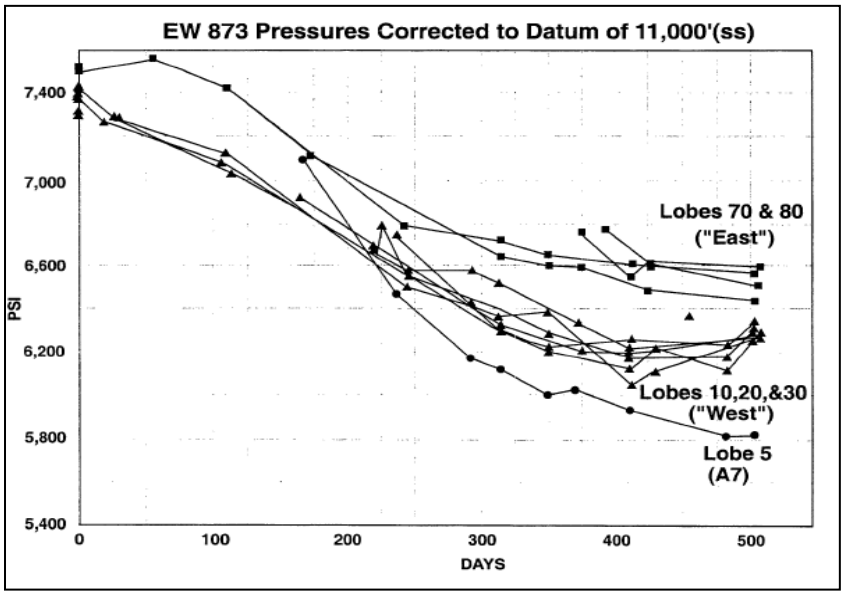

Fig 5-3 Decline in reservoir pressure normalized to 11,000' in the Ewing Bank Block 873. Note the different pressure decline trends where lobe 70 and 80 that display similar trends are located in the east bank, lobes 10, 20 and 30 display similar trends and are mainly located in the west bank. Lobe 5 has its own characteristic pressure decline and is located in the far west bank.

5.3 Well Test Data

Build-up test for 12 wells in the reservoir area (Fig 5-4) were made available by the operator however most tests were only a couple of hours in duration and no boundary effects could be detected in the well test records. From the tests that were of long enough duration, it was clearly seen that the wells were located in channels with the influence of shale boundary clearly seen in the derivative plot.

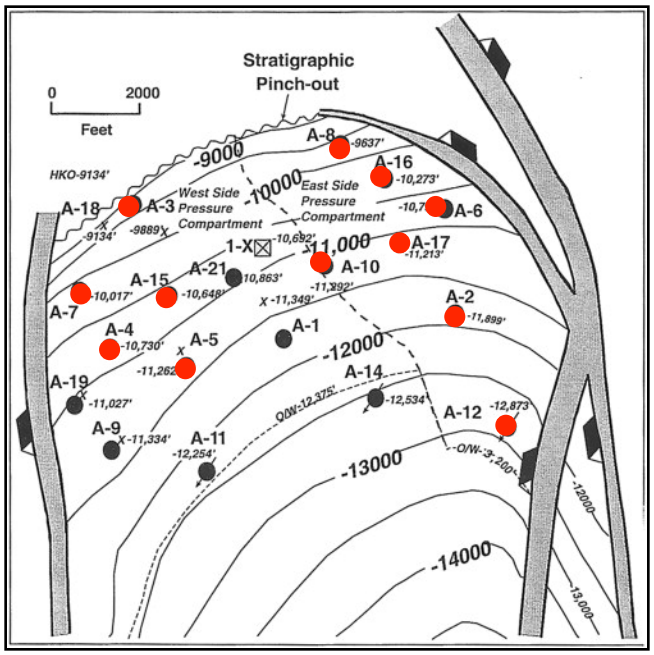

Fig 5-4 The locations of the wells (red dots) where build up test data was available for analysis.

A focus was especially put on the wells located in the eastern region of the reservoir close to the fault boundary. In Well A-6 for example shown in Fig. 5-5, the derivative plot shows the presence of a no-flow boundary exists approximately 200 ft away which can also be seen on the surface map (Fig. 5-4) where a fault is present to the East. The plot shows a change in the slope of the derivative plot (after stabilization of flow) after 0.3 hours indicating that a low permeability/ no flow zone has been detected.

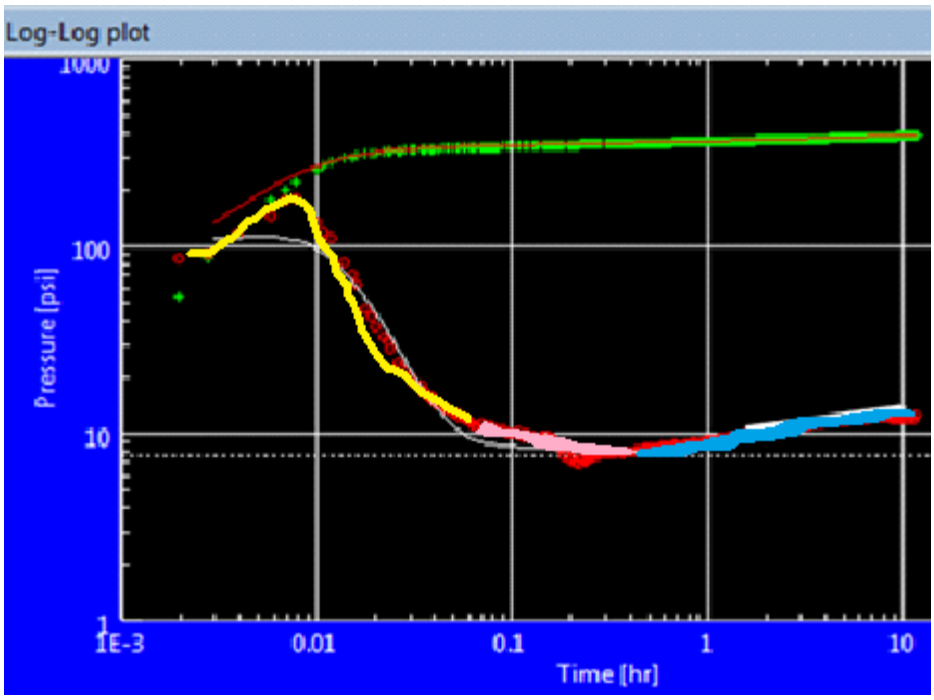

Fig 5-5 Derivative plot for Well A-6 in East bank of Ewing block 873. After the initial wellbore storage (yellow line) there is a change in slope (blue line) after the stabilization period (pink line)is indicative of a no flow boundary

Well A-10 also has been extensively monitored and is expected to be on the border between the eastern region and the middle region. Well A-10 is completed in 3 different sand lobes, lobe 70, lobe 30 and lobe 10. Most of the buildup tests done on this well were carried out for comingled production from the three lobes. The most extensive test was done in Sept 97 where the well was shut in for 1000 hours. The profile for this test can be seen in Fig 5-6a. The profile indicates that the East and west boundaries were calculated to be 1000's of feet away while the north and south boundaries are a couple hundred feet away. These boundaries were outputted from the analysis done in Saphir by Marathon for the Ewing Bank reservoir where a rectangular drainage area was specified.

The boundaries picked up are where the channel lobes meet the shale turbidite regions. . In July 2009 a 10 hour buildup test was done isolating production from lobe 70 alone. This test can be seen in Fig 5-6b. The isolated test picks up boundary effects after only two hours compared to thirty hours for the non-isolated test. This indicated that lobe 70 is not as extensive as the other two lobes. The results of this test allows us to see that lobe 70 only exists in the East bank while lobe 30 and 10 extend further into other reservoir regions.

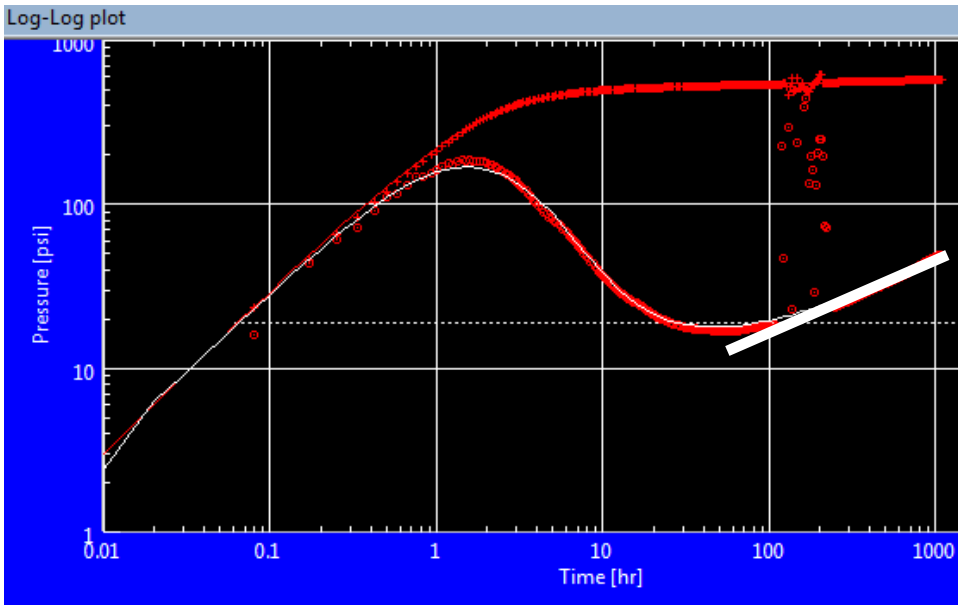

(A)

Fig 5-6

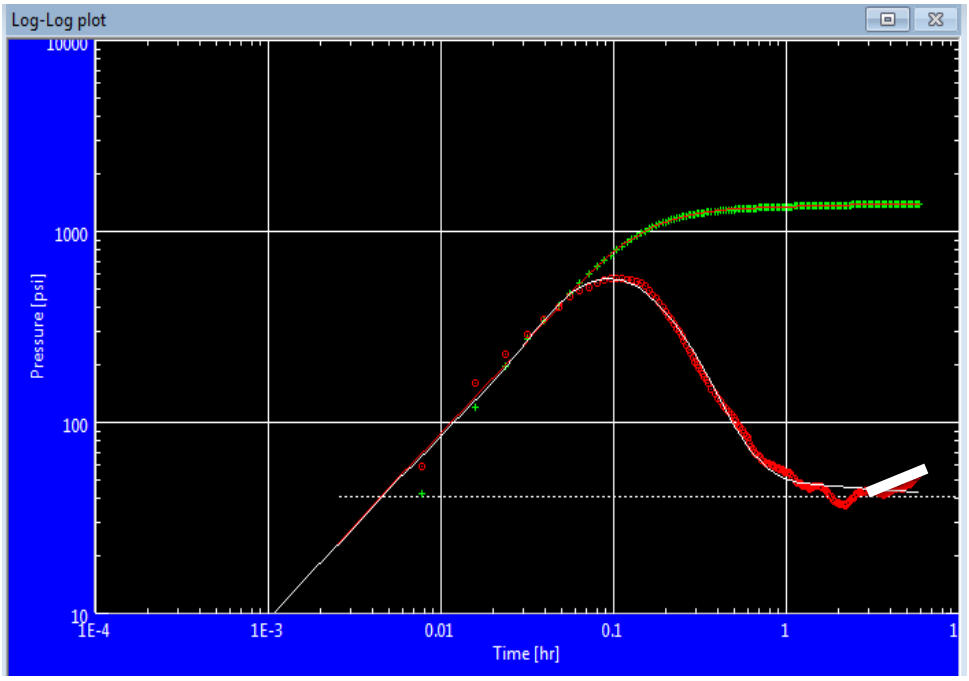

(B)

Fig 5-6 Build up test done on well A-10, (A) 1000 hour shut-in done after flow from three sand lobes 10, 30 and 70. The derivative plot shows a change in slope at 30 hours (white line depicts change) (B) 10 hour shut in done after isolating flow from lobe 70 only, change in slope (indicated by the white line) after two hours depicts boundary.

5.4 Well test interpretation using the multiple point proxy

In this section the wells completed in lobes 10 and 20 will be investigated to see if we can determine proximity of the well to channel or other facies boundaries. For this, we will use a reservoir model for the spatial extent of lobes 10 and 20 that has been developed constrained to the available well information and taking into account the basic physics of turbidite flow. Well test responses will be simulated on the reservoir model and an attempt will be made to try and match the effective permeability values using multiple point statistics and the ω values solved in chapter 4 .

5.4.1 Analysis of well test

Three wells located in lobes 10 and 20 are well A-01, A-04 and A-05. A-04 and A-05 have accompanying build up test profiles and can be seen in Fig 5-7 and fig 5-8 respectively.

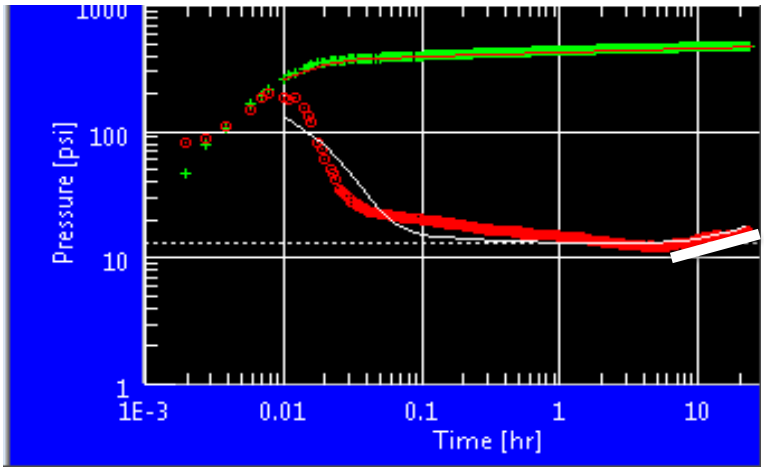

Fig 5-7 Buid up test profile for well A-04 showing the log-log derivative plot showing the presence of a boundary by change of slope at 6 hours (white line)

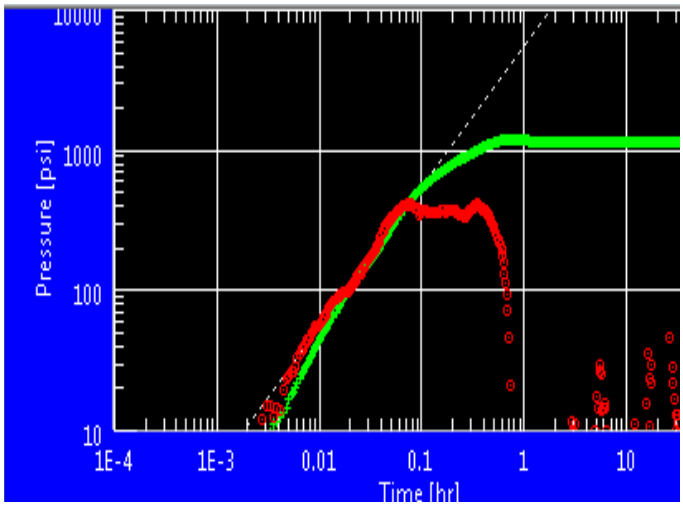

Fig 5-8 Build up test profile for well A-05 showing the log-log derivative plot showing after well bore storage the data becomes noisy and unable to analyze

Looking at the derivative plots for Well A-04 (Fig. 5-7) and that for well A-05 (Fig 5-8) it is clear that the well A-05 data is noisy after the initial wellbore storage period and any interpretation may prove incorrect. Consequently, Zambrano models for the influence of close channel boundaries were used to analyze the results for well A-04.

In well A-04, after the initial wellbore storage, a period of flow stabilization takes place , which is indicated by a straight line of zero slope in the derivative plot. This is followed by a change in slope. Unfortunately due to the inadequate duration of the test we are unsure of how the derivative plot will behave and if it will stabilize and then a slope change will take place as in Fig 2-7 for a well completed in a channel with asymmetric composite thickness profile or if the plot will stabilize and stay straight as in a well within a channel with symmetric composite thickness profile as shown in Fig 2-8. If the derivative plot trend keeps rising and never stabilizes it will indicate that the well is completed in a sinuous channel with constant thickness.

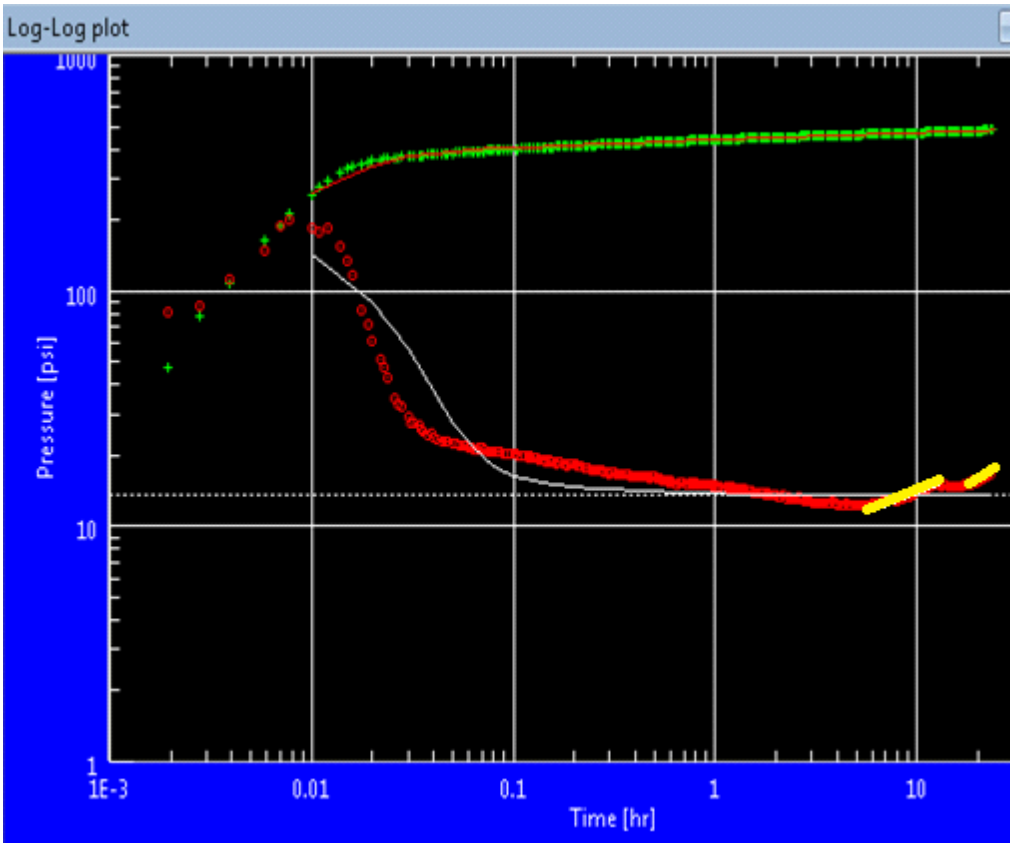

Fig 5-9 The log-log derivative plot for well A-04 enlarged showing the two distinct half slopes (yellow lines) indicating presence of asymmetric channel as in Fig 5-10

Looking closely at the log-log plot and the limited amount of data available, a slight second stabilization period seems to occur followed by a change in slope. This is closely matched by the channel with an asymmetric thickness profile as shown in fig 2-7 and repeated in Fig 5-10

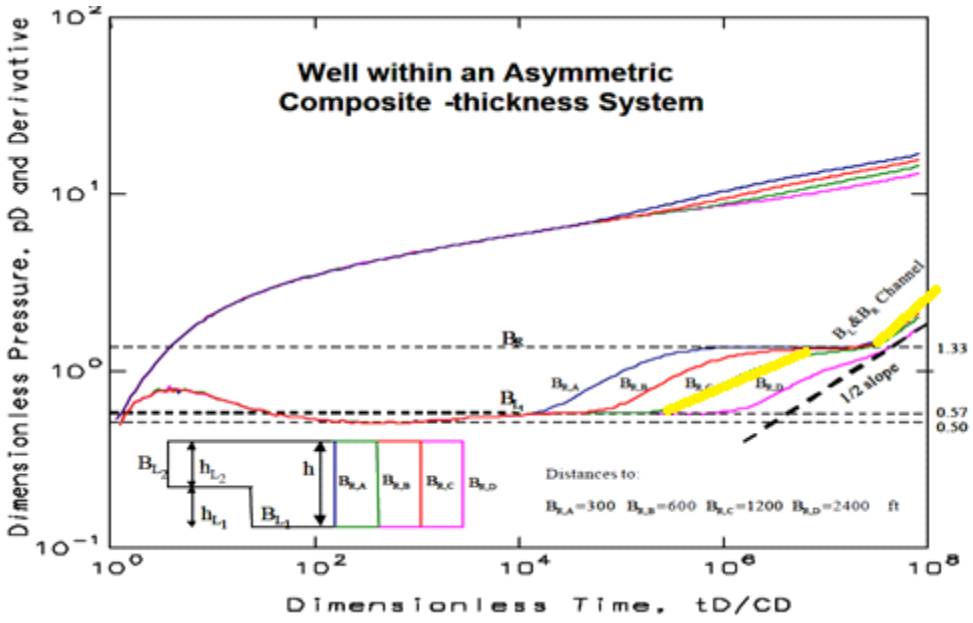

Fig 5-10 Log-log plot of drawdown test on well within a channel with asymmetric composite thickness profile. The change in slope indicates the location of a flow boundary or lower permeability close by. The two yellow lines indicate ½ slopes similar to that of well A-04 as in Fig 5-9

Due to the quick change in slope after the second stabilization after the 10 hour mark it is likely that the channel more follows the pink line in Fig 5-10 indicating that the boundary is far on one end. After performing the analysis of the plots the effective permeability was found to be 1240 md.

5.4.2 Application of the multiple point proxy

A reservoir model was created for the extent of Lobes 10 and 20 in the Ewing Bank area. This model includes the logging data at wells A-01, A-04 and A-05. The details of the model development process are in Srinivasan (2011). The reservoir model can be seen in Fig 5-11 were the permeability values are shown. The model includes

channels (1500md), channel fringe sands (800md), levies (200md) and mudstone (20md). The permeability values assigned to the different facies are typical values. Core data and any other permeability related information was unavailable. The model is a 100x100x10 grid system where thickness has also been modeled to provide a more accurate model.

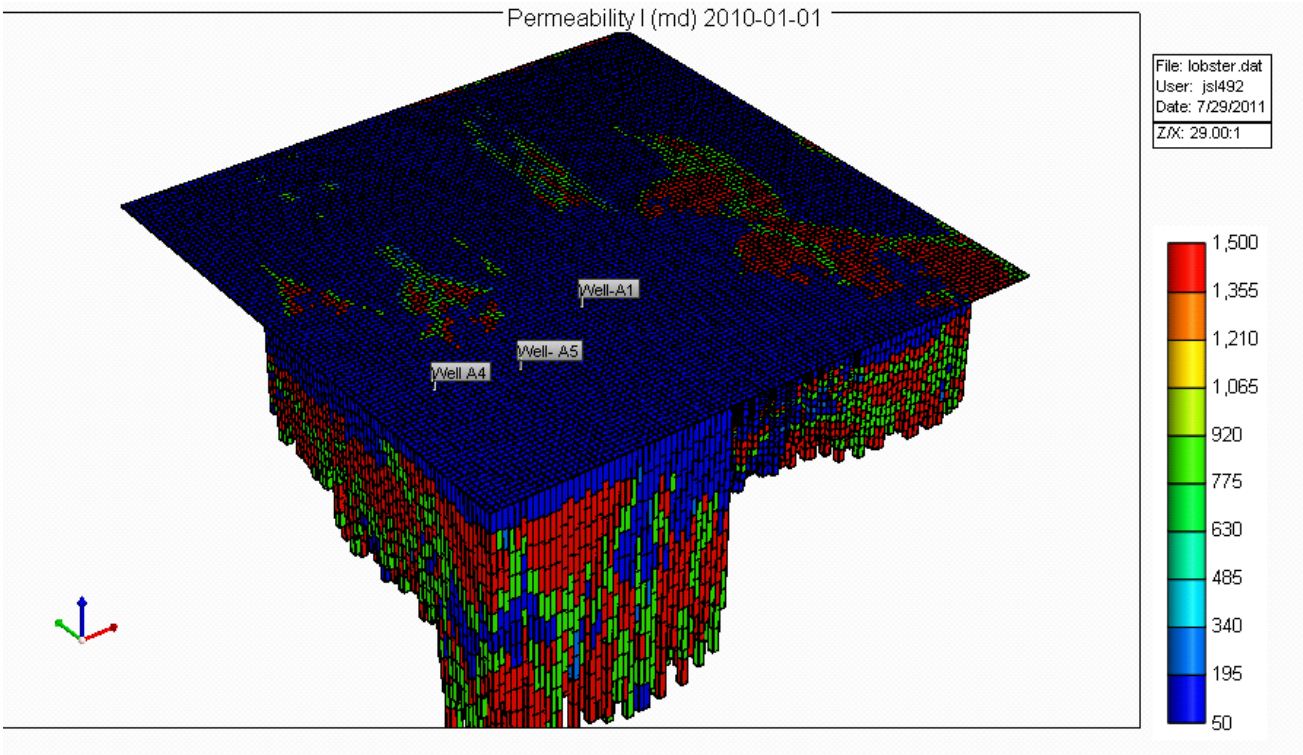

Fig 5-11. 3-D view of the Ewing bank Permeability reservoir model showing the vertical stacking of channel sands.

The permeability variation over each layer of the reservoir model is shown in Figures 5-12a - Fig 5-12, where the location of well A-04 is also identified. To estimate ω parameter values the mode was split up into layers so that we can estimate the channel proximity for each layer individually. The objective is to fit an optimal ω parameter such

that the average of all the layer permeabilities fits the observed effective permeability from the well test.

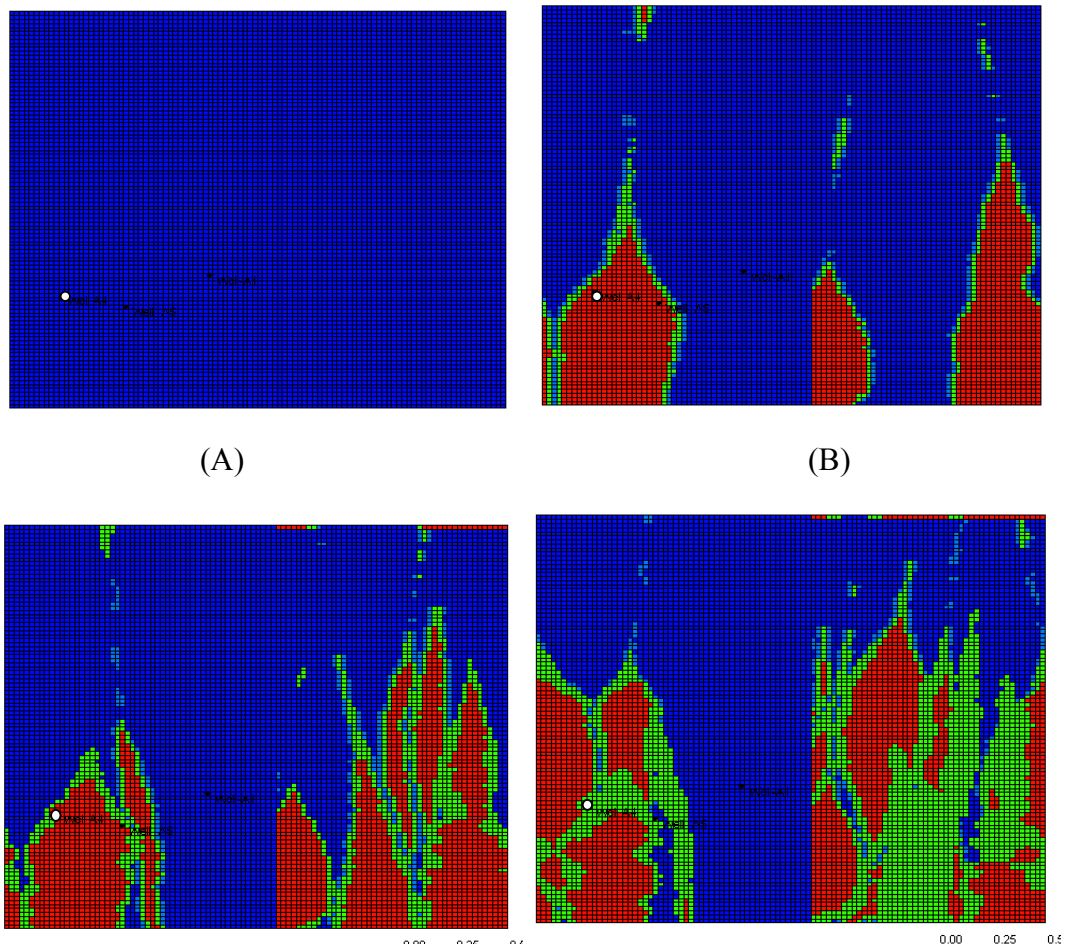

(A) (B)

(C) (D)

Fig 5-12

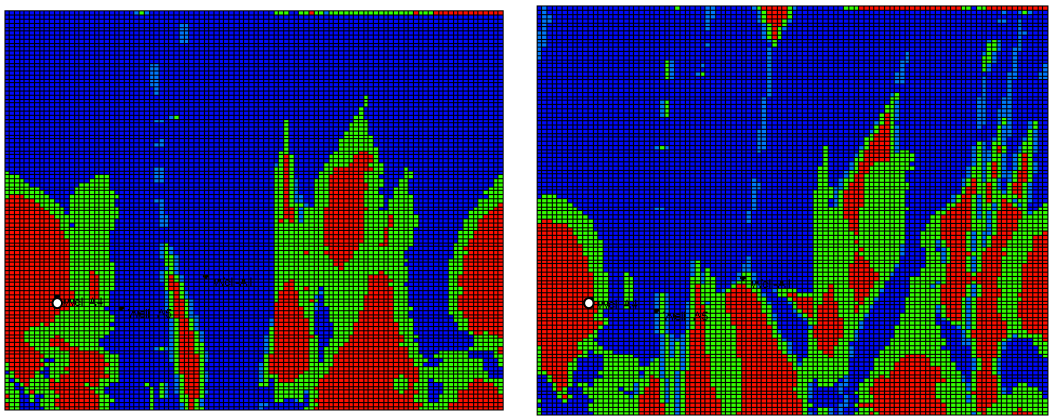

(E) (F)

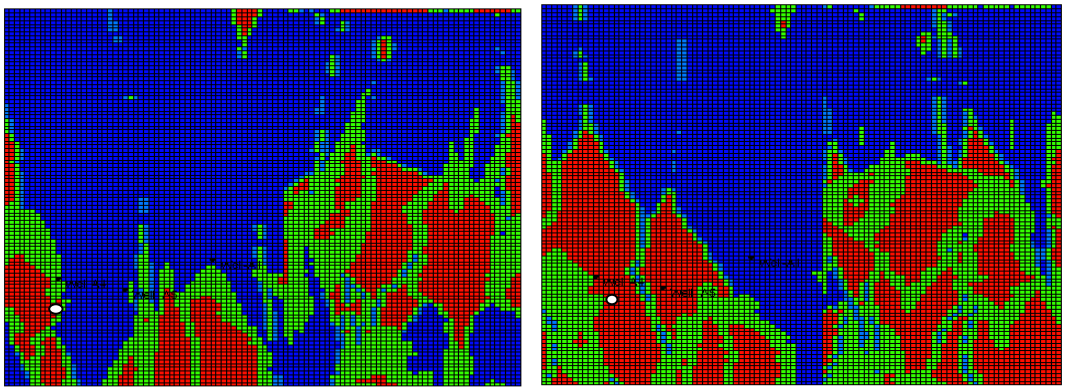

(G) (H)

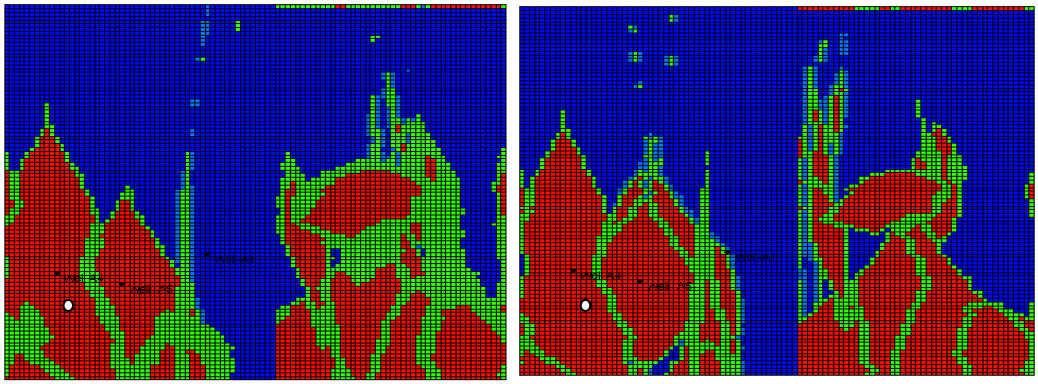

(I) (J)

Fig 5-12 Permeability values for each layer in the Ewing Bank Reservoir model with Well A-04 marked by the white circle for (A) layer 1 (B) layer 2 (C) layer 3 (D) layer 4 (E) layer 5 (F) layer 6 (G) layer 7 (H) layer 8 (I) layer 9 (J) layer 10 where red is channel sands (1500md), green is channel fringe sand (800md) and blue is shale zones (20md

Based on well location in the sands it can be seen that well A-04 is always in a channel lobe while A-5 is only in the channel lobes towards the deeper layers and on the fringes at the shallower depths. Well A-01 is in the mudstone at shallower depths and on the fringes at deeper depths. Since well A-04 is the only well with a full build up analysis done that will be the focus of this study.

5.4.3 Application of multiple point proxy

The simplest model to apply is the single point model as seen in section 4.2. it must be recalled that for zones where the well were far away from any heterogeneity the optimum value of the exponent comes out to be $\omega=1$. As the well moves closer to the boundary of channels, the optimum value of ω starts deviating from 1. For wells located 100ft away ω came out to be 0.8. When the well was in the fringe sands close to the channel ω was shown to tend to 0.1. Using the single point model a permeability of 1,211 md was calculated which is an underestimation of the simulated effective permeability of 1243 md. In this case ω was set equal to one since for most layers the well was completed more than 100 feet away from the channel boundary. After applying the two point model holding ω_1 to be the same as in the single point case and the optimum value of ω_2 came out to be 0.24 which is indicative of a well in the vicinity of a channel boundary. an estimate of 1,242 md was calculated which is close to the effective permeability of the well test.. Using the three point model setting $\omega_2=-1$ and $\omega_3=0.165$ which was the low for a well more than 200 feet away from the boundary a permeability

of 1243 was calculated which is very close to the effective permeability estimated in the well test. These results can be seen in table 5-1.

Single point model		Two point model		Three point model	
	$\omega_1=1$		$\omega_1=1 \omega_2=.24$		$\omega_1=1\ \omega_2=-1\ \omega_3=0.165$
	$K_{average}$		$K_{average}$		$K_{average}$
layer 2	1333	layer 2	1366	layer 2	1370
layer 3	1136	layer 3	1166	layer 3	1170
layer 4	914	layer 4	941	layer 4	943
layer 5	1428	layer 5	1461	layer 5	1465
layer 6	1184	layer 6	1215	layer 6	1219
layer 7	521	layer 7	545	layer 7	548
layer 8	1385	layer 8	1416	layer 8	1420
layer 9	1500	layer 9	1533	layer 9	1537
layer 10	1500	layer 10	1533	layer 10	1537
model average	1211.2	model average	1242.0	model average	1244

Table 5-1 Results of the multiple point models performed on Well A-04 in the Ewing block 873

5.5 Conclusion

The chapter presents the application of the multiple point proxy presented in Chapter 4 to a 3-D field example. By splitting the 3-D block into separate layers and taking arithmetic average of the layers, we get interpretable results for the power exponents. Since well A-04 was primarily more than 150 ft away from a lower permeability zone it was found that a $\omega_1=1$ was the best case followed by a two point model with an $\omega_2=0.24$ or for a three point model $\omega_2=-1$ and $\omega_3=0.165$

Proper analysis of the build-up test data is not possible unless a longer test is done to see the behavior of the log-log plot at later times. From the test data provided, we can

infer that the well is completed in a channel and the boundary is being felt but we cannot pinpoint the size of the channel

Chapter 6: Conclusions and Recommendations for Future Work

6.1Conclusions

Well testing is of primary importance for determining the flow performance and dynamic characteristics of the reservoir. The key objectives of this research work were:

1. To look at the response of the build-up test in different geological environments, and
2. To apply a spatial template to calculate multiple point statistics for wells located at different locations with respect to the channel boundaries and and determine fit parameters to approximate the K_{eff} from well test at those locations.
3. Apply the multiple point models to the Ewing Block 873 deep sea wells and see if conclusions regarding the variations in parameters of the mp proxy are validated for this real field case.

For the fulfillment of the first objective a synthetic reservoir model was built and various channel turbidite reservoir templates were applied to it. Wells were then completed in various locations in channels, shales and at various distances from the boundaries.

- For a well completed far away from any boundary or region of permeability changes the derivative plot levels out after the initial well bore storage.

- For a well completed close to a boundary where it goes from high permeability to a lower permeability across the boundary the derivative plot gets a more positive slope
- For a well completed in a low permeability zone close to a high permeability area the slope of the derivative plot becomes more negative. If it's close enough to the boundary the plot continues going negative straight after the well bore storage giving an almost spherical shape.
- If the well is completed a fair distance from the boundary, for the pressure to stabilize before the boundary is detected, the derivative plot will flatten out and then the slope change will either be positive if going from high-low or negative if going from a low- high permeability zone.

The effective permeability was obtained from the well test for all the cases mentioned above and after applying a template to the reservoir, various models were applied to best try and estimate these effective permeabilities. For wells completed with no boundaries in proximity an arithmetic average of all of the blocks in the 7x7 template provide the best match.

For wells completed at a location close to a channel/shale boundary the best model was a three point power law average. The proxy parameters either scale down the calculated average permeability for a well completed in a channel and scale down the calculated permeability for a well completed in the channel.

If the well was located more than the templates half length away from the boundary and thus have an under representation of either high or low permeability in the template, the multiple point models performed significantly better. The multiple point models tend to capture these transitioning permeability values and thereby fit the well test data better. Two point models and three point models were used in the experiment and it was found that three point models provided the best match.

Values for effective permeability can now be calculated by applying the parameters obtained from the statistics models. The power law parameter, ω, and model to be used depend on the grid location in terms of distance from a boundary and whether the well is completed in a channel or a shale. Due to the variations in the parameter values between different reservoir models a database of well test will need to be available before applying this method to estimate effective permeability values for a well completed at different locations in a reservoir model or for interpreting the proximity of the well to a facies boundary.

6.2 Recommendations for Future Work

The work presented in this thesis is new and needs further investigation to explore its full potential. Based on the work done and results obtained, the following can be recommended for future studies:

- The results obtained were essentially for a single layer reservoir. It would be interested to see the effect of laterally stacked sands on the calculation of the

template and of the calculated average permeability using the multiple statistics models.

- We have seen the effect of changes in the contrast between the channel permeability and shale permeability for a basic case. It would be interesting to see if it holds for the complex channelized reservoirs and over laterally stacked sands.
- Apply the multiple point models on more real life cases instead of synthetic models. A good match was made for the Ewing Bank Well A-04 but it should be tested for more wells.
- The research done in this thesis was purely for short build ups for wells located short distances away from a boundary and thus the transition covered by the template size. If the flow rates were lower and the boundary was not detected it would be interesting to see how this would affect the proxy fit parameters.

Appendix A: Python program for calculating single point statistical model

A.1 Overview

Here we present the code for the calculation of the single point statistical model. The code takes a 200x200x1 grid system and after inputting the grid block where the well is completed a 7x7 template around the well is assigned and a power law average calculated.

A.2 Implementation of Single point power law average

```
import numpy

#-------------------------------------------------
#-------creating 200x200 permeability matrix------
k=numpy.zeros(shape=(200,200))

f=open('perm.txt','r')
grid=[]

for line in f.xreadlines():
   perm, temp =line.split('\n')

   #perm=int(line)
   grid.append(float(perm))
```

```
for i in range(0,200):
    for j in range(0,200):
        k[i,j]=grid[j*200+i]


c,d=input("input block value nb subtract 1 from x,y coordinates (example block
90,105=89,104) =")
print k[c,d]
if c<4 or c>197:
    print ("please pick x,y value greater than 3, less than 197")
#-----------------------------------------------------------------
#---------making 7x7 matrix-------------------------
temp=numpy.zeros(shape=(7,7))
temp[0,0]=k[c-3,d-3]
temp[1,0]=k[c-2,d-3]
temp[2,0]=k[c-1,d-3]
temp[3,0]=k[c,d-3]
temp[4,0]=k[c+1,d-3]
temp[5,0]=k[c+2,d-3]
temp[6,0]=k[c+3,d-3]
temp[0,1]=k[c-3,d-2]
temp[1,1]=k[c-2,d-2]
temp[2,1]=k[c-1,d-2]
temp[3,1]=k[c,d-2]
temp[4,1]=k[c+1,d-2]
temp[5,1]=k[c+2,d-2]
temp[6,1]=k[c+3,d-2]
```

temp[0,2]=k[c-3,d-1]

temp[1,2]=k[c-2,d-1]

temp[2,2]=k[c-1,d-1]

temp[3,2]=k[c,d-1]

temp[4,2]=k[c+1,d-1]

temp[5,2]=k[c+2,d-1]

temp[6,2]=k[c+3,d-1]

temp[0,3]=k[c-3,d]

temp[1,3]=k[c-2,d]

temp[2,3]=k[c-1,d]

temp[3,3]=k[c,d]

temp[4,3]=k[c+1,d]

temp[5,3]=k[c+2,d]

temp[6,3]=k[c+3,d]

temp[0,4]=k[c-3,d+1]

temp[1,4]=k[c-2,d+1]

temp[2,4]=k[c-1,d+1]

temp[3,4]=k[c,d+1]

temp[4,4]=k[c+1,d+1]

temp[5,4]=k[c+2,d+1]

temp[6,4]=k[c+3,d+1]

temp[0,5]=k[c-3,d+2]

temp[1,5]=k[c-2,d+2]

temp[2,5]=k[c-1,d+2]

temp[3,5]=k[c,d+2]

temp[4,5]=k[c+1,d+2]

```
temp[5,5]=k[c+2,d+2]

temp[6,5]=k[c+3,d+2]

temp[0,6]=k[c-3,d+3]

temp[1,6]=k[c-2,d+3]

temp[2,6]=k[c-1,d+3]

temp[3,6]=k[c,d+3]

temp[4,6]=k[c+1,d+3]

temp[5,6]=k[c+2,d+3]

temp[6,6]=k[c+3,d+3]

print temp


#---------------------------------------------------------------------

#grid calculations

#3x3

grid9=(temp[2,2]+temp[3,2]+temp[4,2]+temp[2,3]+temp[3,3]+temp[4,3]+temp[2,4]+tem
p[3,4]+temp[4,4])

#5x5

grid25=(grid9+temp[1,1]+temp[2,1]+temp[3,1]+temp[4,1]+temp[5,1]+temp[1,2]+temp[5
,2]+temp[1,3]+temp[5,3]+temp[1,4]+temp[5,4]+temp[1,5]+temp[2,5]+temp[3,5]+temp[4
,5]+temp[5,5])

#7x7

grid49=grid25+temp[0,0]+temp[1,0]+temp[2,0]+temp[3,0]+temp[4,0]+temp[5,0]+temp[
6,0]+temp[0,1]+temp[6,1]+temp[0,2]+temp[6,2]+temp[0,3]+temp[6,3]+temp[0,4]+temp[
6,4]+temp[0,5]+temp[6,5]+temp[0,6]+temp[1,6]+temp[2,6]+temp[3,6]+temp[4,6]+temp[
5,6]+temp[6,6]

v9=grid9/9

v25=grid25/25

v49=grid49/49
```

```
print "3x3= " +str(v9)

print "5x5= " +str(v25)

print "7x7=" +str(v49)

#-------------------------------------------------------------------------------

#--------------IMPLEMENTING POWER LAW AVERAGE----------------

pa=input("input omega= ")


#power law calculator

geometricaverage=((.020408163)*((temp[0,0]**pa)+(temp[1,0]**pa)+(temp[2,0]**pa)+(
temp[3,0]**pa)+(temp[4,0]**pa)+(temp[5,0]**pa)+(temp[6,0]**pa)+(temp[0,1]**pa)+(t
emp[1,1]**pa)+(temp[2,1]**pa)+(temp[3,1]**pa)+(temp[4,1]**pa)+(temp[5,1]**pa)+(te
mp[6,1]**pa)+(temp[0,2]**pa)+(temp[1,2]**pa)+(temp[2,2]**pa)+(temp[3,2]**pa)+(te
mp[4,2]**pa)+(temp[5,2]**pa)+(temp[6,2]**pa)+(temp[0,3]**pa)+(temp[1,3]**pa)+(te
mp[2,3]**pa)+(temp[3,3]**pa)+(temp[4,3]**pa)+(temp[5,3]**pa)+(temp[6,3]**pa)+(te
mp[0,4]**pa)+(temp[1,4]**pa)+(temp[2,4]**pa)+(temp[3,4]**pa)+(temp[4,4]**pa)+(te
mp[5,4]**pa)+(temp[6,4]**pa)+(temp[0,5]**pa)+(temp[1,5]**pa)+(temp[2,5]**pa)+(te
mp[3,5]**pa)+(temp[4,5]**pa)+(temp[5,5]**pa)+(temp[6,5]**pa)+(temp[0,6]**pa)+(te
mp[1,6]**pa)+(temp[2,6]**pa)+(temp[3,6]**pa)+(temp[4,6]**pa)+(temp[5,6]**pa)+(te
mp[6,6]**pa)))**(1/pa)

print "geometric average=" +str(geometricaverage)
```

A.3 Implementation of two point statistical model

```
#-------To calculate multiple point models the same template was used-------

#-Use outputted answer and apply parameter by using solver to minimize error difference

#---------------------lag1 geometricavg--------------------

#

gc1=(((temp[0,6]*temp[1,5]))+((temp[0,5]*temp[1,4]))+((temp[0,4]*temp[1,3]))+((temp
[0,3]*temp[1,2]))+((temp[0,2]*temp[1,1]))+((temp[0,1]*temp[1,0])))/(6)

gc2=(((temp[1,6]*temp[2,5]))+((temp[1,5]*temp[2,4]))+((temp[1,4]*temp[2,3]))+((temp
[1,3]*temp[2,2]))+((temp[1,2]*temp[2,1]))+((temp[1,1]*temp[2,0])))/(6)
```

```
gc3=(((temp[2,6]*temp[3,5]))+((temp[2,5]*temp[3,4]))+((temp[2,4]*temp[3,3]))+((temp
[2,3]*temp[3,2]))+((temp[2,2]*temp[3,1]))+((temp[2,1]*temp[3,0])))/(6)

gc4=(((temp[3,6]*temp[4,5]))+((temp[3,5]*temp[4,4]))+((temp[3,4]*temp[4,3]))+((temp
[3,3]*temp[4,2]))+((temp[3,2]*temp[4,1]))+((temp[3,1]*temp[4,0])))/(6)

gc5=(((temp[4,6]*temp[5,5]))+((temp[4,5]*temp[5,4]))+((temp[4,4]*temp[5,3]))+((temp
[4,3]*temp[5,2]))+((temp[4,2]*temp[5,1]))+((temp[4,1]*temp[5,0])))/(6)

gc6=(((temp[5,6]*temp[6,5]))+((temp[5,5]*temp[6,4]))+((temp[5,4]*temp[6,3]))+((temp
[5,3]*temp[6,2]))+((temp[5,2]*temp[6,1]))+((temp[5,1]*temp[6,0])))/(6)


twopt=(gc1+gc2+gc3+gc4+gc5+gc6)/6

print"twoptlag1= "+str(twopt)


#---------------------------------------------------------------------

#for lag 2 geometric average

gl1=(((temp[0,6]*temp[2,4]))+((temp[0,5]*temp[2,3]))+((temp[0,4]*temp[2,2]))+((temp[
0,3]*temp[2,1]))+((temp[0,2]*temp[2,0])))/5

gl2=(((temp[1,6]*temp[3,4]))+((temp[1,5]*temp[3,3]))+((temp[1,4]*temp[3,2]))+((temp[
1,3]*temp[3,1]))+((temp[1,2]*temp[3,0])))/5

gl3=(((temp[2,6]*temp[4,4]))+((temp[2,5]*temp[4,3]))+((temp[2,4]*temp[4,2]))+((temp[
2,3]*temp[4,1]))+((temp[2,2]*temp[4,0])))/5

gl4=(((temp[3,6]*temp[5,4]))+((temp[3,5]*temp[5,3]))+((temp[3,4]*temp[5,2]))+((temp[
3,3]*temp[5,1]))+((temp[3,2]*temp[5,0])))/5

gl5=(((temp[4,6]*temp[6,4]))+((temp[4,5]*temp[6,3]))+((temp[4,4]*temp[6,2]))+((temp[
4,3]*temp[6,1]))+((temp[4,2]*temp[6,0])))/5


twoptlag2=(gl1+gl2+gl3+gl4+gl5)/5


print "geometric average lag2=" +str(twoptlag2)

#---------------------------------------------------------------------
```

```
#for lag3 geometric average

ga1=(((temp[0,6]*temp[3,3]))+((temp[0,5]*temp[3,2]))+((temp[0,4]*temp[3,1]))+((temp
[0,3]*temp[3,0])))/4

ga2=(((temp[1,6]*temp[4,3]))+((temp[1,5]*temp[4,2]))+((temp[1,4]*temp[4,1]))+((temp
[1,3]*temp[4,0])))/4

ga3=(((temp[2,6]*temp[5,3]))+((temp[2,5]*temp[5,2]))+((temp[2,4]*temp[5,1]))+((temp
[2,3]*temp[5,0])))/4

ga4=(((temp[3,6]*temp[6,3]))+((temp[3,5]*temp[6,2]))+((temp[3,4]*temp[6,1]))+((temp
[3,3]*temp[6,0])))/4

twoptlag3=(ga1+ga2+ga3+ga4)/4

print "geometric average lag3="+str(twoptlag3)

#-----------------------------------


#for lag 1 reverse geometric average

gq1=(((temp[0,0]*temp[1,1]))+((temp[0,1]*temp[1,2]))+((temp[0,2]*temp[1,3]))+((temp
[0,3]*temp[1,4]))+((temp[0,4]*temp[1,5]))+((temp[0,5]*temp[1,6])))/6

gq2=(((temp[1,0]*temp[2,1]))+((temp[1,1]*temp[2,2]))+((temp[1,2]*temp[2,3]))+((temp
[1,3]*temp[2,4]))+((temp[1,4]*temp[2,5]))+((temp[1,5]*temp[2,6])))/6

gq3=(((temp[2,0]*temp[3,1]))+((temp[2,1]*temp[3,2]))+((temp[2,2]*temp[3,3]))+((temp
[2,3]*temp[3,4]))+((temp[2,4]*temp[3,5]))+((temp[2,5]*temp[3,6])))/6

gq4=(((temp[3,0]*temp[4,1]))+((temp[3,1]*temp[4,2]))+((temp[3,2]*temp[4,3]))+((temp
[3,3]*temp[4,4]))+((temp[3,4]*temp[4,5]))+((temp[3,5]*temp[4,6])))/6

gq5=(((temp[4,0]*temp[5,1]))+((temp[4,1]*temp[5,2]))+((temp[4,2]*temp[5,3]))+((temp
[4,3]*temp[5,4]))+((temp[4,4]*temp[5,5]))+((temp[4,5]*temp[5,6])))/6

gq6=(((temp[5,0]*temp[6,1]))+((temp[5,1]*temp[6,2]))+((temp[5,2]*temp[6,3]))+((temp
[5,3]*temp[6,4]))+((temp[5,4]*temp[6,5]))+((temp[5,5]*temp[6,6])))/6



twoptr=(gq1+gq2+gq3+gq4+gq5+gq6)/6

print"twoptr= "+str(twoptr)
```

```
#-----------------------------------------------

#for lag 2 reverse geometric average

gw1=(((temp[0,0]*temp[2,2]))+((temp[0,1]*temp[2,3]))+((temp[0,2]*temp[2,4]))+((temp
[0,3]*temp[2,5]))+((temp[0,4]*temp[2,6])))/5

gw2=(((temp[1,0]*temp[3,2]))+((temp[1,1]*temp[3,3]))+((temp[1,2]*temp[3,4]))+((temp
[1,3]*temp[3,5]))+((temp[1,4]*temp[3,6])))/5

gw3=(((temp[2,0]*temp[4,2]))+((temp[2,1]*temp[4,3]))+((temp[2,2]*temp[4,4]))+((temp
[2,3]*temp[4,5]))+((temp[2,4]*temp[4,6])))/5

gw4=(((temp[3,0]*temp[5,2]))+((temp[3,1]*temp[5,3]))+((temp[3,2]*temp[5,4]))+((temp
[3,3]*temp[5,5]))+((temp[3,4]*temp[5,6])))/5

gw5=(((temp[4,0]*temp[6,2]))+((temp[4,1]*temp[6,3]))+((temp[4,2]*temp[6,4]))+((temp
[4,3]*temp[6,5]))+((temp[4,4]*temp[6,6])))/5

glag2_rev=(gw1+gw2+gw3+gw4+gw5)/5

print "geometric average lag2 reverse="+str(glag2_rev)

#-----------------------------------------

#for lag 3 reverse geometric average

ge1=(((temp[0,0]*temp[3,3]))+((temp[0,1]*temp[3,4]))+((temp[0,2]*temp[3,5]))+((temp
[0,2]*temp[3,6])))/4

ge2=(((temp[1,0]*temp[4,3]))+((temp[1,1]*temp[4,4]))+((temp[1,2]*temp[4,5]))+((temp
[1,3]*temp[4,6])))/4

ge3=(((temp[2,0]*temp[5,3]))+((temp[2,1]*temp[5,4]))+((temp[2,2]*temp[5,5]))+((temp
[2,2]*temp[5,6])))/4

ge4=(((temp[3,0]*temp[6,3]))+((temp[3,1]*temp[6,4]))+((temp[3,2]*temp[6,5]))+((temp
[3,2]*temp[6,6])))/4

glag3_rev=(ge1+ge2+ge3+ge4)/4


print "geometric average lag3 reverse="+str(glag3_rev)
```

A.4 Implementation of Three Point Model

```
#---three point 45 degrees

pt31=(((temp[0,6]*temp[1,5]*temp[2,4]))+((temp[1,6]*temp[2,5]*temp[3,4]))+((temp[2,
6]*temp[3,5]*temp[4,4]))+((temp[3,6]*temp[4,5]*temp[5,4]))+((temp[4,6]*temp[5,5]*te
mp[6,4])))/5

pt32=(((temp[0,5]*temp[1,4]*temp[2,3]))+((temp[1,5]*temp[2,4]*temp[3,3]))+((temp[2,
5]*temp[3,4]*temp[4,3]))+((temp[3,5]*temp[4,4]*temp[5,3]))+((temp[4,5]*temp[5,4]*te
mp[6,3])))/5

pt33=(((temp[0,4]*temp[1,3]*temp[2,2]))+((temp[1,4]*temp[2,3]*temp[3,2]))+((temp[2,
4]*temp[3,3]*temp[4,2]))+((temp[3,4]*temp[4,3]*temp[5,2]))+((temp[4,4]*temp[5,3]*te
mp[6,2])))/5

pt34=(((temp[0,3]*temp[1,2]*temp[2,1]))+((temp[1,3]*temp[2,2]*temp[3,1]))+((temp[2,
3]*temp[3,2]*temp[4,1]))+((temp[3,3]*temp[4,2]*temp[5,1]))+((temp[4,3]*temp[5,2]*te
mp[6,1])))/5

pt35=(((temp[0,2]*temp[1,1]*temp[2,0]))+((temp[1,2]*temp[2,1]*temp[3,0]))+((temp[2,
2]*temp[3,1]*temp[4,0]))+((temp[3,2]*temp[4,1]*temp[5,0]))+((temp[4,2]*temp[5,1]*te
mp[6,0])))/5

threept=(pt31+pt32+pt33+pt34+pt35)/5

print"threept= "+str(threept)


#--------for three point average 135 degrees--------


lr1=(((temp[6,6]*temp[5,5]*temp[4,4]))+((temp[5,6]*temp[4,5]*temp[3,4]))+((temp[4,6]
*temp[3,5]*temp[2,4]))+((temp[3,6]*temp[2,5]*temp[1,4]))+((temp[2,6]*temp[1,5]*tem
p[0,4])))/5

lr2=(((temp[6,5]*temp[5,4]*temp[4,3]))+((temp[5,5]*temp[4,4]*temp[3,3]))+((temp[4,5]
*temp[3,4]*temp[2,3]))+((temp[3,5]*temp[2,4]*temp[1,3]))+((temp[2,5]*temp[1,4]*tem
p[0,3])))/5

lr3=(((temp[6,4]*temp[5,3]*temp[4,2]))+((temp[5,4]*temp[4,3]*temp[3,2]))+((temp[4,4]
*temp[3,3]*temp[2,2]))+((temp[3,4]*temp[2,3]*temp[1,2]))+((temp[2,4]*temp[1,3]*tem
p[0,2])))/5
```

```
lr4=(((temp[6,3]*temp[5,2]*temp[4,1]))+((temp[5,3]*temp[4,2]*temp[3,1]))+((temp[4,3]
*temp[3,2]*temp[2,1]))+((temp[3,3]*temp[2,2]*temp[1,1]))+((temp[2,3]*temp[1,2]*tem
p[0,1])))/5

lr5=(((temp[6,2]*temp[5,1]*temp[4,0]))+((temp[5,2]*temp[4,1]*temp[3,0]))+((temp[4,2]
*temp[3,1]*temp[2,0]))+((temp[3,2]*temp[2,1]*temp[1,0]))+((temp[2,2]*temp[1,1]*tem
p[0,0])))/5


threeptr=(lr1+lr2+lr3+lr4+lr5)/5

print"threeptr= "+str(threeptr)
```

Bibliography

Abreu, V., Sullivan, M., Pirmez, C., Mohrig, D., (2003). Lateral accretion packages (LAPs): an important reservoir element in deep water sinuous channels. Marine and petroleum Geology 20, 631-648

Chassagne, A., Louis, A.,(1999). Well Testing Technical Challenges in Deep Water Wells, Presented at 1999 SPE/IADC Drilling Conference

Clark, J.D., Pickering, K.T. (1996) Submarine Channels: Processes and Architecture. Vallis Press, London, (231 pp)

Cronin, B.T, (1995). Structurally controlled deep sea channel courses: example from the Miocene of southeast Spain and the Alboran Sea, southwest Mediterranean. Characterization of Deep Marine Clastic Systems: Geological Society Special Publication No. 94 pp. 115-135

Dutton, S.P., Barton, M.D., Asquith, G.B., Malik, M.A., Cole, A.G., Gogas, J., Guzman, J.I.,Clift, S.J.,(1999). Geologic and Engineering Characterization of Turbidite Reservoirs, Forth Geraldine Unit, Bell Canyon Formation, West Texas. Bureau of Economic Geology, Report of investigations no 225

Gringarten, A.C., From Straight Lines to Deconvolution: The Evolution of the State of the Art in Well Test Analysis, Presented at 2006 SPE Annual Technical Conference

Kolla, V., Bourges, P., Urrity, J.M, Saffa, P., (2001). Evolution of deepwater tertiary sinuous channels offshore, Angola (West Africa) and implications to reservoir architecture.AAPG Bulletin 85, 1373-1405

Lassoued, C., Dowla, N., Wendt, R., (2002). Deepwater Improvements Using Real-Time Formation Evaluation. Presented at 2002 SPE International Petroleum Conference

Levitan, M.M, Ward, M.J. (2006). The Use of Well Testing for Evaluation of Connected Reservoir Volume, 2006 SPE Annual Technical Conference

Luchesi, C.F., Gontijo J.E (1998). Deep Water Reservoir Management: the Brazilian Experience. Presented at Offshore Technology Conference

Maher J, (2007). Architecture and Seismic Geomorphology of Shelf Edge Deltas along an Active Tectonic Margin, Eastern Offshore Trinidad. Masters Thesis, University of Texas-Austin

Massonant, G.M., Norris, R.J., Chalmette, J.C., Aquitaine, E. (1993). Well Test Interpretation in Geologically Complex Channelized Reservoirs. 68th Annual SPE Technical Conference

Mayall, M. , Jones, E. and Casey, M. (2006). Turbidite channel reservoir-Key elements in facies prediction and effective development. Marine and Petroleum Geology 23 (2006) 821-841

Mayall, M. Stewart, I.,(2000). The architecture of turbidite slope channels Global deep water reservoirs: Gulf coast section SEPM Foundation 20th Annual Bob F Perkins research conference pp 578-586

Mijiniywa, A. (2008). Influence of geological Features on Well Test Behavior. 2008 SPE Europec/EAGE Annual Conference and Exhibition

Navarre J.C., Claude, D., Librelle, F., Safa, P., Villon, G., Keskes, N. (2002). Deepwater turbidites system analysis, West Africa: sedimentary model and implications for reservoir model construction. The Leading Edge 21, 1132-1139

Remy, N., Boucher, A., Wu, J., (2009). Applied Geostatistics with Sgems. Stanford University

Stow, D. and Mayall, M. (1999). Deep-water sedimentary systems: New models for the 21st century. Marine and Petroleum Geology 17 (2000) 125-135

Strebelle, S., (2002) Conditional simulation of complex geological structures using multiple-point statistics. Math. Geol

Wood, G.A., Orren, R.J., Conway, A.M, (2000). 3D High Resolution Seismic: Case Study Deepwater West Africa. Presented at 2000 Offshore technology conference.

Zambrano, J., Zimmerman, R.W., Gringarten, A.C. (2000). Influence of Geological Features on Well Test Behavior. 2000 SPE Asia Pacific Conference on Integrated Modeling for Asset Management